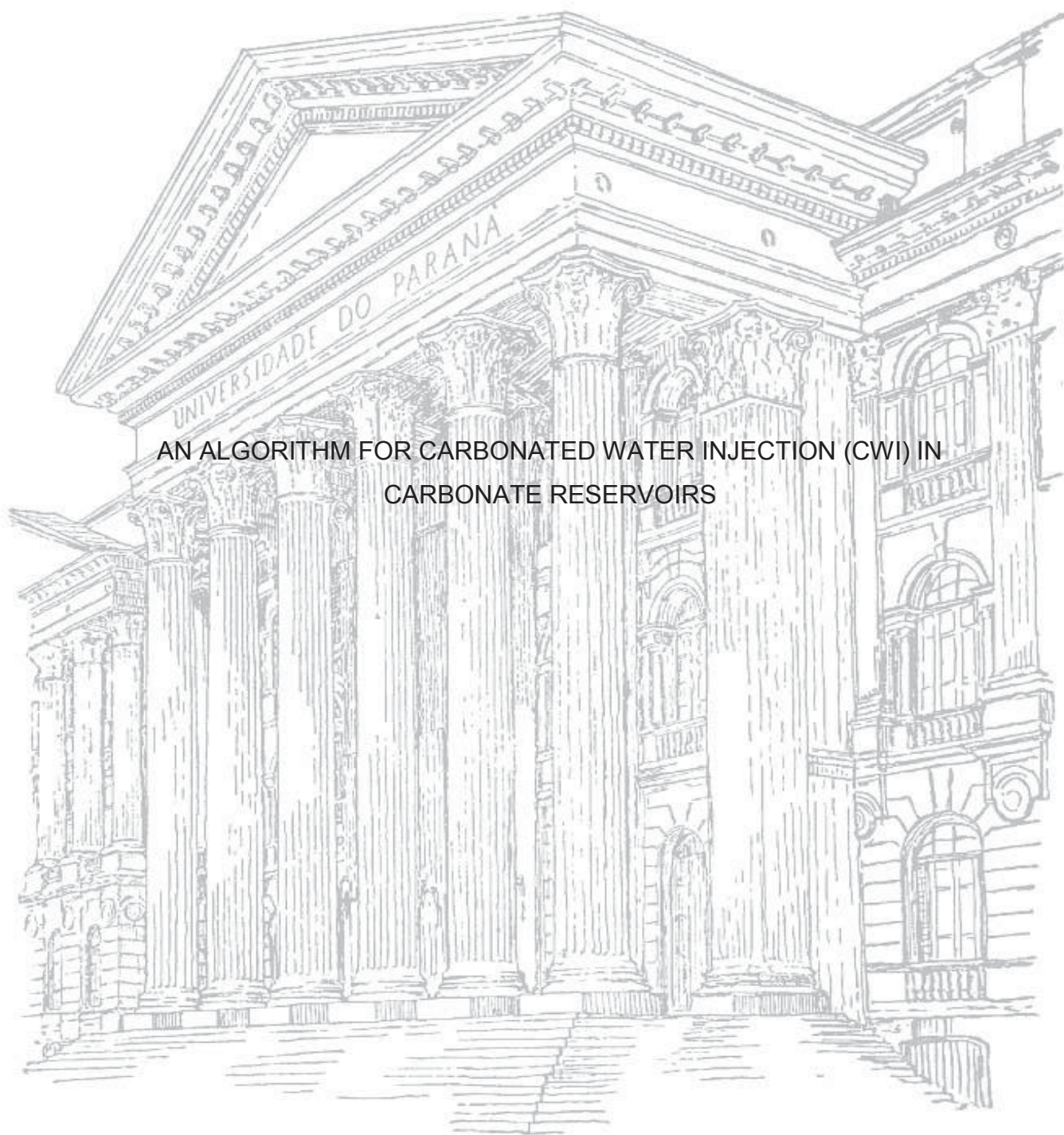


UNIVERSIDADE FEDERAL DO PARANÁ

GUSTAVO LUNARDON QUILLÓ



AN ALGORITHM FOR CARBONATED WATER INJECTION (CWI) IN
CARBONATE RESERVOIRS

CURITIBA

2018

GUSTAVO LUNARDON QUILLÓ

AN ALGORITHM FOR CARBONATED WATER INJECTION (CWI) IN
CARBONATE RESERVOIRS

Dissertação apresentada como requisito parcial à
obtenção do título de Mestre, do Curso de Pós-
Graduação em Engenharia Química, Setor de
Tecnologia, Universidade Federal do Paraná.

Orientador: Prof. Dr. Luiz Fernando Lima Luz Jr.
Coorientador: Prof. Dr. Éliton Fontana

CURITIBA

2018

FICHA CATALOGRÁFICA ELABORADA PELO SISTEMA DE BIBLIOTECAS/UFPR
BIBLIOTECA DE CIÊNCIA E TECNOLOGIA

Q6a Quilló, Gustavo Lunardon
 An algorithm for carbonated water injection (CWI) in carbonate reservoirs / Gustavo Lunardon
 Quilló. – Curitiba, 2018.

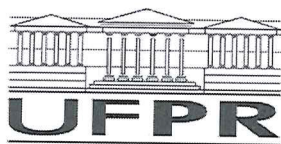
 Dissertação (Mestrado) - Universidade Federal do Paraná, Setor de Tecnologia, Programa de
 Pós-Graduação em Engenharia Química, 2018.

 Orientador: Luiz Fernando Lima Luz Jr.
 Coorientador: Éliton Fontana.

 1. Solubilidade do CO₂. 2. Armazenamento geológico de carbono. 3. Água carbonatada.
 I. Universidade Federal do Paraná. II. Luz Jr, Luiz Fernando Lima. III. Fontana, Éliton.
 IV. Título.

CDD: 660

Bibliotecária: Romilda Santos - CRB-9/1214




MINISTÉRIO DA EDUCAÇÃO
SETOR SETOR DE TECNOLOGIA
UNIVERSIDADE FEDERAL DO PARANÁ
PRÓ-REITORIA DE PESQUISA E PÓS-GRADUAÇÃO
PROGRAMA DE PÓS-GRADUAÇÃO ENGENHARIA QUÍMICA

TERMO DE APROVAÇÃO

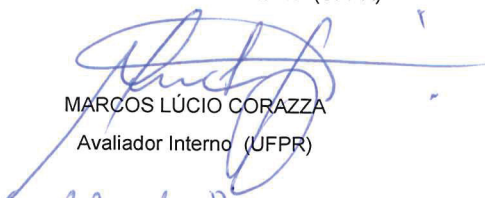
Os membros da Banca Examinadora designada pelo Colegiado do Programa de Pós-Graduação em ENGENHARIA QUÍMICA da Universidade Federal do Paraná foram convocados para realizar a arguição da Dissertação de Mestrado de **GUSTAVO LUNARDON QUILLÓ** intitulada: **AN ALGORITHM FOR CARBONATED WATER INJECTION (CWI) IN CARBONATE RESERVOIRS**, após terem inquirido o aluno e realizado a avaliação do trabalho, são de parecer pela sua APROVAÇÃO no rito de defesa.

A outorga do título de mestre está sujeita à homologação pelo colegiado, ao atendimento de todas as indicações e correções solicitadas pela banca e ao pleno atendimento das demandas regimentais do Programa de Pós-Graduação.

CURITIBA, 23 de Maio de 2018.


LUIZ FERNANDO DE LIMA LUZ JUNIOR
Presidente da Banca Examinadora (UFPR)


ELITON FONTANA
Coorientador - Avaliador Interno (UFPR)


MARCOS LÚCIO CORAZZA
Avaliador Interno (UFPR)


CLÁUDIO DARIVA
Avaliador Externo (UNIT-SE)

I dedicate this work to my parents João and Luciane,
my grandmother Nina, my sister Fernanda and my girlfriend
Annelorie for their endless love, support and encouragement to
chase my dreams and giving me the strength to reach the stars.

ACKNOWLEDGEMENTS

I would like to express my gratitude to my supervisors Professor Luiz Fernando de Lima Luz Jr. and Professor Éliton Fontana for their guidance throughout my studies at UFPR. Their doors were always open for clearing doubts and discussing ideas. Moreover, I am deeply grateful to Professor Marcos Lúcio Corazza for the invaluable insights which considerably improved the quality and structure of this master thesis.

For my parents João and Luciane, who provided me with quality advice and did not measure efforts so I could complete this master's degree. Your contribution starts before I can even remember, before the day you gave me my first book. Thank you for your hard work so I could have more opportunities.

For my girlfriend Annelorie, who supported me in many moments of crisis and for so many reviews and proofreading of my articles. For your comprehension, love and patience, I am forever indebted. Walking alongside you in this journey has been a more enjoyable experience than I could have wished for.

To my grandmother Nina and my sister Fernanda, who cheered me up and brighten my days. You always encouraged me to do my best. I could not express in words how thankful I am for your affection.

Thank you, God, for my good health and for your protection from any dangers, especially while driving in the highway.

To all my friends and family who, in one way or another, accompanied me during this phase in my life. You gave me the tenacity to face this challenge with dignity.

I am grateful for the financial support of CNPq (Conselho Nacional de Desenvolvimento Científico e Tecnológico), grant proc. 480989/2013-3 and the research scholarship granted by CAPES (Coordenação de Aperfeiçoamento de Pessoal de Nível Superior).

Lastly, thank you as a reader. I hope you find the information compiled in this work useful and provide you valuable insights for your own work.

RESUMO

Um algoritmo é apresentado para modelar o comportamento de injeção de água salgada carbonatada em rochas carbonáticas com a finalidade de armazenamento geológico de carbono. A abordagem permite customização de simulações de fluidodinâmica computacional pela inclusão de reações de dissolução de minerais ao integrar um modelo de solubilidade CO_2 , cálculos de especiação, reações cinéticas de dissolução e suas consequentes mudanças nas propriedades do reservatório ao longo do tempo. As reações de equilíbrio e cinética são calculadas sequencialmente, onde um controle adaptativo do passo de tempo garante que a taxa de dissolução seja computada a partir da condição correta de equilíbrio químico. O equilíbrio químico é calculado pela abordagem estequiométrica, em que um sistema de equações algébricas é solucionado pela método de Newton-Raphson com derivadas numéricas na matriz Jacobiana. O reservatório é considerado como um meio pseudo-homogêneo onde as alterações na estrutura da rocha são computadas por uma equação semi-empírica baseada em Kozeny-Carman. Finalmente, um algoritmo de estabilização baseado no gráfico de Bjerrum do H_2CO_3 fornece robustez numérica para os cálculos de especiação. Os resultados são obtidos procurando o menor esforço computacional, permitindo a estimação do intervalo de tempo em que o sistema atinge o equilíbrio e mudanças na estrutura da rocha.

Palavras-chave: dissolução, solubilidade do CO_2 , armazenamento geológico de carbono, água carbonatada, meio poroso.

ABSTRACT

An algorithm for calculating the behavior of carbonated brine injection in calcite rocks aiming at carbon geological storage is presented. The approach is designed to customize computational fluid dynamics simulations to include dissolution chemistry by integrating a CO₂ solubility model, speciation calculations, mineral dissolution reactions and the consequent change in reservoir properties over time. The equilibrium and dissolution reactions are calculated sequentially, where an adaptive control of the time step ensures the rate of dissolution is computed from the correct equilibrium condition. The chemical equilibrium condition is calculated via the stoichiometric approach, where a system of three algebraic equations is solved using Newton-Raphson supplied with numerical derivatives in the Jacobian Matrix. The reservoir is represented as a pseudo-homogeneous medium where alterations in rock properties are computed via a formulation based on Kozeny-Carman. Finally, a stabilization algorithm based on the Bjerrum plot of H₂CO₃ provides numerical robustness for the speciation calculations. The results are obtained attempting the minimum computational effort, allowing the estimation of the time frame for the system to reach the equilibrium condition and changes in rock structure.

Keywords: dissolution, CO₂ solubility, carbon sequestration, carbonated water, porous medium.

LIST OF FIGURES

FIGURE 1 BJERRUM PLOT FOR CARBONIC ACID	26
FIGURE 2 POROSITY HISTOGRAM FOR THE FRANCO FIELD AT PRE SALT IN BRAZIL.....	28
FIGURE 3 PHASES FOR OIL PRODUCTION IN RESERVOIRS.	29
FIGURE 4 CROSS-SECTIONS OF A CALCITE ROCK IN THE PLANE (a) $x = 405$ (b) $y = 440$	33
FIGURE 5 EXAMPLES OF PATTERNS OF DISSOLUTION (a) FACE DISSOLUTION, (b) CONICAL WORMHOLE, (c) DOMINANT WORMHOLE, (d) RAMIFIED WORMHOLE	33
FIGURE 6 FLOW CHART FOR THE MAIN SECTION OF THE ALGORITHM.	37
FIGURE 7 FLOW CHART FOR THE SOLUBILITY CODE	40
FIGURE 8 FLOW CHART FOR THE SPECIATION MODEL.	46
FIGURE 9 FLOW CHART FOR NEWTON-RAPHSON METHOD (INNER LOOP OF THE SPECIATION CODE).....	47
FIGURE 10 STEPWISE CHANGE IN VOLUME FROM RESERVOIR TO SURFACE CONDITIONS.....	50
FIGURE 11 (A) JOINT CONFIDENCE REGION FOR $hCa2 +$ AND $hMg2 +$ AND (B) COMPARISON BETWEEN COMPUTED AND MEASURED $mCO2$ FOR THE FIRST ADJUSTMENT.....	58
FIGURE 12 (A) JOINT CONFIDENCE REGION FOR $hCa2 +$ AND $hMg2 +$ AND (B) COMPARISON BETWEEN COMPUTED AND MEASURED $mCO2$ FOR THE SECOND ADJUSTMENT	59
FIGURE 13 COMPARISON BETWEEN MODEL AND EXPERIMENTAL RESULTS FOR EQUILIBRIUM CO_2 SOLUBILITY IN BRINE. (A) $76\text{ }^\circ\text{C}$ AND 1.05 $mCaCl_2$, (B) $76\text{ }^\circ\text{C}$ AND $2.30\text{ }mCaCl_2$, (C) $101\text{ }^\circ\text{C}$ AND $1.05\text{ }mCaCl_2$, (A) $101\text{ }^\circ\text{C}$ AND $2.30\text{ }mCaCl_2$	60
FIGURE 14 COMPARISON BETWEEN MODEL RESULTS FOR H_2O CONTENT IN THE GAS PHASE AT EQUILIBRIUM. (A) $76\text{ }^\circ\text{C}$ AND $1.05\text{ }mCaCl_2$, (B) $76\text{ }^\circ\text{C}$ AND $2.30\text{ }mCaCl_2$, (C) $101\text{ }^\circ\text{C}$ AND $1.05\text{ }mCaCl_2$, (D) $101\text{ }^\circ\text{C}$ AND $2.30\text{ }mCaCl_2$	61

FIGURE 15 EVOLUTION OF VARIABLES IN TIME (A) PH, (B) DETAILED INFORMATION ON pH, (C) MOLALITY OF CARBON SPECIES (D) PARTIAL BJERRUM PLOT WITH PERCENTAGE OF CARBON SPECIES.....	69
FIGURE 16 ROCK PROPERTIES AS A FUNCTION OF TIME (A) POROSITY AND DISSOLUTION RATE, (B) INDIRECT EFFECT OF DISSOLUTION RATE ON SPECIFIC SURFACE AREA AND PERMEABILITY.....	69
FIGURE 17 EVOLUTION OF IMPORTANT PROPERTIES OF THE SOLUTION IN TIME (A) ACTIVITY OF CO ₂ AND IONIC STRENGTH, (B) MOLALITY OF Ca ²⁺ AND CO ₃ ²⁻	70
FIGURE 18 (A) DATA FIT FOR PARAMETER A _{y,10} , (B) DATA FIT FOR PARAMETER B _{y,10}	83

LIST OF TABLES

TABLE 1 OVERVIEW OF MODELS IN SEVERAL CO ₂ INJECTION TECHNIQUES	22
TABLE 2 MECHANISTIC CALCITE DISSOLUTION REACTIONS	24
TABLE 3 CHEMICAL SYSTEM USED FOR ANALYZING THE BJERRUM PLOT OF H ₂ CO ₃	25
TABLE 4 EXAMPLES OF CHEMICAL SYSTEMS USED IN THE LITERATURE	38
TABLE 5 COEFFICIENTS FOR CALCULATING $V_{CO_2, dis}$	51
TABLE 6 RESULTS FOR EACH PARAMETER ESTIMATION PROCEDURE	58
TABLE 7 VALIDATION OF THE MODIFIED DRUMMOND (2018) AT P = 150 BAR – MgCl ₂	60
TABLE 8 CHEMICAL SYSTEM USED IN THIS WORK AND EQUILIBRIUM CONSTANTS.	63
TABLE 9 NUMBER OF MOLES OF AT THE START OF ANY PART OF THE MODEL.....	64
TABLE 10 NUMBER OF MOLES AT THE END OF EACH PART OF THE MODEL.	64
TABLE 11 EQUILIBRIUM CONSTANTS IN TERMS OF TEMPERATURE [K]	65
TABLE 12 EQUILIBRIUM CONSTANTS IN TERMS OF THE DEGREE OF ADVANCEMENT OF THE REACTIONS	65
TABLE 13 CHEMICAL SPECIES PROPERTIES AND SUMMARY ACTIVITY COEFFICIENT MODELS USED IN THIS WORK.....	66
TABLE 14 MISCELLANEOUS CRITERIA FOR NUMERICAL METHODS IN THE EXAMPLE.	66
TABLE 15 CALCITE DISSOLUTION PARAMETERS	67
TABLE 16 COMPARISON BETWEEN DIFFERENT THERMODYNAMIC MODELS AT $T = 60\text{ }^{\circ}\text{C}$, $PEQ = 100\text{ BAR}$, $m_{NaCl} = 0.5\text{ mol/kgH}_2\text{O}$ AND $m_{CaCl_2} =$ $0.1\text{ mol/kgH}_2\text{O}$	71
TABLE 17 DATA USED FOR COMPUTING DEBYE-HÜCKEL PARAMETERS.....	82

LIST OF SYMBOLS

Nomenclature			
a	Activity [-]	SSA_t	Specific surface area [m ² m ⁻³]
a_{WATEQ}	WATEQ parameters	s	Newton-Raphson method variable [mol]
b_{WATEQ}			
$A_{\gamma,10}$	Debye-Hückel parameters	S	Reactive surface area [m ²]
$B_{\gamma,10}$			
C_{KC}	Constant for Kozeny-Carman	S_{wt}	Salinity [wt%]
E_a	Activation energy [J mol ⁻¹]	t	Time [s]
F_{VAL}	Objective function values	tol	tolerance
h	Empirical parameter [-]	T	Temperature [K] (or otherwise indicated)
it	Iteration number [-]	u	Mechanism index [-]
I	Ionic strength [mol kg _{H2O} ⁻¹]	V	Volume [m ³]
J	Jacobian matrix	$V_{min,i}$	Molar volume of mineral i [m ³ mol ⁻¹]
k	Kinetic constant	y	Molar fraction in the gas phase [-]
K	Equilibrium constant	z	Ion charge [-]
m	Molality of species i [mol kg _{H2O} ⁻¹]	β	Empirical parameter [-]
$mass$	Mass [kg]	γ	Activity coefficient [-]
MW	Molar weight [g mol ⁻¹]	Δt	Time step [s]
n	Order of reaction [-]	Δt_{small}	Reduced time step [s]
N	Number of moles [mol]	$\Delta \xi$	ξ step used in CDS-2 [mol]
N_{aq}	Number of aqueous species	θ	Void fraction [-]
N_{EQ}	Number of equilibrium reactions	σ	Permeability [m ²]
N_{min}	Number of minerals	ξ	Extent of reaction [mol]
N_{parts}	Number of parts [-]	ν	Stoichiometric coefficient [-]
p, q	Empirical parameters [-]	ρ	Density
P	Pressure [bar]	ω	Empirical parameter [-]
R	Gas constant [cm ³ bar mol ⁻¹ K ⁻¹]		
Subscripts and superscripts			
c	Critical	mix	Mixture property
$cell$	Pertinent to the control volume	ref	Reference
$crit$	Criterion	$stab$	From the stabilization code
EQ	Equilibrium	sim	Simulation
g	Gas / vapor / supercritical phase	t	At time t
$guess$	Guess for the numerical solution	tot	Total
i	Species i	u	Mechanism number u
j	Reaction number j	x	Molar fraction scale
k	Salt k	●	Final (iteration end)
l	Liquid phase	□	Initial (iteration start)
m	Molality scale	0	At $t = 0$
min	Mineral	ξ	Extent of reaction

ACRONYMS

a.k.a – Also known as

ANSYS® – American computer-aided engineering software developer

CDS-2 - 2nd order central differencing scheme

CFD – Computer fluid dynamics

CGS – Carbon dioxide geological storage

CPA – Cubic plus association EoS

CWI – Carbonated water injection

e.g. – *Exempli gratia* (latin)

EOR – Enhanced oil recovery

EoS – Equation of state

FDM – Finite difference method

FEM – Finite element method

FSM – Fractional step method

FVM – Finite volume method

IAP – Ion Activity Product

i.e. – *id est* (latin)

INDC - Intended Nationally Determined Contribution

IOR – Improved oil recovery

LAMIR - Laboratory of Analysis of Minerals and Rocks

LSW – Low salinity water injection

MATLAB® – Matrix laboratory. A language for technical computing

Micro-CT – Computer micro-tomography

MIP – Mercury intrusion porosimetry

N.A. – Not applicable

PISO – Pressure Implicit with Splitting of Operator

PNM – Pore network modeling

PHREEQC – PH (pH) REdox EQUilibrium C (program written in C)

PSO – Particle Swarm optimization

RK – Redlich-Kwong EoS

SEM – Scanning electron microscopy

SIMPLE – *Semi-Implicit Method for Pressure-Linked Equations*

SIMPLEC – SIMPLE-consistent

SIMPLER – SIMPLE-revised

UDF – User Defined Function

UNFCCC - United Nations Framework Convention in Climate Change

WAG – Water alternating gas

SUMMARY

1	INTRODUCTION	16
1.1	MOTIVATION AND GOALS	17
1.1.1	Specific goals	20
2	CRITICAL ANALYSIS OF THE RELEVANT LITERATURE	21
2.1	DISSOLUTION AND PRECIPITATION REACTION RATES	23
2.2	BJERRUM PLOT	24
2.3	DIFFUSION COEFFICIENT	26
2.4	POROUS MEDIUM REPRESENTATION	27
2.5	BRIEF NOTES ON OIL-RELATED EFFECTS	29
2.6	TOPICS ABOUT SIMULATION OF CWI IN CARBONATE RESERVOIRS ..	32
2.6.1	Pressure-velocity coupling	33
2.6.2	Numerical methods	34
2.7	STATE OF THE ART – SUMMARY	35
3	ALGORITHM STRUCTURE AND CONSIDERATIONS	36
3.1	GENERAL STRUCTURE OF THE ALGORITHM	36
3.2	CHEMICAL SYSTEM	38
3.3	SOLUBILITY CODE	39
3.3.1	Modification of γ_{CO_2}	41
3.4	SPECIATION MODEL: MULTICOMPONENT CHEMICAL EQUILIBRIUM ..	43
3.5	ACTIVITY OF CHEMICAL SPECIES	47
3.5.1	Activity of water	48
3.5.2	Activity of ions	48
3.6	DENSITY AND VISCOSITY OF THE BRINE	49
3.7	SEMI-EMPIRICAL DESCRIPTION OF DISSOLUTION AND PRECIPITATION RATE	52
3.8	POROUS MEDIUM PROPERTIES	54
3.9	CARBONATE RESERVOIR SAMPLE USED IN THIS WORK	56
4	RESULTS AND DISCUSSION	57
4.1	PARAMETER ESTIMATION FOR γ_{CO_2}	57
4.2	EXAMPLE OF CARBONATED WATER INJECTION INTO A CALCITE SALINE AQUIFER	62
4.3	ACTIVITY CONCENTRATION SCALE AND COMPARISON BETWEEN MODELS	70

5	CONCLUSIONS	72
	REFERENCES	74
	APPENDIX 1 – FIT OF DATA FROM HELGESON (1981) FOR EXTENDED DEBYE-HÜCKEL PARAMETERS	82
	APPENDIX 2 – BRIEF NOTES REGARDING THE EXPERIMENTS CWI IN CARBONATE MINERALS	84
	ANNEX 1 – CALCULATION OF CO₂-BRINE EQUILIBRIUM.....	86
	ANNEX LIST – VIRTUAL DOCUMENTS.....	91

1 INTRODUCTION

Carbonated water injection (CWI) is a technique primarily applied for CO₂ geological sequestration (CGS) or for enhanced oil recovery (EOR) processes. In carbonated water, CO₂ exists as a dissolved phase thus the contrast between carbonated water and reservoir fluid mobility is less than it would be compared to its alternative techniques (e.g. pure CO₂-floods and water alternating gas). Conventional CO₂-EOR, where CO₂ exists predominantly as a free phase, experiences more technical problems such as gravity segregation, leakages, poor sweep efficiency, fingering flow and gas channeling. As a result, CWI leads to safer storage of a substantial amount of CO₂ and a more efficient oil recovery than conventional CO₂-EOR (TAVAKOLIAN et al., 2012).

Carbon dioxide geological storage (CGS) in saline aquifers and depleted reservoirs represents an important process for reducing emissions of this greenhouse gas and one of its techniques is the carbonated water injection (CWI). The technology of CWI in carbonate reservoirs is particularly attractive for the pre-salt region reservoirs in Brazil, where the CO₂ content ranges from 1 to 20% (BOYD et al., 2015; DOS SANTOS et al., 2017). Hence, re-injecting the gas into the fields overcomes the hurdle of providing a CO₂ supply at an affordable price for CWI.

This research will focus on CWI in carbonate reservoirs since this is the type of geological formation in more than half of petroleum reserves in the world (BURCHETTE, 2012) and this is the main type of mineral in several fields in the pre-salt layer in Brazil (BOYD et al., 2015; DOS SANTOS et al., 2017). Moreover, CGS is particularly important for Brazil, since it submitted an Intended Nationally Determined Contribution (INDC) in United Nations Framework Convention on Climate Change (BRAZIL, 2015) to reduce its greenhouse gas emissions by 37% below 2005 levels in 2025 (REUTERS, 2015), proving its commitment with climate change control.

Despite its inherent advantages compared to other CO₂-EOR or CGS techniques, CWI still needs some countermeasures to assure that the whole process operates smoothly and the results match with the goals of the stakeholders. Dissolution and precipitation caused by the carbonated water could be either helpful or alarming. Chemical interactions between the carbonated water and the reservoir rock may

promote the development of high or low-permeability regions in the reservoir depending on the system conditions. These regions are troublesome because they can significantly decrease the overall sweep efficiency or even cause mechanical damage to the injection equipment. Thus, the existence of a model that could predict the conditions where the aforementioned problems do not arise could be particularly useful to support the engineering department with data so as to avoid major errors in planning. In summary, technical reasons for modeling CWI and CO₂-enhanced oil recovery (CO₂-EOR) in general are (GRAVA, 2014):

- Flow assurance, predict alterations in reservoir porosity and permeability;
- Provide information on the thermodynamic behavior of reservoir fluids;
- Tracking the injected CO₂ (environmental safety and stability of the operation);
- Secure the integrity of materials and equipment;
- Optimize characteristics of the injected fluid (e.g. flow rate, composition);
- Reservoir monitoring and control.

Chemical interactions between injected carbonated water and the reservoir rocks are a major aspect of CO₂-EOR and CGS. Carbonated water is an acidic solution able to react with the rocks, particularly when these contain carbonate minerals (e.g. calcite, dolomite, aragonite, dawsonite, magnesite). Modeling and simulation of CWI are crucial because the companies responsible for the process must assure that the operation will not have a detrimental effect on the reservoir quality and stability due to dissolution and precipitation of the carbonate minerals, leading to changes in porosity and permeability. Consequently, several concerns arise from CGS and CO₂-EOR techniques, such as the development of “wormholes” (high permeability channels) causing preferential flow, local wellbore instability, the motion of landmass and precipitation in high pH conditions, increasing the costs in the injection process (IGLAUER, 2011).

1.1 MOTIVATION AND GOALS

The development of a model capable of representing the region of interest in the reservoir is a complex task so the research project at UFPR planned comprehensible steps for its implementation. This work pertains to the early stage of

this project and will focus on the relevant chemical system, modifications on rock structure and, above all, how to compile this information in a working and resourceful mathematical model that could be extended to tackle other phenomena. Thus, this work is part of an ambitious research to create and implement a model capable of handling all the nuances in CWI in small samples (e.g. capillary flow, oil swelling and rock compressibility), so large-scale simulators can improve their predictions.

The scientific community has not studied carbonated water injection (CWI) extensively (SOHRABI et al., 2009). Other techniques such as WAG (water alternating gas) and LSW (low salinity water) have more complete models and simulators. Moreover, the models available in the literature do not facilitate customization by adding or removing species or changing the reactions in the system so the user cannot adapt the model to their own problem. Besides, these models do not handle many important physical processes present in CWI in carbonate rocks in particular.

The goal of this work is to develop a versatile algorithm capable of modeling carbonated water (CO₂-enriched) injection in a carbonate reservoir. For example, the model should calculate the solubility of CO₂ in brine, along with the activities of the chemical species at equilibrium condition. Furthermore, it must address physical changes in the rock caused by kinetic reactions of dissolution and precipitation since they directly impact the flow. Besides, the algorithm should provide the freedom to customize the model while building the foundations needed for structuring an even more complex model, e.g. by adding an oil phase or a gas phase.

The purpose of the algorithm proposed in this work is to complement computer fluid dynamics (CFD) software capabilities since they generally do not include solution chemistry in the base software. CFD programs are general purpose tools that primarily focus on many aspects relating to numerical methods to discretize flow equations and cannot anticipate all user needs. Nonetheless, these programs provide means for including self-programmed utilities, e.g. UDFs (user-defined functions) in ANSYS® Fluent, which significantly enhance their capabilities. The existence of this feature allows the development of a model in an external source and subsequent conversion to the UDF structure in the C language, which is ultimately used in ANSYS® Fluent. This work developed the algorithm in MATLAB®, while its conversion to the best UDF structure is part of a later stage in the research project at UFPR.

In addition, in CFD any saving in computational effort per time step affects the overall simulation time. The algorithm hereby proposed attempts to keep math complexity to a minimum and can be implemented with just the essential thermodynamic inputs. The algorithm was tested in MATLAB® to calculate the CO₂ solubility in brine, the chemical equilibrium condition, and mineral dissolution rates, along with their implications on the porosity, permeability and surface area of a porous medium in a cell of constant volume.

The underlying physical processes and pore-scale mechanisms in CWI have been studied isolated from one another in the literature. In contrast, the proposed algorithm attempts to capture the whole scenario of these techniques, which is accomplished by a compilation of carefully chosen models that provide key information to CFD simulations for CWI. Ideally, this algorithm should approach the problem armed with detailed computer codes that operate with a lower computational effort than the models found in the literature.

The research group at UFPR started its studies with the algorithm for CWI in saline aquifers developed in Machado (2015). The previous algorithm, however, made several strong hypotheses that either resulted in a loss of physical significance or caused instabilities during the simulation. In addition, the previous code accepted many input parameters that were either collected graphically or estimated so the user had to know the programming language and read the entire code to change the inputs and simulate other conditions. The present algorithm should bear with a minimum set of inputs and compute all secondary variables so as to simplify its usage. In addition, it should verify the conservation of mass, the charge balance and allow scale-up to consider greater regions of the reservoir.

The present code also tackles CWI in a carbonate aquifer, as it is a comprehensive step towards implementing dissolution and its effects in an oil reservoir at a later stage of the research. This is reasonable because the H⁺ ion, which is responsible for the dissolution, exists predominantly in the aqueous phase so the inclusion of the oil phase would affect this facet of the problem by changing the flow and incorporating CO₂ into its phase and not by significantly contributing to the dissolution. Naturally, there is also the issue that the oil, as an emulsion, incorporates some water from the aqueous phase.

1.1.1 Specific goals

The algorithm presented in this work prioritizes versatility, allowing the user to freely select the chemical system and dissolution reactions and thus control the model complexity. This flexibility is provided through all topics covered by the algorithm that allow extension without major alterations in their structure and inputs. The steps needed to include these features in the model are briefly summarized as:

1. Develop a versatile algorithm capable of handling CWI in different carbonate reservoirs and test it in MATLAB®
 - 1.1. Include the effect of pressure and temperature in the model by calculating the solubility of CO₂ in the brine and the density and viscosity of the brine;
 - 1.2. Correct liquid density in time and properly link dissolution and precipitation kinetics to solution chemistry;
 - 1.3. Associate the rate of kinetic reactions with current reservoir porosity and surface area, which provide information on the saturation index as well;
 - 1.4. Track the transport of mass between the rock and aqueous phase to verify the conservation of mass both during the simulation;
 - 1.5. Solve the chemical equilibrium using a numerical approach;
2. Develop a model for calculating the activity coefficient of CO₂ for chloride salts in general so it is easily extendable to more situations;
3. Provide general workflow strategies for approaches other than the pseudo-homogeneous for modeling the porous system;
4. Implement a reactive system for the dissolution/precipitation of calcite that allows the extension to other minerals;

2 CRITICAL ANALYSIS OF THE RELEVANT LITERATURE

There is a great interest in the development of more complete, customizable models that are able to be scaled up, afford better physics or provide estimates of important information at low computational effort. This has been a dynamic challenge as technologies related to experimental equipment, software for computer fluid dynamics (CFD) and software for image processing are improved continually.

Literature has developed a series of excellent but highly dedicated models for CGS and CO₂-EOR, i.e. models for a specific reservoir, where a huge number of chemical species and reaction rates are important and must be modeled (see TABLE 1). Few models attempted to describe CWI in particular and these models are rigid in the sense they are difficult to adapt to other situations, where less or different minerals, chemical species or phases are present.

There are several CWI coreflood experiments in the literature but the simulation studies are rare. Most of the simulation studies, some shown in TABLE 1, are not directly suitable for CFD simulations because they are elaborated in a different scope, work as a standalone application or make assumptions that hamper the application of specific numerical methods (e.g. LEAL et al., 2015). Thus, it is cumbersome and time-consuming to adapt these models.

One of the most recent validated simulation studies was developed by SANAEI et al. (2018), who used a 3D commercial reservoir simulator called UTCOMP coupled with the geochemical package IPhreeqc/PHREEQC to model the CWI process. SANAEI et al. (2018) further studied the main drive mechanism for oil recovery using CWI and concluded that the presence of CO₂ plays a major role in the recovery of the oil not displaced during the initial coreflooding. These authors do not provide details on the equations and theories used to model each aspect of CWI, referring only to the commercial software package. In contrast, this work will provide all equations and develop an open-source software.

TABLE 1 OVERVIEW OF MODELS IN SEVERAL CO₂ INJECTION TECHNIQUES

Authors	Technique	Model Dimension	Source of rock structure	Fluids	Number of phases	Model Type	Software	Comments
Moortgat et al. (2012)	CGS and CO ₂ -EOR: WAG	2D	Pseudo-homogeneous medium	CO ₂ , pure water, oil	3	FEM	Not reported	Rigorous phase instability analysis and three-phase-split computations. Use of PR and CPA EOS to capture polar interactions. Uses higher-order FE to tackle viscous and gravitational fingering. ΔP from Darcy's law.
Zaretskiy et al. (2012)	CO ₂ -EOR: LSW	3D	X-ray computer tomography	Low salinity water and oil	2	FEM-FVM	CSMP++ C++ PHREEQC	Uses Delaunay triangulation and Godunov operator splitting. Does not detail thermodynamics nor the oil. Constant ρ and ΔP from Stokes equation.
Fan et al. (2012)	CGS CO ₂ -EOR: CWI	3D	Pseudo-homogeneous medium	CO ₂ and brine	2	FVM	PFLOTTRAN	Uses PR and CPA for phase behavior, B-dot for activity coefficient of ions and Darcy's law for ΔP . Constant isotropic permeability. Large scale simulator in a real aquifer over a wide time scale. Simulations with several minerals.
Hao et al. (2013)	CO ₂ -EOR: CWI WAG	3D	Micro-CT MIP SEM	Brine and carbonated brine	1	FDM	NUFT	Validated with experimental data. Integrates kinetic and equilibrium reactions and Darcy's law for ΔP . Tracks the evolution of the surface area and permeability via empirical functions. Partial equilibrium assumption in an extended chemical system where equilibrium is defined minimizing the Gibbs free energy. Considers an expandable cell at constant pressure and does not track the evolution of porosity, permeability and surface area. Considers 5 minerals and 77 species.
Leal (2014)	CGS CWI WAG	Single cell	Assumption of properties of a rock from Qatari reservoir	CO ₂ and carbonated brine	2	FVM under development	Reaktoro C++	

The dimension of the model serves as a measure of its stage of development because it relates to the value of the resulting information in terms of engineering applications. Nonetheless, 2D or 3D models may only cover system thermodynamics and the flow, ignoring chemical reactions and its implications. Thus, further studying the core principles and phenomena taking place can add to what has already been developed in similar models, giving rise to a more valuable representation of the true physics of the process. In the following sections, each of the important aspects present in CWI on each model will be addressed in detail.

2.1 DISSOLUTION AND PRECIPITATION REACTION RATES

There are many challenges in modeling the kinetics of the dissolution and precipitation of carbonate minerals under reservoir conditions. This leads to large uncertainties in the calculations and gaps in current knowledge that call for more research, justifying some of the spreading of dissolution data found in the literature and emphasizing that there is no consensus in the literature.

For example, few experiments were performed in the temperature and pressure range of interest for carbon sequestration (POKROVSKY et al., 2009). Moreover, there is a considerable uncertainty of the estimation of the initial reactive surface area from the geometric surface area ignoring the roughness of surface (GUNTER et al., 2000), e.g. (CHOU et al., 1989; PLUMMER et al., 1978) and the evolution of said surface and porosity in time (LEAL, 2014).

Besides, models usually attempt to represent complex surface chemistry with different mechanisms depending on experiment conditions (T , P_{CO_2} , pH) using simple equations in the form of power law or empirical dissolution/precipitation rates as a function of some measure of the disequilibrium (INSKEEP and BLOOM, 1985). In addition, reaction rates are dependent on solution and mineral compositions, e.g. precipitation of siderite ($FeCO_3$) ultimately alter the rate of calcite dissolution (PERKINS et al., 1995).

Plummer et al. (1978) were pioneers who investigated calcite dissolution kinetics, analyzing the effect of each parameter in his model and using a formal approach. For the first time, rate equations were formulated in terms of the activities of reactants. Using both “pH-stat” and “free-drift” methods, Plummer et

al. (1978) studied how the system responded to changes in the range of pH (2 - 7), P_{CO_2} (0,0003 - 1 bar) and temperature (5 – 60 °C), identifying three independent simultaneous reactions. They proposed the macroscopic mechanistic reaction system for calcite ($CaCO_3$) shown in TABLE 2.

TABLE 2 MECHANISTIC CALCITE DISSOLUTION REACTIONS

Index	Reaction
1	$Calcite + H^+ \rightleftharpoons Ca^{2+} + HCO_3^-$
2	$Calcite + H_2CO_3^* \rightleftharpoons Ca^{2+} + 2 HCO_3^-$
3	$Calcite \rightleftharpoons Ca^{2+} + CO_3^{2-}$

SOURCE: (PLUMMER et al., 1978)

- a) At low pH (below 3.5) and all values of P_{CO_2} , reaction 1 is important and explains the dependence on the activity of H^+ ;
- b) At moderate pH (above 3.5 – 5.5) and high P_{CO_2} , reaction 2 accounts for the linear dependence on the total concentration of CO_2 . Note that $H_2CO_3^*$ acts as a pseudospecies representing the convention $H_2CO_3 + CO_{2(sc)}$. As H_2CO_3 is unstable, most of $H_2CO_3^*$ is $CO_{2(aq)}$;
- c) At high pH (above 5.5) and $P_{CO_2} \ll 0.1$ bar, the rate is nearly constant and independent of the composition aqueous phase, as in reaction 3.

2.2 BJERRUM PLOT

A Bjerrum plot is a graph of the concentrations of the different species of a polyprotic acid (e.g. carbonic acid) versus the pH of the solution at chemical equilibrium (HANRAHAN, 2012). It is a convenient tool to introduce concepts and is used to analyze how the total dissolved inorganic carbon (DIC) distributes into CO_2 , HCO_3^- and CO_3^{2-} at equilibrium condition in the CWI context.

The saturation index (SI) in eq. (1) is a comparison of the current activities of the ions from dissolution with the solubility product (K_{SP}) and serves to evaluate the state of the solution with respect to the equilibrium condition.

$$SI = \log\left(\frac{Q}{K_{SP}}\right) \quad (1)$$

Manipulation of the equilibrium constants given TABLE 3 leads to eq. (2) and (3). Assuming all carbon in the aqueous phase is distributed in CO_2 , HCO_3^-

and CO_3^{2-} , the total number of moles of dissolved inorganic carbon (N_{DIC}) is constant within the time step and is given by eq. (4) and eq. (5).

TABLE 3 CHEMICAL SYSTEM USED FOR ANALYZING THE BJERRUM PLOT OF H_2CO_3

Reaction	Reaction	Equilibrium constant
1	$H_2O \rightleftharpoons OH^- + H^+$	$K_1 = K_w = \left[\frac{a_{OH^-} \cdot a_{H^+}}{a_{H_2O}} \right]_{eq}$
2	$CO_2 + H_2O \rightleftharpoons HCO_3^- + H^+$	$K_2 = \left[\frac{a_{HCO_3^-} \cdot a_{H^+}}{a_{H_2O} \cdot a_{CO_2}} \right]_{eq}$
3	$HCO_3^- \rightleftharpoons CO_3^{2-} + H^+$	$K_3 = \left[\frac{a_{CO_3^{2-}} \cdot a_{H^+}}{a_{HCO_3^-}} \right]_{eq}$

$$a_{HCO_3^-} = m_{HCO_3^-} \cdot \gamma_{HCO_3^-} = \left(\frac{K_2 \cdot a_{H_2O}}{a_{H^+}} \right) a_{CO_2} \therefore m_{HCO_3^-} = \left(\frac{K_2 \cdot a_{H_2O}}{a_{H^+} \gamma_{HCO_3^-}} \right) a_{CO_2} \quad (2)$$

$$a_{CO_3^{2-}} = m_{CO_3^{2-}} \cdot \gamma_{CO_3^{2-}} = \left(\frac{K_2 K_3 a_{H_2O}}{(a_{H^+})^2} \right) a_{CO_2} \therefore m_{CO_3^{2-}} = \left(\frac{K_2 K_3 a_{H_2O}}{(a_{H^+})^2 \gamma_{CO_3^{2-}}} \right) a_{CO_2} \quad (3)$$

$$N_{DIC} = (m_{CO_2} + m_{HCO_3^-} + m_{CO_3^{2-}}) \cdot mass_{H_2O} \quad (4)$$

$$N_{DIC} = \left[\frac{1}{\gamma_{CO_2}} + \left(\frac{K_2 \cdot a_{H_2O}}{a_{H^+} \gamma_{HCO_3^-}} \right) + \left(\frac{K_2 K_3 a_{H_2O}}{(a_{H^+})^2 \gamma_{CO_3^{2-}}} \right) \right] \cdot a_{CO_2} \cdot mass_{H_2O} \quad (5)$$

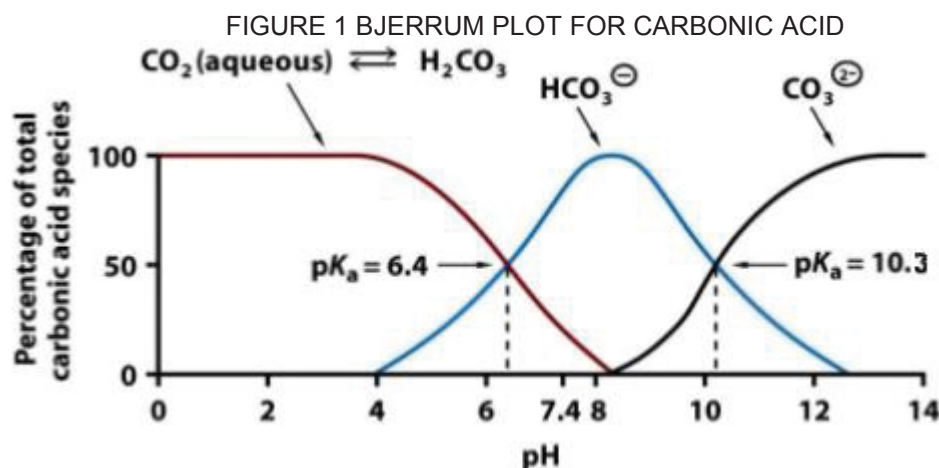
Alternatively, it is possible to write the same information in terms of concentration [mol/L], as in eq. (6) to (9), if the system is ideal ($\gamma_i \approx 1 \forall i$). These equations can be modified to obtain these concentrations as a function of pH and then create a Bjerrum plot for the carbonic acid, as shown in FIGURE 1.

$$DIC = [CO_2]_{eq} \left\{ \frac{([H^+]_{eq})^2 + K_2[H^+]_{eq} + K_2K_3}{([H^+]_{eq})^2} \right\} \quad (6)$$

$$[CO_2]_{eq} = \left\{ \frac{([H^+]_{eq})^2}{([H^+]_{eq})^2 + K_2[H^+]_{eq} + K_2K_3} \right\} DIC \quad (7)$$

$$[HCO_3^-]_{eq} = \left\{ \frac{K_2[H^+]_{eq}}{([H^+]_{eq})^2 + K_2[H^+]_{eq} + K_2K_3} \right\} DIC \quad (8)$$

$$[CO_3^{2-}]_{eq} = \left\{ \frac{K_2K_3}{([H^+]_{eq})^2 + K_2[H^+]_{eq} + K_2K_3} \right\} DIC \quad (9)$$



This plot shows that at a low pH the dissolved carbon is mostly CO_2 and as pH increases the molality of CO_2 decreases while HCO_3^- becomes more important. Further on, at $\text{pH} \cong 10.3$, CO_3^{2-} becomes the predominant species.

2.3 DIFFUSION COEFFICIENT

Diffusion is the process by which a substance is transported due to random molecular motions (CRANK, 1975) and its driving force is a gradient in chemical potential. The diffusion of CO_2 in brine and in oil is important for calculating the oil swelling effect and changes in the brine chemistry. According to Zarghami et al. (2017), there is a significant decrease in the rate of CO_2 diffusion in brine as salinity increases. Moreover, at the same salinity, the diffusion coefficient decreases significantly as the system reaches equilibrium.

Moortgat et al. (2012) used Fickian diffusion across the phases in their model (oil, water, gas). They created a matrix of composition-dependent, multicomponent diffusion coefficients and calculated their values for non-aqueous phases according to the work by Leahy-dios and Firoozabadi (2007), and the aqueous phase coefficient by Mutoru et al., (2011). In contrast, Hao et al. (2013) evaluated the Peclet number and considered that advective and reactive transport are dominant over diffusive transport and assigned a constant value for the diffusion coefficient, ignoring the effect of the pore radius.

Most models found in the literature assume the diffusion coefficient is constant. Examples are the models of Hao et al. (2013) and Machado (2015). Another approach is to consider the diffusivity to be a function of porosity and tortuosity, requiring further image processing to collect such values.

A common definition of tortuosity is the path distance divided by the straight line distance but this is far too simple to be applied in a 3D object where pores form branches and may or not reach the boundaries of the object. A free MATLAB® application that can be used to calculate the tortuosity of a complex 3D porous medium such as rocks or bones from binary data is called TauFactor, but it requires that the medium is permeable, i.e. there must be at least one pore that connects one side of the object to the other (COOPER et al., 2016).

Gommes et al. (2009) proposed methodologies for measuring the tortuosity of porous materials from binary tomographic reconstructions. One of them uses a fully penetrable sphere (FPS) model to represent the solid phase of the porous material, where the tortuosity and porosity are used to relate the diffusion coefficient of hindered and unhindered flow.

The dissolution and precipitation reactions alter the pore structure so tortuosity values would need to be recalculated each time step along with porosity. Moreover, measuring tortuosity for 3D objects generated from micro-CT data is non-trivial and the diffusion coefficients in each coordinate would be different according to each value of tortuosity, possibly carrying significant errors. Additionally, it is just in recent years that the unhindered diffusion coefficient for CO₂ in water and brine were studied in greater detail at elevated pressures, i.e. pressures higher than 1 MPa (CADOGAN et al., 2014).

2.4 POROUS MEDIUM REPRESENTATION

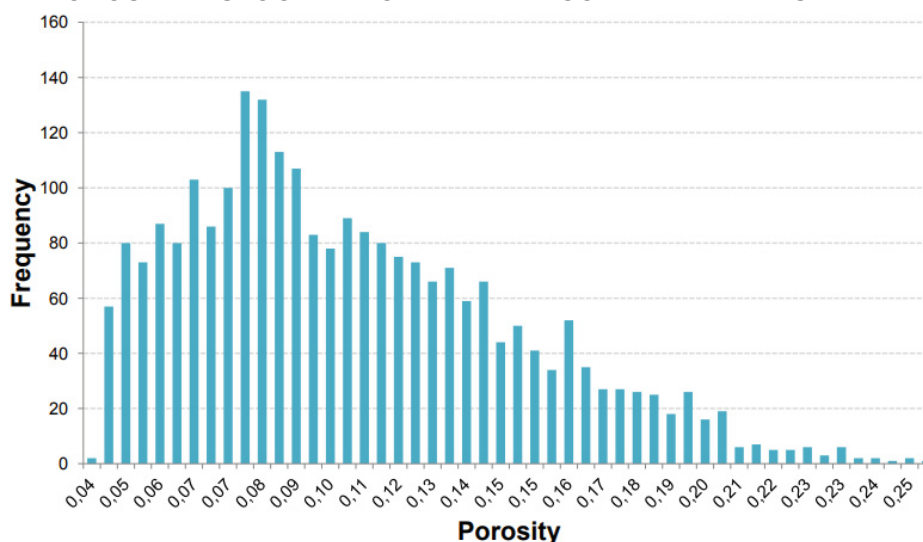
There are three main ways to represent the porous medium in the context of computational simulations (BLUNT et al., 2013):

- Direct approach: discretizes the voids using Cartesian grid derived from a binarized 3D image, honoring the geometry of pore space. This type of model is computationally expensive and better suited for computing single-phase flow properties and transport, despite being extendable for multi-phase flow. This approach has difficulties to capture capillary controlled displacement. Examples are particle-based methods (e.g. lattice Boltzmann), smooth particle hydrodynamics, density functional modeling and graphical processing units.

- Pseudo-homogeneous medium: regard the medium as a continuum, inheriting properties as porosity, permeability and tortuosity, where the medium has constant spatial properties inside each cell. The limitations are similar to the direct approach.
- Network modeling: extracts networks from a representation of the pore space. Idealize pores as larger voids in the rock called pore bodies that interconnect by narrower pathways called throats. Both pore bodies and throats receive different inputs, e.g. size or volume, cross-sectional shape, etc. This approach can also accommodate irregular lattices, wetting layer flow, arbitrary wettability multiphase flow, phase exchange, non-Newtonian displacement, non-Darcy flow and reactive transport.

The pseudo-homogenous approach has difficulties to represent capillary flow because during the conversion from the micro-CT scans to cell properties (e.g. porosity), information regarding the structure of the pores and pore size distribution is lost. One point that supports the use of this approach, however, is that it is extendable to the field scale by enlarging the size of the cell. There is equipment to determine the porosity in the field, and histograms such as the one shown in FIGURE 2 can supply information to the algorithm.

FIGURE 2 POROSITY HISTOGRAM FOR THE FRANCO FIELD AT PRE SALT IN BRAZIL



SOURCE: (PETERSOHN; ABELHA, 2013).

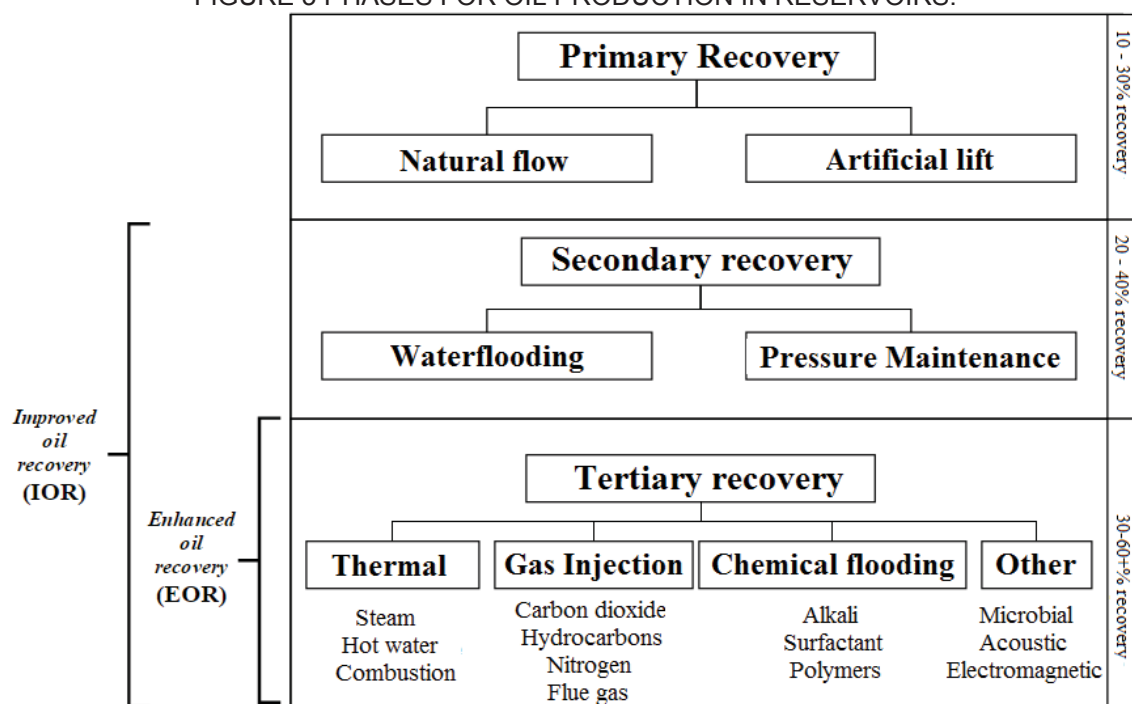
The dissolution reactions can be applied in any virtual representation of the rock. For instance, Raoof et al. (2013) simulated a reaction system in a pore

network model, changing the radius of pore throats (affects permeability) and the size of pore bodies (affects storage capacity).

2.5 BRIEF NOTES ON OIL-RELATED EFFECTS

Crude oil development involves different phases (see FIGURE 3). Even after primary and secondary recoveries, much of the oil and remain inside the pores in the rocks. Thus, when conventional techniques fail or lose efficiency, enhanced oil recovery (EOR) techniques assume the tasks.

FIGURE 3 PHASES FOR OIL PRODUCTION IN RESERVOIRS.



ADAPTED FROM: (AL-MUTAIRI; KOKAL, 2011)

In the past years, EOR technologies are receiving an increasingly important role to cope with the simultaneous rise in demand and high prices of oil. Thus, EOR techniques need continuous upgrades in terms of better models and simulators to attain superior control of the field, improve predictions for future reservoir behavior and provide some aid during the allocation of the wells, taking production to the next level.

Enhanced recovery techniques aim to increase the mobility of the oil in the reservoir by altering its properties, thereby facilitating the displacement of formation fluids (e.g. oil, gas) from the pore space toward the production wellbore,

increasing oil recovery rate. During contact time between the aqueous and oil phase, the higher solubility of CO_2 in oil provokes mass diffusion of CO_2 to the oil phase and causes the oil to swell, reduce its viscosity and its interfacial tension with water (FOROOZESH et al., 2016). Adequate phase equilibria calculations can provide the partition coefficient of CO_2 and the molar volume of oil and water.

On the aqueous phase, the presence of CO_2 induces a drop in pH that ultimately causes the dissolution of calcite, changing its pore structure. Moreover, as the carbonated water reaches previously closed pores, it incorporates more oil into the stream and further increases oil recovery. CWI alters the wettability of the rock as well, which increases capillary flow (SOHRABI et al., 2009).

The ratio of the density of the liquid after incorporating the dissolved gas with respect to the original density is what literature calls the swelling factor. Azin et al. (2013) studied the diffusion of CO_2 in water at mild temperatures and pressures between 5.8 and 6.9 MPa and discovered that the swelling factor for this system is about 2%, so it can be neglected in the absence of oil. Despite this, it is evident that the content of CO_2 itself in the aqueous phase is an important piece of data. In three-phase flow, one approach to calculate the CO_2 content is to assume isofugacity for all species present in all phases (MOORTGAT et al., 2012). In contrast, Foroozesh et al. (2016) included swelling effects using measured solubility data.

A commendable effort to include proper thermodynamics in the model was carried out by Moortgat et al. (2012). They combined flow equations with rigorous phase instability analysis and three-phase split computations. These authors modeled the flow of up to three hydrocarbon phases by PR-EoS with the transfer of all species between all phases. They also modeled the flow of one or two hydrocarbon phases coexisting with one aqueous phase using CPA-EoS. Moortgat et al. (2012) emphasized the importance of the bilinear discontinuous Galerkin (DG) since it allowed sharp discontinuities in phase properties without disrupting the numerical simulation. However, Moortgat et al. (2012) did not include kinetic reactions in their model and it does not account for any changes in rock structure. The effects of capillarity were not included either so their model excels at phase equilibria but fails to capture fluid-rock interactions.

A comprehensive approach to compute capillary pressure in a pore network model (PNM) was implemented by Raoof et al. (2013). They considered

that the progress of the displacement is controlled by capillary forces at low flow rates, forming the basis for their invasion–percolation algorithm. They considered that at every stage of the process, the non-wetting phase invades all accessible pore bodies and throats with the lowest entry capillary pressure. This entry capillary pressure is computed from the Laplace equation, calculating the mean radius of curvature from the Young–Laplace's equation. Both Zaretskiy et al. (2012) and Raoof et al. (2013) chose the criterion that the invading fluid enters and fills an available pore throat only if the injection pressure is equal to or larger than the entry capillary pressure of the pore. Alternatively, Foroozesh et al. (2016) computed capillary pressure from the Brooks-Corey correlation.

In addition, Zaretskiy et al. (2012) adopted an algorithm similar to the one presented by Silin and Patzek (2006) and assumed that the capillary pressure at a given point in the pore space is equivalent to the pressure exerted on a spherical bubble inscribed inside the pore space and covering that point. These authors justified that this is merely an approximation since the interface between two fluids does not necessarily assume a spherical shape and, even then, this is only valid when capillary forces dominate viscous forces.

Wang et al. (2013) used the capillary number and the viscosity ratio to describe the displacement of a wetting fluid by a non-wetting fluid in a 2D network. They found that these numbers can help to identify different mechanisms for the flow. Examples characterized are capillary fingering, viscous fingering, stable displacement and a transition regime. They showed that viscous fingering happens closer to the injection well whereas capillary fingering is more important in regions of lower velocities, e.g. far from the injection well. This type of flow results in poor efficiency due to preferential flow, causing low area coverage.

Including the capillary effect in a model that uses a pseudo-homogeneous representation of the porous medium is difficult since it intrinsically disregards pore-scale information, which is required to model capillarity and wettability when an oil phase is added to the system. Consequently, before tackling these phenomena, one must perform further process the original micro-CT images to retrieve properties such as surface area and pore size distribution.

2.6 TOPICS ABOUT SIMULATION OF CWI IN CARBONATE RESERVOIRS

The Navier-Stokes equations are widely used to describe the free flow in conduits. Meanwhile, Darcy's law is often chosen to model flows that are confined to a matrix (CHEN et al., 2010). The Darcy-Brinkman formulation (DBF) has the advantage of representing in a single equation the flow in the porous medium and the free flow (Stokes regime) without additional equations to specify boundary and interface conditions (IZGEC, 2009; MACHADO, 2015).

The DBF formulation performs better than Darcy's law in larger pores because Darcy's law does not take into account the viscous resistance and convective acceleration terms, what imposes limitations on the range of Reynolds number (Re) it can be applied, i.e. it is valid only for flows with low Re. As flow velocity increases, Darcy's linear relationship between pressure gradient and velocity breaks down. So in order to correct this issue, Brinkman (1949) proposed an extension of Darcy's model for systems with higher porosity and velocity, taking into account the presence of a solid boundary by adding a viscous term to the original Darcy's law (GUTA and SUNDAR, 2010). This term is analogous to the Laplacian found in the Navier-Stokes equation (MACHADO, 2015).

The dissolution of a porous medium, especially one that may already contain large empty spaces such as carbonate rocks (see FIGURE 4, where high porosity regions may exist), can create conditions for highly conductive channels called wormholes (see FIGURE 5) where the original Darcy's law may yield poor results. These dissolution patterns depend ultimately on the pH of the incoming solution and the injection rate (GOLFIER et al., 2002).

Fan et al. (2012), Hao et al. (2013) and Moortgat et al. (2012) used Darcy's law to calculate pressure drop. In a carbonate reservoir simulation, a better decision should use Darcy-Brinkman equation instead of Darcy (MACHADO, 2015). Moreover, the diffusive viscous term in the Darcy-Brinkman equation is able to describe the boundary layer type of flow that develops close to the interface in the porous zone. (GOLFIER et al., 2002). Applications of the Darcy-Brinkman equation in this context is found in the work of Golfier et al. (2002, 2004, 2006) for injection of HCl solutions and Machado (2015) for CWI.

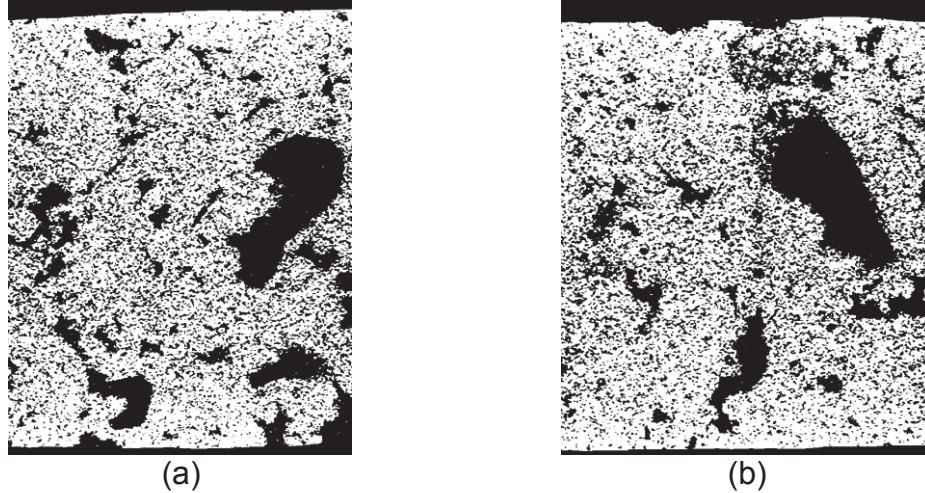
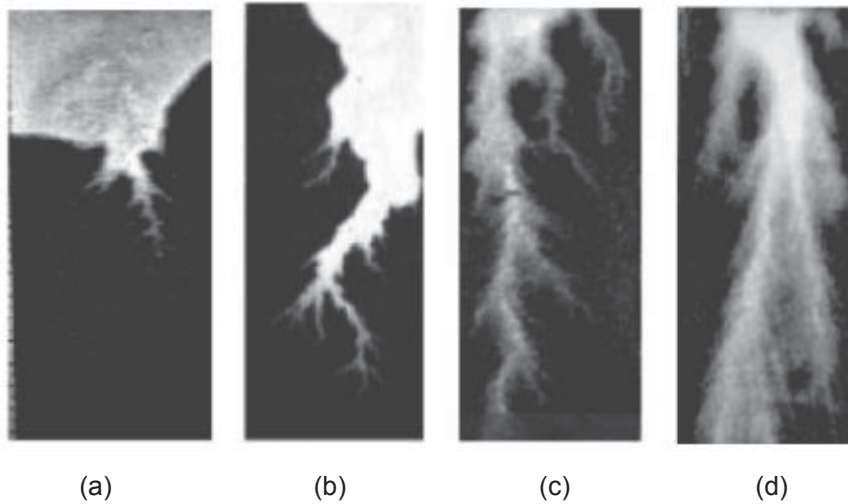
FIGURE 4 CROSS-SECTIONS OF A CALCITE ROCK IN THE PLANE (a) $x = 405$ (b) $y = 440$ 

FIGURE 5 EXAMPLES OF PATTERNS OF DISSOLUTION (a) FACE DISSOLUTION, (b) CONICAL WORMHOLE, (c) DOMINANT WORMHOLE, (d) RAMIFIED WORMHOLE



A possibly better approach would be to establish a threshold for the porosity value and apply Darcy or Darcy-Brinkman according to this criterion. This could reduce the simulation running time since Darcy's law require less mathematical operations. There is no article in the CWI literature that apply both equations so the impact on the numerical simulation is yet to be evaluated.

2.6.1 Pressure-velocity coupling

The velocity-pressure coupling scheme is necessary for the discretized version of Navier-Stokes equations because these variables depend on each other. A tactic to provide this coupling is to use schemes such as SIMPLE, SIMPLER, SIMPLEC, PISO in segregated solvers, but it is possible to solve this

system for Navier-Stokes equations in a coupled way, tackling the inter-equation coupling in a single matrix. For example, the Help from ANSYS Fluent® 17.0 (ANSYS, [s.d.]) states that PISO moves the repeated calculations required by SIMPLE and SIMPLEC to the solution stage of the equation responsible for pressure correction. In PISO, there is a loop called “neighbor correction” to improve the solution the corrected velocities provide for the continuity and momentum equation. The PISO algorithm demands more computational effort per solver iteration but it can reduce the number of iterations required for convergence, particularly for transient problems.

2.6.2 Numerical methods

The numerical method used in the simulation has implications in the solution, e.g. FVM is expected to offer better results than FDM due to its inherent conservative characteristics. FVM starts with conservation laws and discretizes the equations in their integrated form whereas FDM discretizes the equations in their differential form (e.g. using Taylor expansion). This makes the FVM more robust, i.e. not so easily affected by instabilities in the numerical simulation. Hao et al. (2013) could improve their work if they used FVM or FEM instead of FDM because of the advantages regarding stability, convergence, and accuracy. FEM is very robust because it works with finite volumes or finite elements and weighs the equations before they are integrated, working with the variational form of the equations. Using mixed FEM-FVM like Zaretskiy et al. (2012) provides flexibility, e.g. they used the Godunov operator splitting so they could calculate the diffusion terms with FEM and advection terms with FVM.

While numerical approaches are able to cope with more details in the model, analytical solutions are also useful to benchmark numerical methods and provide key insights to understand complicated fluid-fluid and fluid-rock interactions in the flow (ZARETSKIY et al., 2012). Furthermore, they can also be used as grid-free methods to shorten computation time. A major downside associated with analytical methods is the serious limitation to represent all the nuances of the multi-component multi-phase flow. None of the articles for CWI

modeling provided a benchmark of their numerical solutions using an analytical solution and just Hao et al. (2013) validated the model with a real sample.

2.7 STATE OF THE ART – SUMMARY

The best aspects of the current CWI models are good models considering rigorous multiphase thermodynamics, such as in MOORTGAT et al. (2012) and SANAEI et al. (2018) and schemes for discretization of flow and pressure drop equations in space and time such as in ZARETSKIY et al. (2012).

The most insufficient aspect of CWI models in carbonate rocks concerns the rate of dissolution and precipitation of carbonate minerals. The mathematical models were often developed based on experiments performed under conditions that differ substantially from the reservoir, leading to potential errors. Besides, there is not a clear consensus on the variables that must be included in the equation describing the rate of reaction of dissolution/precipitation because the set of important variable may differ depending on the rock and brine composition.

Moreover, the link between chemical reactions and changes in the rock matrix has received considerably less attention, i.e. how changes in pore radius, porosity, and surface area (or other properties depending on the virtual representation of the rock) affect solution chemistry and the rate of dissolution and precipitation.

Finally, while there are many coreflood experiments in the literature, mathematical and simulation studies are very uncommon. Moreover, several of them use very specific commercial software. The present model was developed in MATLAB® to be implemented in ANSYS® Fluent, which are widely used in diverse areas, what is already an advantage in itself. Despite this, as an open-source model developed with public financial support, the model proposed in this work can be easily converted to the C language, Scilab or GNU Octave to be used with OpenFoam® on a later stage, possibly saving several thousands of dollars in licenses.

3 ALGORITHM STRUCTURE AND CONSIDERATIONS

Reactive flow simulation in reservoirs is a diversified problem given the variety of mathematical models, discretizing schemes and velocity-pressure coupling methods in the literature. Furthermore, different authors make their own simplifications in the phase behavior, porous medium, in solution chemistry and composition. A cartesian point of view may prove useful in the sense of dividing this intricate problem into smaller parts and treat each of them accordingly, placing the various pieces of the puzzle in place in a logical order. Then it will be possible to create increasingly complex algorithms until the nature, quantity, and quality of data produced are in accordance of the requirements of the project.

The algorithm proposed in this work is divided into six subroutines called “codes”, describing the (1) calculation of CO₂ solubility in a synthetic brine of chloride salts, (2) distribution of chemical species in the chemical equilibrium condition, (3) adaptive time step scheme, (4) kinetic rate of dissolution and its implications on the porous medium (5) the stabilization procedure for the numerical method and (6) density calculations of the carbonated brine. These subroutines are discussed in the following sections and are applied in a certain order, described the general structure of the algorithm. Finally, the algorithm is applied to CWI in a calcite reservoir and the results of the speciation code are compared with rigorous models such as electrolyte-NRTL and Pitzer.

3.1 GENERAL STRUCTURE OF THE ALGORITHM

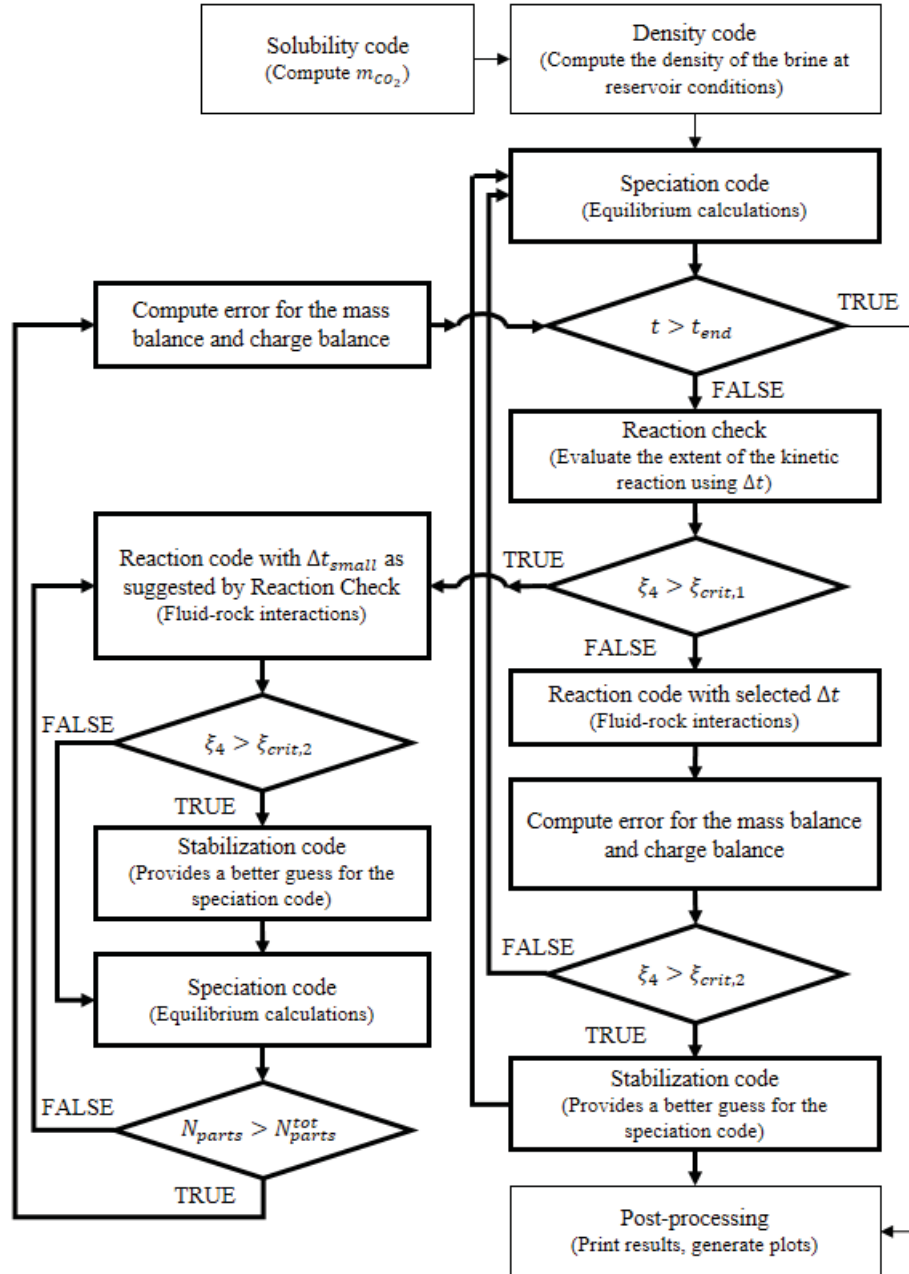
Assuming that the equilibrium reactions are infinitely faster than kinetic reactions, a procedure is proposed in which the calculations of kinetics and equilibrium are alternated each time step to ensure the kinetic reaction rates are computed in a condition that is not too far from chemical equilibrium. A general overview of the structure of the algorithm is shown in FIGURE 6.

The main algorithm uses the following specific subroutines:

- The solubility code calculates the molality values for all aqueous species;
- The density code calculates the initial density and mass of the solution;
- The speciation code is always called before computing kinetic reactions;
- The reaction rate is evaluated for a proper selection of the time step;

- Reservoir structure is a function of the extent of mineral dissolution, which impacts porosity directly and permeability and surface area indirectly;
- The stabilization procedure activates if dissolution exceeds ξ_{crit} ;
- The mass balance and charge balance are checked to verify consistency.

FIGURE 6 FLOW CHART FOR THE MAIN SECTION OF THE ALGORITHM.



3.2 CHEMICAL SYSTEM

Aspen Plus® (ASPEN TECHNOLOGY, 2000) or SUPCRT92 (JOHNSON et al., 1992) can be used to detect possible aqueous species and linearly independent reactions of dissociation and ionization. The procedure decreases the time required for brainstorming to create a consistent chemical system for the specific mineralogy of the reservoir. The steps of this procedure involve informing all neutral (e.g. CO₂, H₂O, salts) and mineral species and proceed to the selection of the reactions according with its impact on the rate of dissolution, which is a function of pH. Next, they must be classified as equilibrium or kinetic reactions according to their respective rates.

Models that simulate CGS over a wide range of pH often choose extended chemical systems, as shown in TABLE 4.

TABLE 4 EXAMPLES OF CHEMICAL SYSTEMS USED IN THE LITERATURE

Plummer et al. (1978)	Li et al. (2008)	Hao et al. (2013)	Machado (2015)	Leal (2014)	Reaction
✓	✓	✓	✓	✓	$\text{Calcite} + \text{H}^+ \rightleftharpoons \text{Ca}^{2+} + \text{HCO}_3^-$
✓	✓				$\text{Calcite} + \text{H}_2\text{CO}_3^* \rightleftharpoons \text{Ca}^{2+} + 2 \text{HCO}_3^-$
				✓	$\text{Calcite} + \text{H}_2\text{O}_{(l)} + \text{CO}_{2(aq)} \rightleftharpoons \text{Ca}^{2+} + 2 \text{HCO}_3^-$
✓	✓		✓		$\text{Calcite} \rightleftharpoons \text{Ca}^{2+} + \text{CO}_3^{2-}$
		✓	✓	✓	$\text{CO}_{2(aq)} + \text{H}_2\text{O} \rightleftharpoons \text{H}^+ + \text{HCO}_3^-$
				✓	$\text{CO}_3^{2-} + \text{H}^+ \rightleftharpoons \text{HCO}_3^-$
		✓		✓	$\text{CaCO}_{3(aq)} + \text{H}^+ \rightleftharpoons \text{Ca}^{2+} + \text{HCO}_3^-$
	✓	✓	✓		$\text{CaHCO}_3^+ \rightleftharpoons \text{Ca}^{2+} + \text{HCO}_3^-$
	✓	✓	✓		$\text{CaCl}^+ \rightleftharpoons \text{Cl}^- + \text{Ca}^{2+}$
	✓	✓	✓	✓	$\text{CaCl}_{2(aq)} \rightleftharpoons 2 \text{Cl}^- + \text{Ca}^{2+}$
		✓			$\text{NaCl}_{(aq)} \rightleftharpoons \text{Na}^+ + \text{Cl}^-$
				✓	$\text{NaCl}_{(s)} \rightleftharpoons \text{Na}^+ + \text{Cl}^-$
	✓		✓	✓	$\text{H}_2\text{O} \rightleftharpoons \text{H}^+ + \text{OH}^-$
	✓			✓	$\text{H}_2\text{CO}_{3(aq)} \rightleftharpoons \text{H}^+ + \text{HCO}_3^-$
	✓				$\text{H}_2\text{CO}_{3(aq)} \rightleftharpoons 2 \text{H}^+ + \text{CO}_3^{2-}$
	✓		✓		$\text{Ca}^{2+} + \text{OH}^- \rightleftharpoons \text{CaOH}^+$
	✓		✓		$\text{H}^+ + \text{Cl}^- \rightleftharpoons \text{HCl}_{(aq)}$
		✓	✓	✓	$\text{CO}_{2(g)} \rightleftharpoons \text{CO}_{2(aq)}$
		✓		✓	$\text{H}_2\text{O}_{(g)} \rightleftharpoons \text{H}_2\text{O}_{(l)}$

These extended chemical systems can be optimized if the operation involves a smaller pH range. Caution is recommended during this selection

process of the chemical reactions that will be considered in the model, as it must ascertain the inclusion of species that have a buffering effect on the solution, e.g. CaHCO_3^+ and MgHCO_3^+ at intermediate pH (>5) and CaOH^+ and MgOH^+ at high pH (>8). Moreover, some chemical species that are unstable at the beginning of the simulation may become more important due to an increase in activity at different pH conditions or in the presence of ions produced from mineral dissolution reactions. As a consequence, an oversimplified chemical system may provide inaccurate results (LEAL et al., 2015).

Other ways to build an optimal chemical system representation include heuristics, special schemes that classify the species as primary or secondary (SAALTINK et al., 1998) or sensitivity analysis to identify main reaction paths and their implications (MORBIDELLI and VARMA, 1987).

3.3 SOLUBILITY CODE

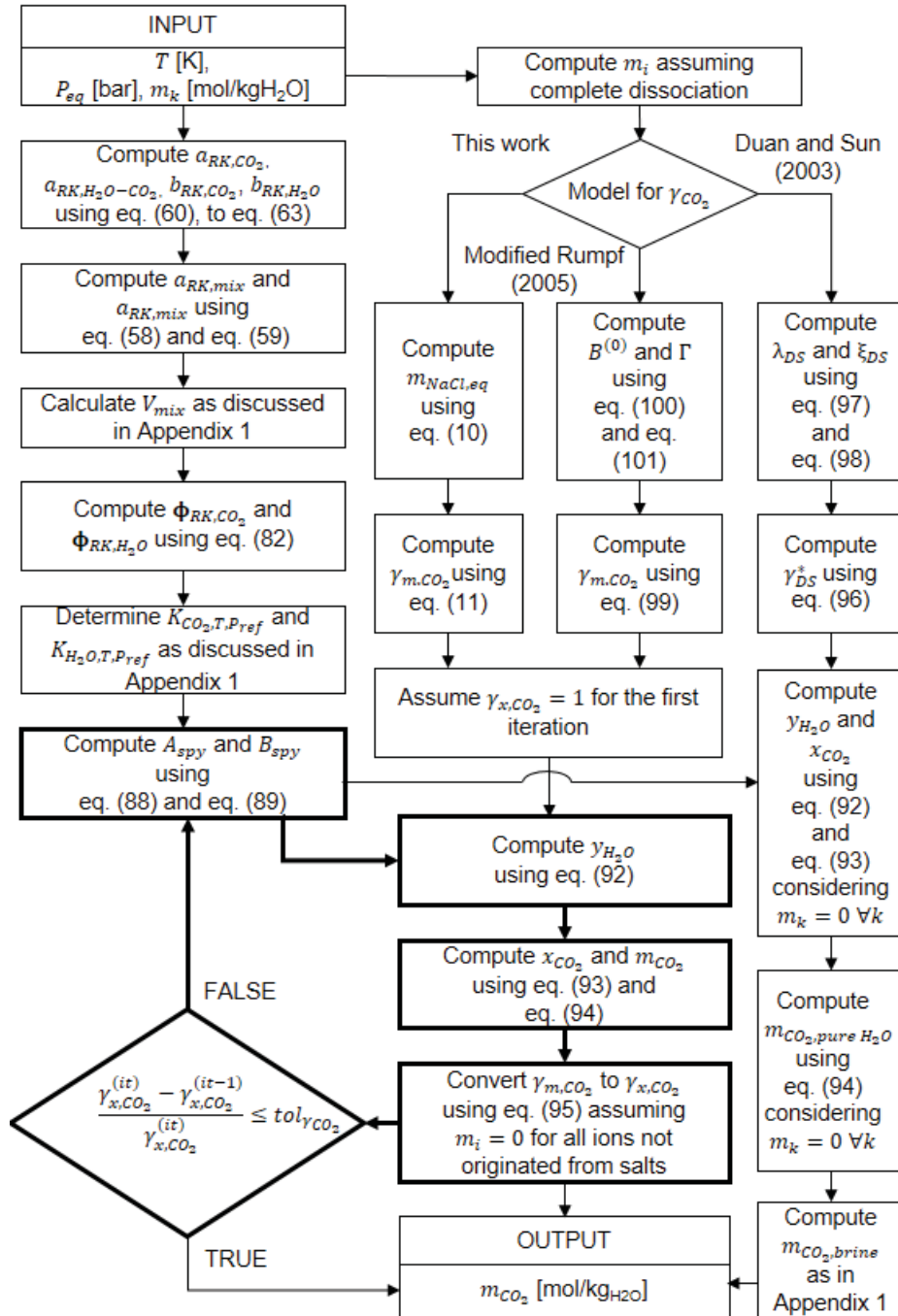
The dissolution rate is dependent on pH, which depends on the content of CO_2 in brine. Thus, the initial value of m_{CO_2} plays an important role in all calculations hereby considered, including changes in rock porosity. Essentially, the solubility model idealizes the situation where the brine reaches equilibrium with the CO_2 -rich phase at temperature T and equilibrium pressure P_{EQ} . Next, the contact with the CO_2 -rich phase is ceased and the solution is pressurized to injection pressure P_{sim} , which should be lower than the mechanical fracture pressure to avoid compromising the stability of the reservoir (HAO et al., 2013).

Apart from the content of CO_2 in brine, this part of the algorithm calculates the composition of the vapor phase in equilibrium with the CO_2 -saturated aqueous phase so it can be used to determine the composition of a bubble in phase equilibrium calculations in a later version of this algorithm.

This work used the model proposed by Spycher and Pruess (2005) (see Annex 1), which calculates the CO_2 solubility in a brine solution and tested their model in solutions of NaCl and CaCl_2 . Their implementation procedure is straightforward and includes solving a modified Redlich-Kwong EOS, selecting the root corresponding to the molar volume of the stable phase and the appropriate Henry constant. Their solubility model itself is non-iterative but it receives an external model for γ_{CO_2} , which should be computed in mole fraction

scale. If γ_{CO_2} is computed in a different concentration scale (e.g. molality scale), a loop is added to convert γ_{CO_2} to the mole fraction scale and solve the dependencies between m_{CO_2} and γ_{CO_2} . In this case, the procedure requires very few iterations to achieve the convergence tolerance $tol_{\gamma_{CO_2}}$. The calculation procedure for the solubility code is given in FIGURE 7.

FIGURE 7 FLOW CHART FOR THE SOLUBILITY CODE



This work offers three different models for the activity of aqueous CO₂ (γ_{CO_2}) in the solubility code: (1) Duan and Sun (2003), (2) the modification by Spycher and Pruess (2005) of the model originally proposed by Rumpf et al. (1994) and (3) the modification by this work of the Drummond (1981) model.

The solubility model proposed by Spycher and Pruess (2005) assumes (1) isofugacity for all species present in both phases, (2) their modified Redlich-Kwong EOS represents the CO₂-rich phase, (3) all ions are non-volatile, (4) infinite dilution of water in the CO₂-rich phase when applying classical mixing rules, (5) the water activity is close enough to unity, (6) all inorganic carbon is the CO₂ present in that phase and (7) complete dissociation of salts in water.

Spycher and Pruess (2005) modified the original version of Rumpf et al. (1994) so it would be able to calculate γ_{CO_2} for solutions of few chloride salts because the original version of could be applied just for solutions of NaCl. Both the models of Duan and Sun (2003) and the modified of Rumpf et al. (1994) are described in Annex 1, along with their implementation procedure.

Alternatively, the model of developed in Spycher and Pruess (2010) could be used as an upgrade to simulate the H₂O-CO₂-salt system in higher conditions of temperature. Other models for calculating P-V-T or P-V-x properties of H₂O-CO₂-salt systems are available in literature e.g. Duan et al. (1992) but it relies on a fifth-order virial expansion in volume with a plethora of parameters, which cannot be efficiently implemented in numerical flow simulations.

3.3.1 Modification of γ_{CO_2}

In the present work, the formulation of Spycher and Pruess (2005) was slightly changed in order to make it applicable even when both salts are present in the solution and developed a new modification of the model developed in Drummond (1981). Spycher and Pruess (2005) tested different formulations to calculate γ_{CO_2} in their model. They found that the model by Duan and Sun (2003) and Rumpf et al. (1994) yielded the best results, but they do not account for the presence of chloride salts other than NaCl, KCl, CaCl₂, and MgCl₂. Moreover, the calculation of the activity coefficient of CO₂ by Duan and Sun (2003) in the form

proposed by Spycher and Pruess (2005) is just a parameter that relates the m_{CO_2} in pure water with m_{CO_2} in brine and cannot be used in speciation calculations.

It is proposed a simpler solution to capture the behavior of γ_{CO_2} , which extends the formulation of Drummond (1981) from aqueous solutions of NaCl to solutions of chloride salts in general that have similar effects than NaCl on γ_{CO_2} . The modification relies on a parameter that expresses the amount of NaCl equivalents instead of using the ionic strength as a substitute of the molality of NaCl such as in Spycher and Pruess (2005), which yielded poor results.

Firstly, the molality of each ion originated from the salts m_i is calculated assuming complete dissociation in water and weighted by its effect on the solubility of CO_2 is considered by eq. (10) according to an adjustable parameter h_i which imbues the effect of ion charge, ionic radius and chemical interactions.

$$m_{NaCl, equivalent} = \frac{1}{2} \left(\sum_{i=1}^N m_i h_i \right) \quad (10)$$

Both the modification using the ionic strength and the modification using NaCl equivalents return to the original form of Drummond (1981) for NaCl using $h_{Na^+} = 1$ and $h_{Cl^-} = 1$ in eq. (10) and the original model is shown in eq. (11).

$$\ln(\gamma_{CO_2, m}) = \left(-1.0312 + 1.2806 \times 10^{-3} T + \frac{255.9}{T} \right) m_{NaCl, equivalent} - (0.4445 - 1.606 \times 10^{-3} T) \left(\frac{m_{NaCl, equivalent}}{m_{NaCl, equivalent} + 1} \right) \quad (11)$$

This work used a hybrid form of the stochastic algorithm Particle Swarm Optimization (PSO) and the deterministic algorithm interior-point, available in the MATLAB® Global Optimization Toolbox™ (THE MATHWORKS INC., 2016). This optimization algorithm was used to determine the best value of h_i for chloride solutions of $CaCl_2$ and $MgCl_2$.

Particle swarm optimization (PSO) is a stochastic method. Each particle is a solution candidate moving at a certain speed across a constrained region (search-region) specified by a lower and upper bound for each parameter. This

method works as a group of particles looking for the global solution, where the best solution candidate so far informs its location to the others.

This PSO optimization method is initialized with a group of particles randomly scattered in the search region and calculation of the objective function at the coordinates of each particle. At every iteration, each particle has its coordinates updated according to a function of its position and velocity along with a random effect and the function values are recalculated. The process is repeated until the solution converges, i.e. the particles swarm towards a single point.

3.4 SPECIATION MODEL: MULTICOMPONENT CHEMICAL EQUILIBRIUM

Chemical equilibrium is common in nature and is present in many geochemical applications. These calculations may follow a stoichiometric or non-stoichiometric approach, where the former uses a set of non-linear equations and the later solves a constrained minimization of Gibbs free energy (LEAL, 2014). There are alternative formulations such as the one proposed in Saaltink et al. (1998), who incorporated equilibrium and kinetic reactions simultaneously in a matrix representation of the transport equations exploring the concept of primary or secondary species. Another option are the Monte Carlo methods, as in López-Castillo and de Souza Filho (2007) and Turner et al. (2008).

In the context of CWI, the speciation code describes how this dissolved CO₂ changes the chemical equilibrium causing the acidification of the solution. Moreover, this part of the algorithm should provide information on how the ion species are distributed in that system condition, i.e. calculate the solution composition in terms of molality of ions in the water.

Equilibrium reactions are considered to be faster than kinetic reactions. Hence, the system must attain the chemical equilibrium within every time step and kinetic reactions may be treated as disturbances applied to a system previously in equilibrium. This is equivalent to the partial equilibrium assumption, where the system is in equilibrium with respect to some reactions and out of equilibrium for others. In geochemical simulations, mineral dissolution can be considered kinetic reactions when compared to aqueous and gaseous reactions because their rate of reaction is usually slower (LEAL et al., 2015).

When local equilibrium is invalid, kinetically reactions can be integrated into thermodynamically based speciation models, where kinetics intercalate with equilibrium calculations to accommodate the evolution of variables in time.

This work uses the stoichiometric approach, which explores the fact the equilibrium constant of a reaction can be obtained by a function of: (1) temperature and pressure, (2) the activity of the chemical species at equilibrium condition and (3) Gibbs free energy, with the reservation that the numerical value of K_{EQ} should be the same regardless of the way it is obtained.

The equilibrium condition can be calculated solving a series of non-linear algebraic equations where each term corresponds to one equilibrium reaction, following the structure is given in eq. (12). There is only one unknown extent of reaction for each equation, i.e. the degree of freedom is zero. Thus, the system is both consistent and exactly determined, i.e. it provides only one solution that satisfies the set of equations. This problem can be solved by the method of Newton-Raphson to find the zero of each element of F_{VAL} simultaneously.

$$F_{VAL}(j) = \prod_i^{N_i} \left[\left(m_i + \sum_{j=1}^{N_{EQ}} v_{i,j} \xi_j \right) \gamma_i \right]^{v_{i,j}} - K_{EQ,j}(T, P) \quad (12)$$

An advantage of writing the speciation problem in terms of the extent of the reactions instead of calculating the molality of the species directly is that it is theoretically impossible to violate the mass or charge balances. Note the charge balance condition is implicitly enforced by the mass balance since it is linearly dependent on it. Nonetheless, all calculations are subjected to the computer accuracy and small errors may still occur in both balances.

The Jacobian matrix is given by eq. (13), where the derivatives can be represented by a second-order central differencing scheme (CDS-2) using a step on the extent of the reaction ($\Delta\xi$) instead of the analytical derivatives. Another option for more complex chemical systems is the automatic differentiation, which is harder to implement but exploits the chain rule to compute analytical derivatives with working accuracy, avoiding truncation errors from discretizing schemes and many sources of numerical instabilities (GRIEWANK and WALTHER, 2003). An analytical approach to determine the Jacobian Matrix in the CWI context is

available in Leal et al. (2015), who used Lagrange multipliers and a matrix representation to compute each partial derivative.

$$\mathbf{J}^{it_{EQ}} = \begin{bmatrix} \frac{\delta \mathbf{F}_{VAL}(1)}{\delta \xi_1} & \dots & \frac{\delta \mathbf{F}_{VAL}(1)}{\delta \xi_{N_{EQ}}} \\ \vdots & \dots & \vdots \\ \frac{\delta \mathbf{F}_{VAL}(N_{EQ})}{\delta \xi_1} & \dots & \frac{\delta \mathbf{F}_{VAL}(N_{EQ})}{\delta \xi_{N_{EQ}}} \end{bmatrix}_{N_{EQ} \times N_{EQ}} \quad (13)$$

The solution of the Newton-Raphson method is given by eq. (14) to (15).

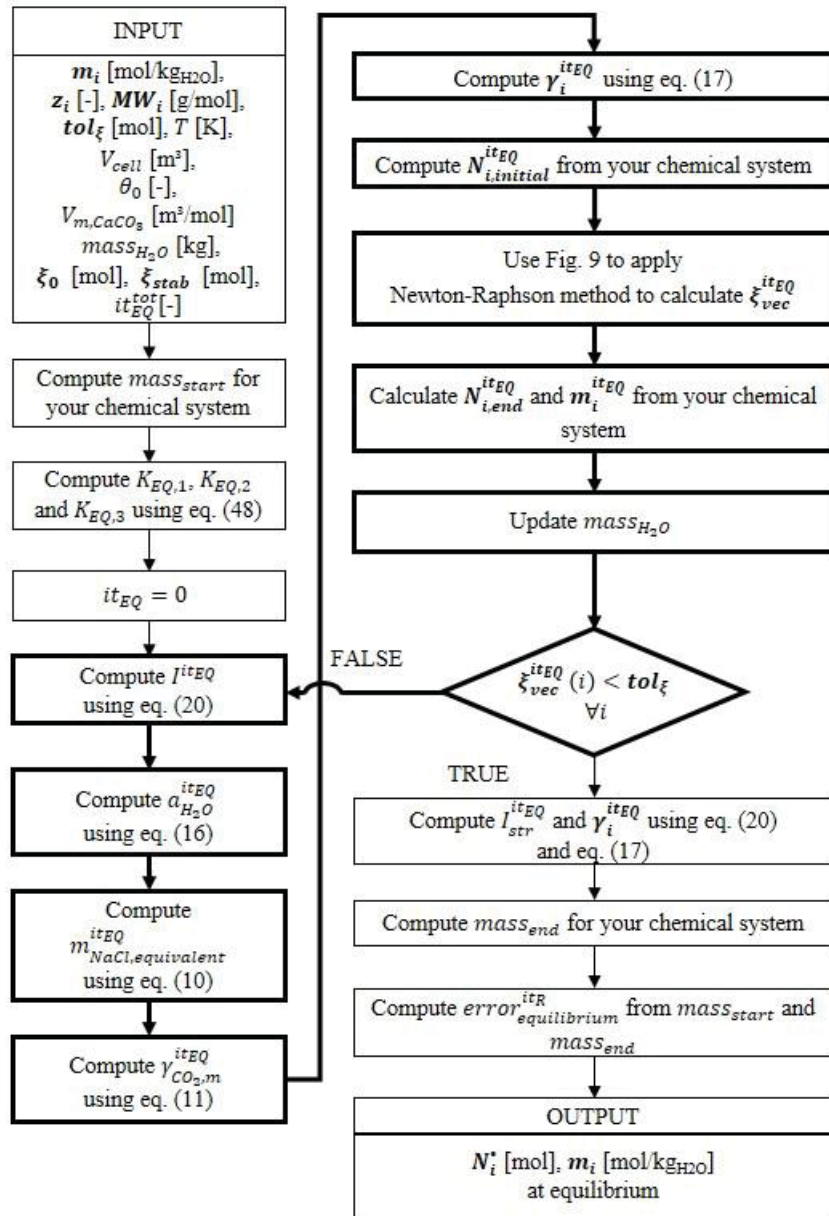
$$\mathbf{J}^{it_{EQ}} \mathbf{s}^{it_{EQ}} = -\mathbf{F}_{VAL}^{it_{EQ}} \quad (14)$$

$$\xi^{it_{EQ}+1} = \mathbf{s}^{it_{EQ}} + \xi^{it_{EQ}} \quad (15)$$

The algorithm responsible for the equilibrium calculations is presented in FIGURE 8, while the inner loop is detailed in FIGURE 9. Note that the mass of H₂O is updated because it participates in the reactions.

In order to increase convergence speed, the algorithm provides the solution of the last iteration as an estimation for the Newton-Raphson method after updating the values of the activity coefficients in the outer loop. The problem was structured so that the numerical method pursues the best solution while maintaining the activity coefficient vector constant in the inner loop.

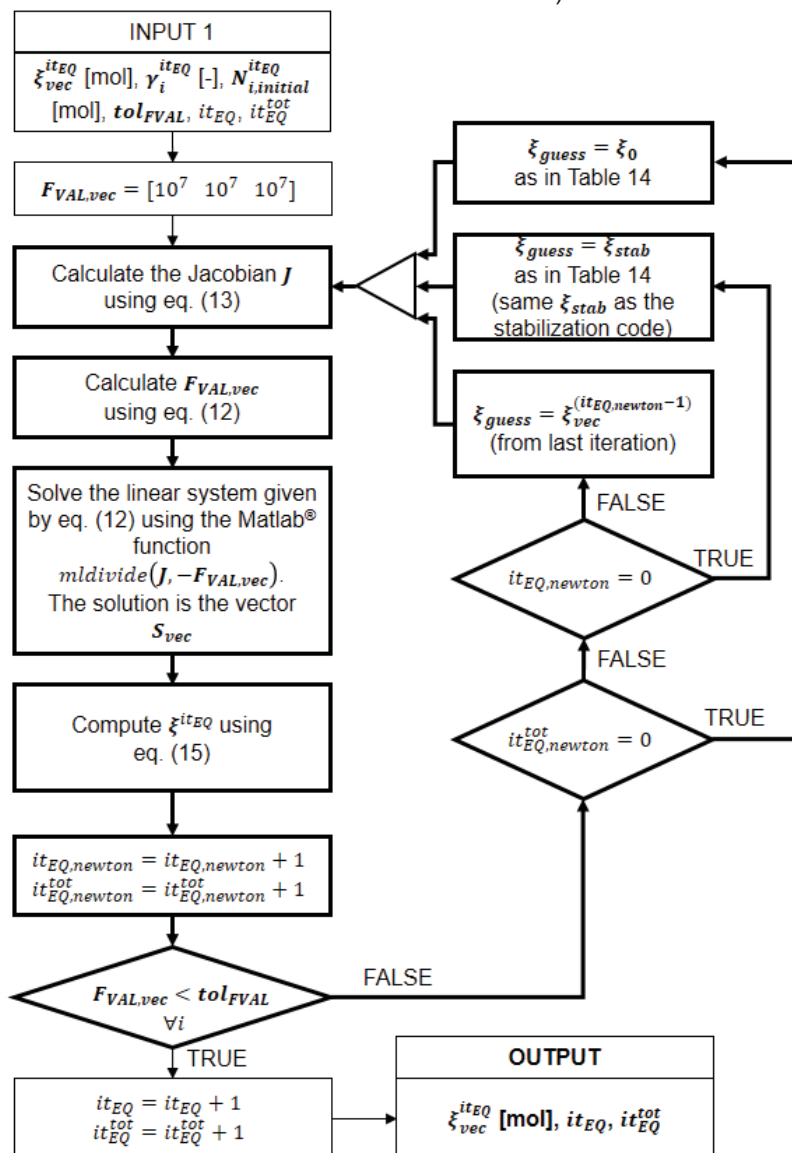
FIGURE 8 FLOW CHART FOR THE SPECIATION MODEL.



Chemical equilibrium state means the rate for the direct and reverse reactions are equal, hence the extent of reactions should be zero for any equilibrium reaction. This makes for the stopping criteria of the outer loop ($\xi_{vec}^{itEQ} \rightarrow 0 \forall j$), while the values for each element of F_{VAL} are used in the inner loop ($F_{VAL,j} \rightarrow 0 \forall j$), which are represented by the specified tolerance for the condition for the outer loop (tol_{ξ}) and inner loop (tol_{FVAL}) of the speciation code.

Alternatively, the speciation could be calculated by an optimization algorithm (e.g. Levenberg-Marquardt) but it is computationally more expensive than a method to find the zero of a function (e.g. Newton-Raphson) in general.

FIGURE 9 FLOW CHART FOR NEWTON-RAPHSON METHOD (INNER LOOP OF THE SPECIATION CODE).



3.5 ACTIVITY OF CHEMICAL SPECIES

The activity of a chemical species requires the definition of a standard state and can be expressed in many concentration scales (e.g. mole fraction, molality). The value of the activities (a_i) and activity coefficients (γ_i) vary according to each of these choices. It follows that thermodynamic methods that use one scale must not be mixed with another convention before a proper conversion between scales. This work deals exclusively with molality based activities. Notice that regardless of the choice of the concentration scale used to for a_i and γ_i , the numerical value for the equilibrium constant should be the same.

3.5.1 Activity of water

As the brine in CGS or CWI applications is complex and have a reasonable CO₂ content, this work chose to use the same empirical formula used by PHREEQC for calculating the activity of water (PARKHURST and APPELO, 2013) This equation is given by eq. (16), where n_i is the number of moles, N_{aq} is the total number of aqueous species and m_i is the molality of the species.

$$a_{H_2O} = 1 - 0.017 \sum_{i=1}^{N_{aq}} m_i \quad (16)$$

3.5.2 Activity of ions

The WATEQ Debye-Hückel equation can be used to calculate the activity coefficient of the ions and provides some versatility in terms of adding or removing species to the model without major alterations in any part of the algorithm. This model is an extension of Debye-Hückel valid in the interval of 0 and 100 °C which shows reliable results up to the ionic strength of seawater (~0.72 m), although it usually agrees well with the results using Pitzer for higher ionic strengths (BALL and NORDSTROM, 1991).

Despite the visual similarity, the WATEQ and B-dot equations are different. In the WATEQ equation, \dot{a}_i and b_i are determined for each ion by fitting measured activities of pure salt solutions. On the other hand, \dot{B} is a function of temperature and \dot{a}_i can be collected from Kielland (1937) (THOENEN et al., 2014). A third option is the Davies equation, often used when the values for \dot{a}_i and b_i are unknown, e.g. uncommon ions. The downsides of this equation are that the only ion-specific parameter is the ion charge and it works well just for temperatures near 25 °C and ionic strengths of a few tenths of molal (WOLERY and DAVELER, 1992). This feature is implemented in PHREEQC (THOENEN et al., 2014). The value for $C_{D,Davies}$ was initially taken as equal to 0.2 in early works but was reviewed and taken as 0.3 nowadays (THOENEN et al., 2014).

These three models are given by eq. (17) to (19).

$$\text{WATEQ} \quad \log_{10}(\gamma_i) = \frac{-A_{\gamma,10} z_i^2 \sqrt{I}}{1 + B_{\gamma,10} a_i \sqrt{I}} + b_i I \quad (17)$$

$$\text{B-dot} \quad \log_{10}(\gamma_i) = \frac{-A_{\gamma,10} z_i^2 \sqrt{I}}{1 + B_{\gamma,10} a_i \sqrt{I}} + \dot{B} I \quad (18)$$

$$\text{Davies} \quad \log_{10}(\gamma_i) = -A_{\gamma,10} z_i^2 \left(\frac{\sqrt{I}}{I + \sqrt{I}} - 0.3I \right) \quad (19)$$

The stoichiometric ionic strength I is computed from eq. (20) from the molality (m_i) and charge (z_i) of the aqueous species, while $A_{\gamma,10}$ and $B_{\gamma,10}$ are parameters dependent on temperature and the solvent (water), calculated in Appendix 1 for the range $273.15 \text{ K} < T < 373.15 \text{ K}$, where T is in kelvin. These equations were obtained from regression of data provided by Helgeson et al. (1981) as demonstrated in Appendix 1.

$$I = \frac{1}{2} \sum_i m_i z_i^2 \quad (20)$$

3.6 DENSITY AND VISCOSITY OF THE BRINE

The density of brine at reservoir conditions can be computed from the correlation of (MCCAIN JR, 1991), which uses the United States customary units (USCS). The water formation volume factor (B_w) symbolizes a change in volume of the brine as it is transported from reservoir conditions to surface conditions and is typically used by oil companies to calculate the flow and design the storage tanks. The units for this parameter are reservoir barrel per surface barrel at standard condition (res bbl/STB). The standard condition is 14.7 psia and 60 °F.

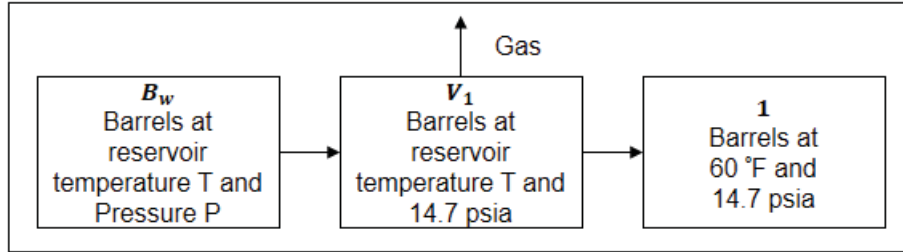
There are three effects involved in this parameter (MCCAIN, 1990):

1. The development of bubbles as the pressure decreases;
2. The expansion of the brine as the pressure decreases;
3. The contraction of the brine as the temperature decreases;

The first effect is smaller on brines than it is on oils and the second and third effect partially offset each other, hence the water formation volume factor is usually close to unity, rarely surpassing 1.06 res bbl/STB (MCCAIN JR, 1991)

The water formation volume factor (B_w) is computed from ΔV_{wP} and ΔV_{wT} as in eq. (21), (22) and (23), where the pressure is in psia and temperature is in °F, following the stepwise procedure is given in FIGURE 10 (MCCAIN JR, 1991).

FIGURE 10 STEPWISE CHANGE IN VOLUME FROM RESERVOIR TO SURFACE CONDITIONS.



SOURCE: (MCCAIN, 1990).

$$B_w = (1 + \Delta V_{wP})(1 + \Delta V_{wT}) \quad (21)$$

$$\Delta V_{wP} = -1.95301 \times 10^{-9} PT - 1.72834 \times 10^{-13} P^2 T - 3.58922 \times 10^{-7} P - 2.25341 \times 10^{-10} P^2 \quad (22)$$

$$\Delta V_{wT} = -1.0001 \times 10^{-2} + 1.33391 \times 10^{-4} T + 5.50654 \times 10^{-7} T^2 \quad (23)$$

The density of the brine at standard conditions (ρ_{wSTD} [lbm/ft³]) is obtained by eq. (24), where the solid weight percentage (S_{wt}) is computed by eq. (25). The standard conditions are 14.65 psia and 60 °F (MCCAIN, 1990).

$$\rho_{wSTD} = 62.368 + 0.438603 S_{wt} + 1.60074 \times 10^{-3} S_{wt}^2 \quad (24)$$

$$S_{wt} = 100 \left(\frac{\sum m_i MW_i}{1000 + \sum m_i MW_i} \right)_{i \neq CO_2} \quad (25)$$

The density (ρ_{w,CO_2-free} [kg/m³]), molar weight (MW_{w,CO_2-free} [g/mol]) and molar volume of CO₂-free (V_{w,CO_2-free} [m³/mol]) brine at reservoir conditions are obtained by eq. (26), (27) and (28), respectively.

$$\rho_{w,CO_2-free} = 16.0185 \frac{\rho_{wSTD}}{B_w} \quad (26)$$

$$V_{w,CO_2-free} = \frac{(MW_{w,CO_2-free}/1000)}{\rho_{w,CO_2-free}} \quad (27)$$

$$MW_{w,CO_2-free} = \frac{1000 + \sum m_i MW_i}{\frac{1000}{MW_{H_2O}} + \sum m_i} \quad (28)$$

The density of water increases when CO₂ is dissolved. Generalizing the same concept to brine, the density of CO₂-brine solution is calculated using eq. (29) (MCBRIDE-WRIGHT et al., 2015), where x_{CO_2} is the molar fraction of CO₂, obtained by the solubility model proposed by (SPYCHER and PRUESS, 2005). The partial molar volume of dissolved CO₂ ($V_{CO_2,dis}$ [cm³/mol]) is computed by an empirical function of temperature and pressure according to eq. (30) with coefficients given in TABLE 5 (MCBRIDE-WRIGHT et al., 2015).

$$\rho_{w,CO_2-mix} = \frac{x_{CO_2}MW_{CO_2} + (1 - x_{CO_2})MW_{w,CO_2-free}}{1000(x_{CO_2}(V_{CO_2,dis}/100^3) + (1 - x_{CO_2})V_{w,CO_2-free})} \quad (29)$$

$$V_{CO_2,dis} = \sum_{i=0}^2 \sum_{j=0}^1 a_{ij} T^i P_{EQ}^j \quad (30)$$

TABLE 5 COEFFICIENTS FOR CALCULATING $V_{CO_2,dis}$

$i \backslash j$	0	1
0	51.19	-6.0708×10^{-2}
1	-0.15575	5.5026×10^{-4}
2	3.2955×10^{-4}	-1.2114×10^{-6}

Salinity effects in $V_{CO_2,dis}$ in water are not considered in this study since they are weak and within experimental uncertainty (GARCÍA, 2001). As the effect of CO₂ on density is substantially smaller than the effect of salinity, it is often ignored. Nonetheless, it is important to simulate convective mixing during numerical simulations (GARCÍA, 2001). Lastly, the information on density and composition of brine and volume of the cell can be worked in eq. (31) and (32) to compute the mass of the solution and water in the cell.

$$mass_{solution} = V_{cell} \rho_{w,CO_2-mix} \theta_0 \quad (31)$$

$$mass_{H_2O} = \frac{1000 mass_{solution}}{\sum m_i MW_i + 1000} \quad (32)$$

The correlation relating the viscosity of the brine with temperature and atmospheric pressure is given by eq. (33) to (35). The units are viscosity μ_{w1} [cP], salinity [wt%] and temperature [°F]. McCain Jr. (1991) declares that this

correlation fits an existing graphical correlation to within 5% at temperatures between 38 °C and 204 °C and salinities up to 26 wt% NaCl.

$$\mu_{w1} = \Lambda T^{-\tau} \quad (33)$$

$$\Lambda = 109.574 - 8.40564 S_{wt} + 0.313314 S_{wt}^2 + 8.72213 \times 10^{-3} S_{wt}^3 \quad (34)$$

$$\tau = 1.12166 - 2.63951 \times 10^{-2} S_{wt} + 6.79461 \times 10^{-4} S_{wt}^2 + 5.47119 \times 10^{-5} S_{wt}^3 - 1.55586 \times 10^{-6} S_{wt}^4 \quad (35)$$

The viscosity of water at reservoir pressure is obtained through the correction given by eq. (36), where the pressure is expressed in psia. Again, McCain Jr. (1991) affirms that this equation fits data from 35 to 75 °C and below 689 bar within 6% and in the interval between 689 bar and 1034 bar within 7%.

$$\frac{\mu_w}{\mu_{w1}} = 0.9994 + 4.0295 \times 10^{-5} P + 3.1062 \times 10^{-9} P^2 \quad (36)$$

3.7 SEMI-EMPIRICAL DESCRIPTION OF DISSOLUTION AND PRECIPITATION RATE

Any rate equation implemented in computer modeling must include only parameters obtainable during program execution. In order to develop a rate with such characteristics, Palandri and Kharaka (2004) collected data for many minerals and adjusted parameters for a semi-empirical rate equation of the form of eq. (37), where each term represents a dissolution mechanism. The rate constant at the reaction temperature ($k_{T,j}$) is computed by eq. (38). The rate is limited by the ratio of the ionic product (Q_j) and the equilibrium constant of the reaction ($K_{eq,j}$), calculated by eq. (39) and (40), where $\nu_{i,j}$ is the stoichiometric coefficient of species i in the reaction j (PALANDRI and KHARAKA, 2004).

$$R_m = -S_{min,i} \sum_j^{NM} \left\{ k_{T,j} \prod_i a_{i,j}^{n_{i,j}} \prod_g P_{g,j}^{n_{g,j}} \left[1 - \left(\frac{Q_j}{K_{eq,j}} \right)^{p_j} \right]^{q_j} \right\} \quad (37)$$

$$k_{T,j} = k_{T_{ref},j} e^{-\left[\frac{E_{a,j}}{R} \left(\frac{1}{T} - \frac{1}{T_{ref}} \right) \right]} \quad (38)$$

$$Q_j = \left[\prod_i a_{i,j}^{v_{i,j}} \right]_{\text{evaluated at current condition}} \quad (39)$$

$$K_j = \left[\prod_i a_{i,j}^{v_{i,j}} \right]_{\text{evaluated at equilibrium}} \quad (40)$$

The reaction rate is R_m [mol/s], $S_{min,i}$ is the reactive surface area of the mineral i [m²], k_0 is a pre-exponential factor [mol m⁻² s⁻¹], E_a is the activation energy [J/mol], $n_{i,j}$ is the order of reaction with respect to component i in reaction j , $a_{i,j}$ is the activity of the i -th species in reaction j and P_g is the partial pressure of the g -th gaseous species in reaction j . The reaction rate may be tuned to the rock characteristics using the empirical parameters p_j and q_j .

The choice of which kinetic reaction represents each mechanism does not matter if chemical equilibrium is reached within the time step. Nonetheless, it may affect the numerical convergence and stability of other parts of the algorithm.

This method of representation of mineral dissolution and precipitation has its roots in the Transition State Theory. For what concerns its limitations, the equations adjusted data from experiments performed under conditions of temperature and pressure what may not represent reservoir conditions. Moreover, they neglected the temperature dependence of the pre-exponential factor or a possible dependence of pH or composition on the activation energy.

Finally, the rate of the precipitation does not necessarily follow the same structure as the rate of dissolution, possibly being faster or slower as the precipitated carbonate may be metastable components. Despite this, the method proposed by PALANDRI and KHARAKA (2004) is a useful representation that uses parameters from the bulk solution.

There are other approaches to model dissolution and precipitation of the carbonate mineral calcite, e.g. POKROVSKY et al. (2009), who studied the dissolution of calcite varying pH, temperature and partial pressure of CO₂ and developed an empirical equation relating these variables to dissolution rate. Another example is ZARETSKIY et al. (2012), who provided equations to regard the reactions in terms of Langmuir adsorptions and accounted for changes in permeability using the Kozeny-Carman relation. Besides that, they adopted a

grid-based method to consider changes in rock structure in greater detail than network models since grid-based methods honor pore structure.

3.8 POROUS MEDIUM PROPERTIES

The porous medium in this work is modeled as a pseudo-homogeneous medium, implicitly assuming that the aqueous species are well mixed within the time step. The values for porosity and other relevant properties must be assigned to the volume mesh on a cell-to-cell basis. The porosity of the cell is updated each time step according to eq. (41), where $N_{min,i}^*$ is the number of moles of mineral i at the end of the time step. This discounts the volume occupied by each mineral in the cell and assumes an ideal solid mixture of minerals.

$$\theta_t = 1 - \frac{1}{V_{cell}} \sum_{min=1}^{N_{min}} N_{min,i}^* V_{min,i} \quad (41)$$

The reactive surface area ($S_{min,i}$) is calculated as in eq. (42), where the specific surface area (SSA) is the surface area per total cell volume (units of m^2/m^3 or m^{-1}). This equation assumes all minerals are available to reactions according to the volume each mineral occupies. The reactive surface areas may be 1-3 orders of magnitude lower than geometrical surface areas depending on the complexity of the rock (GUNTER et al., 2000), suggesting there may be an overestimation of the dissolution rate if geometrical surface areas are used.

$$S_{min,i} = V_{cell} SSA_t \left(\frac{N_{min,i}^* V_{min,i}}{\sum_{min=1}^{N_{min}} N_{min,i}^* V_{min,i}} \right) \quad (42)$$

The initial values for porosity and surface area of the rock can be retrieved from micro-CT data, while the permeability can be calculated or determined experimentally. The initial permeability [m^2] can be obtained by a lumped form of the Kozeny-Carman (KC) equation as in eq. (43), where the empirical constant C_{KC} imbues the concept of the particle diameter and tortuosity and generally given the value 5.0 (MOSTAGHIMI, 2012).

$$\sigma_0 = 9.87 \times 10^{-13} \frac{1}{C_{KC}} \frac{\theta_0^3}{\frac{SSA_0}{(1000^2)} (1 - \theta_0)^2} \quad (43)$$

Mostaghimi (2012) took measurements of two carbonate rocks and calculated the values for C_{KC} , resulting in 14.77 and 130.14, highlighting the differences between the two rock samples.

Both the specific surface area and permeability must be updated as a function of porosity, which changes in time as well. This macroscopic relationship is important for modeling flow or reactive transport in the pseudo-homogeneous approach and partially compensates for the gap of information on the real pore structure of the system, which is unavailable during the simulation as dissolution or precipitation changes it continuously. An analytical description of this relationship is, however, not practical for reactive transport. Hence, Panga et al. (2005) proposed semi-empirical relations based on Kozeny-Carman, given by eq. (44) and (45). The empirical parameter β depends on the rock sample and the correlation returns to the original Kozeny-Carman equation for $\beta = 1$. The advantage of using the model proposed by Panga et al., (2005) is its theoretical grounds and the necessity to adjust only one parameter (β).

$$\sigma_t = \sigma_0 \frac{\theta_t}{\theta_0} \left(\frac{\theta_t(1 - \theta_0)}{\theta_0(1 - \theta_t)} \right)^{2\beta} \quad (44)$$

$$SSA_t = SSA_0 \frac{\theta_t}{\theta_0} \sqrt{\frac{\sigma_0 \theta_t}{\sigma_t \theta_0}} \quad (45)$$

Another approach that provides fair results for describing the surface area-permeability-porosity relationship is the sugar-lump model and Darcy's law (NOIRIEL et al., 2009). The sugar-lump is an empirical model of four parameters where the rock matrix is approximated as a cluster of spherical grains that dissociate into smaller grains, increasing the solution-exposed surface area. Alternatively, HAO et al. (2013) used a power-law to describe the surface area-permeability-porosity relationship, as in eq. (46) and eq. (47).

$$\sigma_t = \sigma_0 \left(\frac{\theta_t}{\theta_0} \right)^\omega \quad (46)$$

$$SSA_t = SSA_0 \left(\frac{1 - \theta_t}{1 - \theta_0} \right)^{2/3} \left(\frac{\theta_t}{\theta_0} \right)^{2/3} \quad (47)$$

3.9 CARBONATE RESERVOIR SAMPLE USED IN THIS WORK

Carbonate reservoirs are porous and permeable sedimentary rocks that can contain hydrocarbons. These rocks are mainly comprised of anionic complexes of $(\text{CO}_3)^{2-}$ and divalent metallic cations, the most common carbonate minerals being calcite (CaCO_3) and dolomite ($\text{CaMg}(\text{CO}_3)_2$). Carbonate rocks consist of component particles and some lime mud matrix (AHR, 2008).

The Laboratory of Analysis of Minerals and Rocks (LAMIR) donated a sample of a carbonate rock from the region of Pamukkale in Turkey and performed micro-computed tomography (micro-CT) scans using a Bruker Skycan 1272 and other experiments, determining that calcite is the predominant mineral in the sample. Micro-CT is a non-invasive non-destructive imaging technique used to collect cross-sectional images of a 3D object with high resolution. These images can be analyzed, binarized and organized in a manner to create a 3D representation of the rock, including its internal structure (XIONG et al., 2016). Further processing of the micro-CT data leads to a virtual model of the rock in a format readable by the CFD software. Moreover, it is believed that this rock has similar properties to the ones taken from the pre-salt region in Brazil. The research group at UFPR performed initial image processing on these images obtained from X-ray micro-CT scans with a resolution of 10 μm .

4 RESULTS AND DISCUSSION

In this section, the parameters for the modification of Drummond (1981) are estimated and the algorithm is applied to a particular case of CWI into a calcite aquifer as a means of demonstration on how to implement the methodology proposed in this work. Finally, the results of the equilibrium calculations are compared with rigorous models such as electrolyte-NRTL and Pitzer.

4.1 PARAMETER ESTIMATION FOR γ_{CO_2}

The particle swarm algorithm for parameter estimation was set up with a swarm size of 500 in the search region of [0.1; 3.0] to fit the parameters h_i in eq. (10) to 99 experimental points taken from Liu et al. (2011) and Tong et al. (2013), who performed experiments to determine the content of CO_2 in solutions of NaCl, KCl, $CaCl_2$ and $MgCl_2$. These authors do not provide values of this content of CO_2 in terms of molality. Rather, they used units the CO_2 weight percentage or CO_2 mole fraction in a salt-free water. Thus, conversion to molality is needed in order to compare the values. A MATLAB® routine was created to convert the data from these articles to the molality scale and is available as an annex of this thesis.

The optimization led to $h_{Ca^{2+}} = 2.2951 \pm 0.4414$ and $h_{Mg^{2+}} = 2.5994 \pm 0.5646$ for an individual confidence interval of 95% using the Student's t distribution. All seven optimization procedures used agreed very well, differing in the fifth decimal digit while the error is in the first decimal digit. The optimization techniques used were: (1) particleswarm: hybrid PSO + interior point, fminsearch: SIMPLEX, (3) fmincon: interior-point, (4) fmincon: SQP, (5) fmincon: active set, (6) lsqnonlin: trust-region-reflexive and (7) lsqnonlin: levenberg-marquadt.

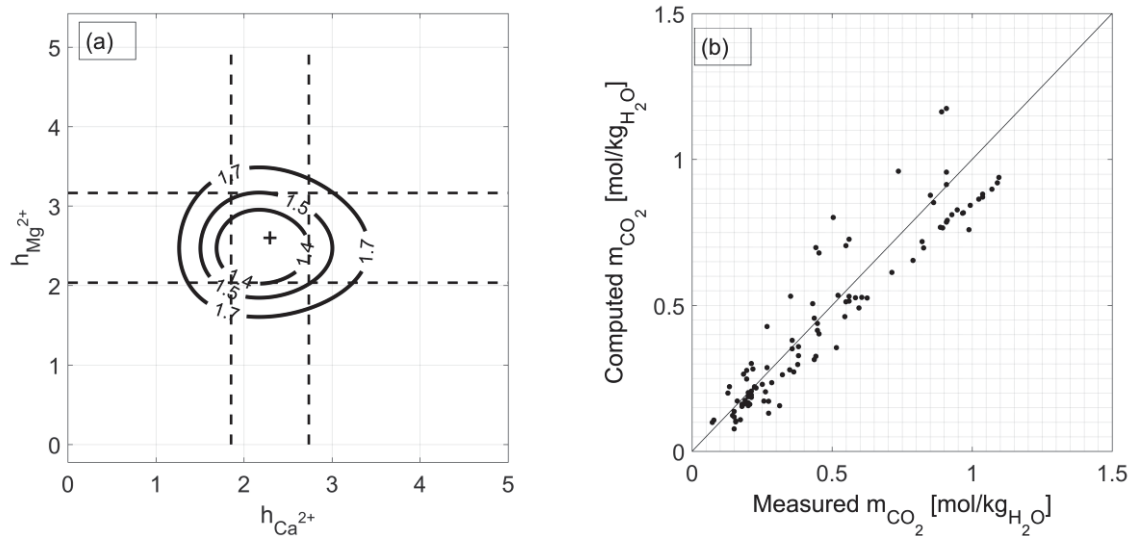
Conditions with higher temperatures and salinities lead to larger values of γ_{CO_2} which decrease the molality of CO_2 in brine, implying in values of $h_i > 1$. Furthermore, a cation with greater charge density (e.g. Ca^{2+} or Mg^{2+}) seems to imply in a stronger decrease in CO_2 solubility in brine than monovalent cations as Na^+ .

TABLE 6 RESULTS FOR EACH PARAMETER ESTIMATION PROCEDURE

Dataset used for training	First adjustment	Second adjustment
Liu et al. (2011)	✓	✓
Tong et al. (2013)	✓	✓
Prutton and Savage (1945)		✓
Zhao et al. (2015)		✓
LSE for the best fit (PSO+ interior point)	1.208	1.681
Number of measurements (n_{meas})	99	183
Number of parameters (n_{par})	2	
$h_{Ca^{2+}}$ with significance level $\alpha = 5\%$	2.2951 ± 0.4414	2.1939 ± 0.1940
$h_{Mg^{2+}}$ with significance level $\alpha = 5\%$	2.5994 ± 0.5646	2.4430 ± 0.3563

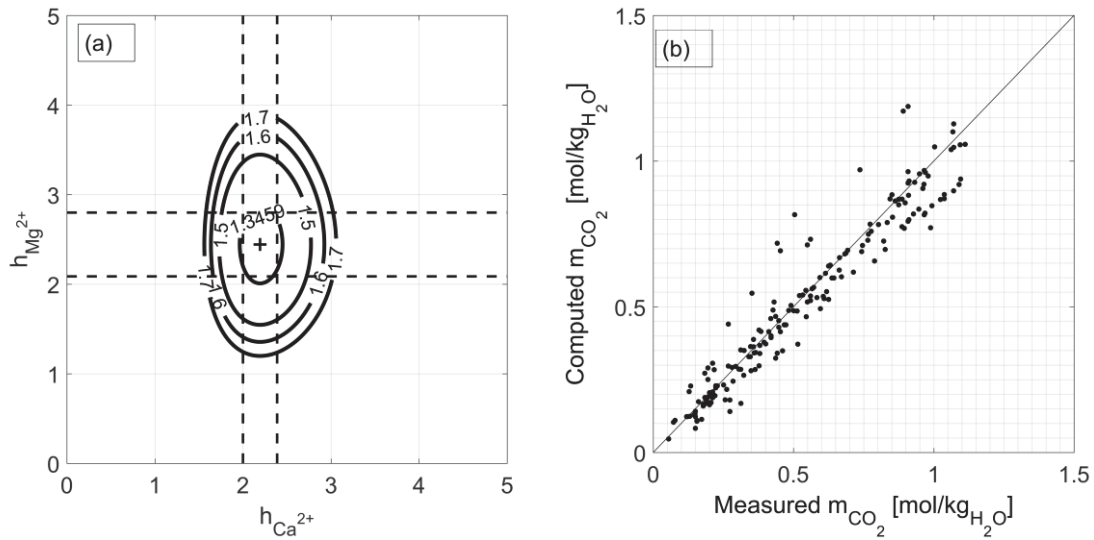
Later, the validation dataset was combined with the training dataset to reduce the confidence interval. The joint confidence interval for the first adjustment is shown in FIGURE 11(a), is equal to 1.2854 for the first adjustment and 1.3459 for the second adjustment using the F distribution with 95% confidence level.

The modification of Drummond (1981) proposed in this work slightly underestimates the solubility of CO_2 but still outperformed the modification proposed by Spycher and Pruess (2005) using the ionic strength for all test cases (Modified Drummond 2005). This bias is shown in FIGURE 11(b) and is mainly due to the choice of keeping the original coefficients in the Drummond (1981) formulation. The new modification is equivalent or better than the γ_{CO_2} model of Duan and Sun (2003) for milder system conditions (m_{salt}, T, P).

FIGURE 11 (A) JOINT CONFIDENCE REGION FOR $h_{Ca^{2+}}$ AND $h_{Mg^{2+}}$ AND (B) COMPARISON BETWEEN COMPUTED AND MEASURED m_{CO_2} FOR THE FIRST ADJUSTMENT

The results for the second adjustment are displayed in FIGURE 12. This second adjustment provides better and less biased predictions for the molality of the CO_2 in the brine but caution is advised when using the resulting parameters for the second adjustment because the errors may be too optimistic due to the inclusion of validation data in the training dataset.

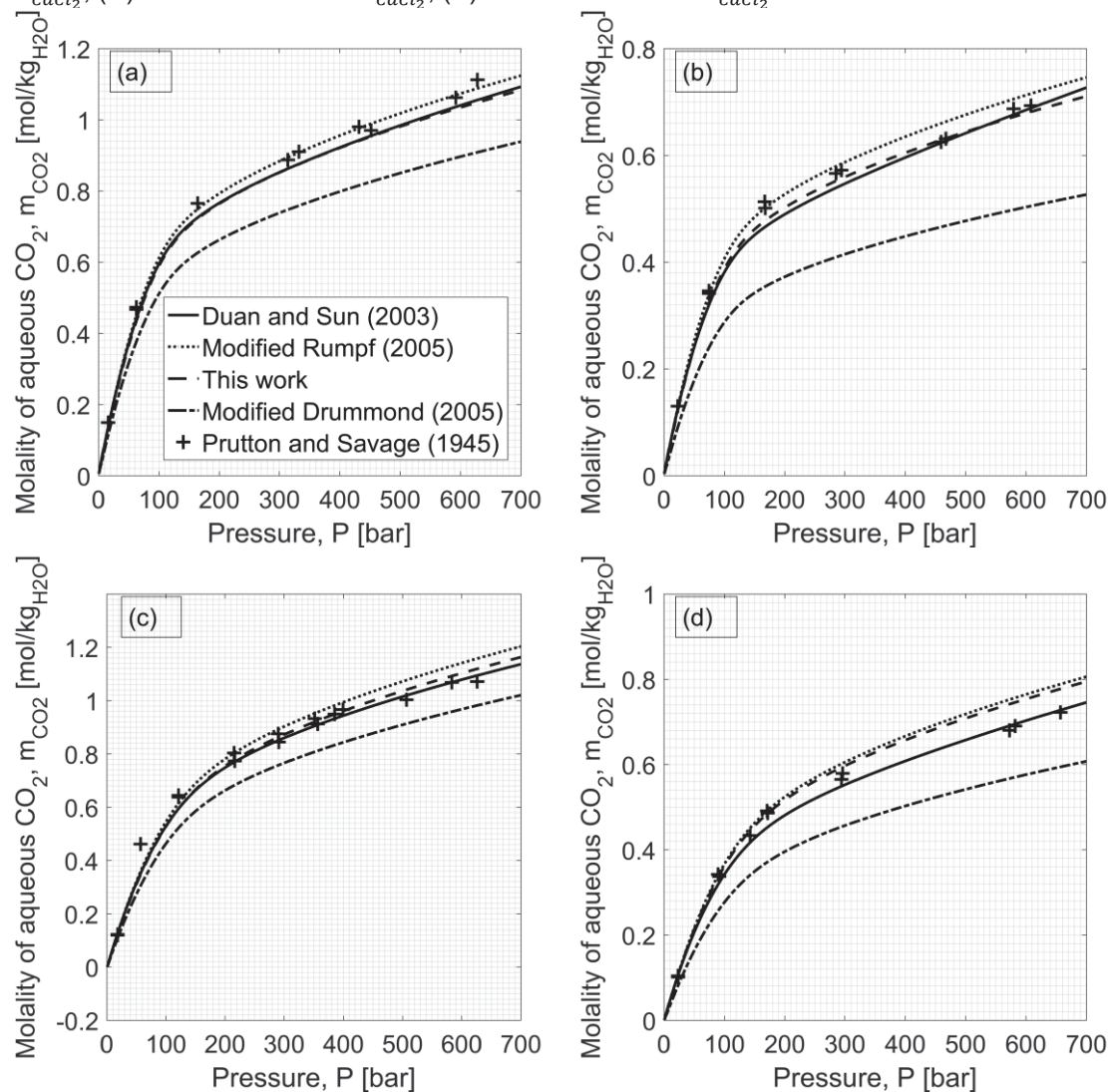
FIGURE 12 (A) JOINT CONFIDENCE REGION FOR $h_{\text{Ca}^{2+}}$ AND $h_{\text{Mg}^{2+}}$ AND (B) COMPARISON BETWEEN COMPUTED AND MEASURED m_{CO_2} FOR THE SECOND ADJUSTMENT



The performance of the solubility model of Spycher and Pruess (2005) with each external model of γ_{CO_2} were evaluated with validation data taken from Prutton and Savage (1945), as in FIGURE 13. In contrast, the parameter $h_{\text{Mg}^{2+}}$ was validated against data from Zhao et al. (2015), resulting in a mean absolute percentage error of 9% as shown in TABLE 7. Moreover, the model seems to be more reliable in higher temperatures, since the errors of the experiments at 373 K are more insensitive to changes in salinity than their counterpart at 323 K, as can be seen in TABLE 7.

TABLE 7 VALIDATION OF THE MODIFIED DRUMMOND (2018) AT P = 150 BAR – MgCl₂

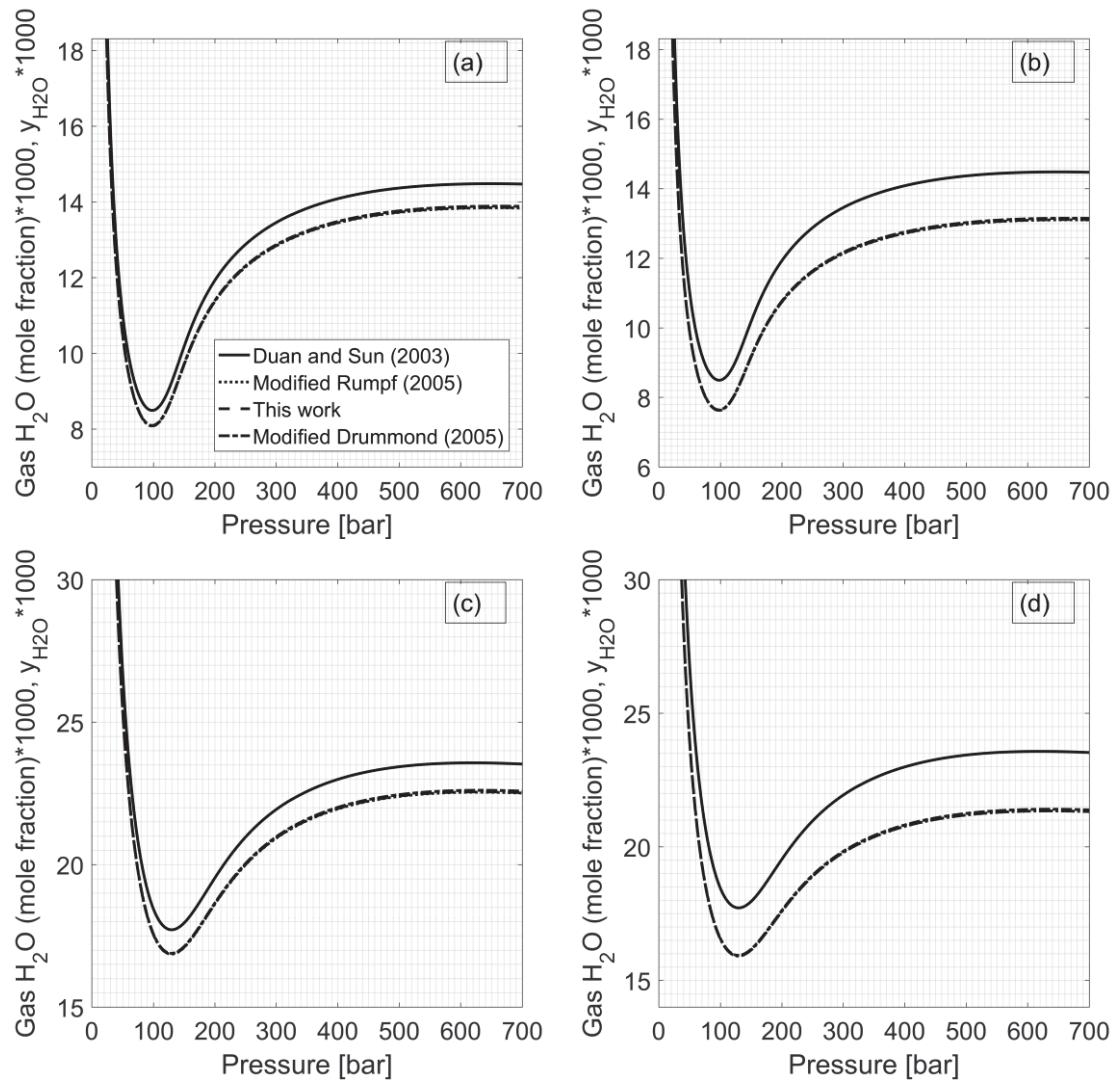
T [K]	m_{MgCl_2} [mol/kgH ₂ O]	Measured	m_{CO_2} [mol/kgH ₂ O]		Error M1 (%)	Error M2 (%)
			Model from 1 st adjustment	Model from 2 nd adjustment		
323	0.333	1.071	1.041	1.047	2.8	2.2
323	0.667	0.961	0.896	0.906	6.7	5.7
323	1.000	0.834	0.777	0.789	6.8	5.4
323	1.333	0.743	0.676	0.689	9.0	7.2
323	1.667	0.671	0.589	0.603	12.3	10.1
323	2.000	0.609	0.513	0.528	15.7	13.3
373	0.333	0.875	0.846	0.850	3.3	2.8
373	0.667	0.767	0.743	0.749	3.2	2.3
373	1.000	0.664	0.591	0.669	10.9	-0.7
373	1.333	0.594	0.531	0.600	10.7	-1.1
373	1.667	0.533	0.531	0.540	0.5	-1.4
373	2.000	0.483	0.477	0.487	1.3	-0.9

FIGURE 13 COMPARISON BETWEEN MODEL AND EXPERIMENTAL RESULTS FOR EQUILIBRIUM CO₂ SOLUBILITY IN BRINE. (A) 76 °C AND 1.05 m_{CaCl_2} , (B) 76 °C AND 2.30 m_{CaCl_2} , (C) 101 °C AND 1.05 m_{CaCl_2} , (D) 101 °C AND 2.30 m_{CaCl_2} .

Additionally, the solubility model calculates the content of water in the CO₂-rich phase, as shown in FIGURE 14. This information is useful for calculating

the water content of natural gas, which is usually collected from general water content charts which are, however, unavailable for CO₂ in equilibrium with brine (SALARI et al., 2011). This information may also be used to calculate the composition of a bubble that forms from the carbonated water stream that suffered enough pressure drop.

FIGURE 14 COMPARISON BETWEEN MODEL RESULTS FOR H₂O CONTENT IN THE GAS PHASE AT EQUILIBRIUM. (A) 76 °C AND 1.05 m_{CaCl_2} , (B) 76 °C AND 2.30 m_{CaCl_2} , (C) 101 °C AND 1.05 m_{CaCl_2} , (D) 101 °C AND 2.30 m_{CaCl_2} .



Using the CO₂ activity model by Duan and Sun (2003) in the context of the model by Spycher and Pruess (2005) will result in the calculation of the H₂O content in the CO₂-rich phase considering the absence of salts, i.e. the equilibrium curve of pure water and CO₂. This curve was used by Salari et al. (2011) together with a correction based on the salinity of the brine to develop a graphical form to determine the CO₂ content in equilibrium with brine. In

contrast, the activity model by Rumpf et al. (1994) and the modification of Drummond (1981) proposed in this work leads to the water content in equilibrium with the carbonated brine directly, avoiding the use of any chart.

4.2 EXAMPLE OF CARBONATED WATER INJECTION INTO A CALCITE SALINE AQUIFER

Petroleum reservoirs at the pre-salt in Brazil are deep (e.g. about 2150 m for the Lula Field in the Santos Basin) and the formation fluids are under pressures usually in the interval of 480 to 950 bar (FORMIGLI, 2007; GRAVA, 2014). Due to its proximity to the mantle of the Earth, the temperature is around 60 °C to 95°C (PETERSOHN; ABELHA, 2013). The salt layer is a better heat conductor than sedimentary rocks so the reservoir temperatures are lower than expected for rocks at this depth (LITTKE et al., 2008).

In order to apply the methodology presented in the previous sections, this work considers a single cell of constant volume that represents a well-mixed batch reactor simulating a portion of the Santos Basin in the pre-salt region of Brazil undergoing CWI. The mineralogy in the Santos Basin is predominantly calcite, with varying quantities of dolomite and quartz (BOYD et al., 2015), but for the purpose of creating a simple example, it is assumed only calcite is present.

The calculations assumed a subsurface fluid with at $T = 60\text{ °C}$, $m_{NaCl} = 0.5\text{ mol/kgH}_2\text{O}$ and $m_{CaCl_2} = 0.1\text{ mol/kgH}_2\text{O}$. The brine assumed equilibrium with CO_2 at $P_{EQ} = 600\text{ bar}$ prior to pressurization to injection pressure $P_{sim} = 650\text{ bar}$. In the context of CWI, the injection pressure is well above P_{EQ} and in the case considered the pressure drop will not be enough to cause the formation of a vapor phase so flash calculations are not required.

The cell size of 1 m^3 represents a segment of a calcite rock with a porosity of 0.29. The initial reactive surface area of calcite was assumed to be equal to $1.5\text{ m}^2/\text{m}^3$ of mineral. This choice was based according to the work of Leal (2014), while initial permeability was computed from eq. (43) assuming $C_{KC} = 14.77$ as in Mostaghimi (2012). Both the specific surface area and the permeability were updated according to the KC-based formulation proposed by Panga et al. (2005). The compressibility of the rock was neglected and the value for the molar volume

of calcite ($V_{m,CaCO_3}$) was considered to be equal to $3.693 \times 10^{-5} \text{ m}^3/\text{mol}$ ("Calcite - Institute of Experimental Mineralogy of Moscow", 1989).

Furthermore, computing chemical equilibrium requires a well-defined chemical system. Besides, the stoichiometric approach demands mass action equations describing the relations between the different components. Considering complete dissociation of salts in water and considering a system at low pH, the chemical system is represented by the reactions given in Table 8. This is the minimum set of equilibrium equations to depict the system, taking into account the aforementioned reservations relating to the choice of the reactions. Other equilibrium reactions should be easily added using CDS-2 numerical derivatives in the Jacobian Matrix.

The best set of reactions is the minimum set of independent reactions that captures the essence of what is occurring in the chemical level for the range of pH considered, to keep the matrices used in the calculations in a tolerable size so the simulations run faster.

The rationale is to use just reactions that carry enough valuable information to the system to compensate for the computational effort its inclusion would imply. In the context of this work, each equilibrium reaction increases the size of the Jacobian matrix by one column and one line, meaning that there is one more variable and one more equation to solve per iteration of the chemical equilibrium calculations, which are performed multiple times each time step.

Thus, the inclusion of this kind of reaction unnecessarily would just make the model slower without significantly improve the quality of its results for the pH range considered. Therefore, this work chose to prioritize efficiency and dealt with the set of chemical reactions shown in TABLE 8.

TABLE 8 CHEMICAL SYSTEM USED IN THIS WORK AND EQUILIBRIUM CONSTANTS.

j	Reaction	Type	Equilibrium constant
1	$H_2O \rightleftharpoons OH^- + H^+$	Equilibrium	$K_{EQ,1} = \left[\frac{m_{H^+} \cdot \gamma_{H^+} \cdot m_{OH^-} \cdot \gamma_{OH^-}}{a_{H_2O}} \right]_{EQ}$
2	$CO_2 + H_2O \rightleftharpoons HCO_3^- + H^+$	Equilibrium	$K_{EQ,2} = \left[\frac{m_{HCO_3^-} \cdot \gamma_{HCO_3^-} \cdot m_{H^+} \cdot \gamma_{H^+}}{m_{CO_2} \cdot \gamma_{CO_2}} \right]_{EQ}$
3	$HCO_3^- \rightleftharpoons CO_3^{2-} + H^+$	Equilibrium	$K_{EQ,3} = \left[\frac{m_{CO_3^{2-}} \cdot \gamma_{CO_3^{2-}} \cdot m_{H^+} \cdot \gamma_{H^+}}{m_{HCO_3^-} \cdot \gamma_{HCO_3^-}} \right]_{EQ}$
4	$\text{Calcite(s)} \rightleftharpoons Ca^{2+} + CO_3^{2-}$	Kinetic	$K_{EQ,4} = \left[\frac{a_{Ca^{2+}} a_{HCO_3^-}}{a_{H^+}} \right]_{EQ}$

The initial number of moles in the system at the start of any part of the model is calculated using the equations in TABLE 9, whereas the number of moles at the end of each iteration is calculated from the equations in TABLE 10.

TABLE 9 NUMBER OF MOLES OF AT THE START OF ANY PART OF THE MODEL.

i	Species	Moles at the start of the iteration it_{EQ}, N_i^\square [mol]
1	H ₂ O	$\frac{mass_{H_2O}(t)}{\frac{MW_{H_2O}}{1000}}$
2	CO ₂	$m_{CO_2}(t).mass_{H_2O}(t)$
3	CaCO ₃	$(1 - \theta(t)).V_{cell}.\left(\frac{1}{V_{m,CaCO_3}}\right)$
4	H ⁺	$m_{H^+}(t).mass_{H_2O}(t)$
5	OH ⁻	$m_{OH^-}(t).mass_{H_2O}(t)$
6	HCO ₃ ⁻	$m_{HCO_3^-}(t).mass_{H_2O}(t)$
7	CO ₃ ²⁻	$m_{CO_3^{2-}}(t).mass_{H_2O}(t)$
8	Ca ²⁺	$m_{Ca^{2+}}(t).mass_{H_2O}(t)$
9	Na ⁺	$m_{Na^+}.mass_{H_2O}(t)$
10	Cl ⁻	$m_{Cl^-}.mass_{H_2O}(t)$

The mass of any species is computed from the conversion from moles at any time except $t = 0$, where the mass of water is calculated from the initial density of the carbonated brine. Likewise, the molality of any species is calculated by dividing the number of moles by the mass of water.

TABLE 10 NUMBER OF MOLES AT THE END OF EACH PART OF THE MODEL.

i	Species	N_i^\bullet [mol] Speciation code	N_i^\bullet [mol] Reaction code	N_i^\bullet [mol] Stabilization code
1	H ₂ O	$N_{H_2O}^\square - \xi_1 - \xi_2$	$N_{H_2O}^\square$	$N_{H_2O}^\square - f_{H^+}.\xi_4 + f_{HCO_3^-}.\xi_4$
2	CO ₂	$N_{CO_2}^\square - \xi_2$	$N_{CO_2}^\square$	$N_{CO_2}^\square + f_{HCO_3^-}.\xi_4$
3	CaCO ₃	$N_{CaCO_3}^\square$	$N_{CaCO_3}^\square - \xi_4$	$N_{CaCO_3}^\square$
4	H ⁺	$N_{H^+}^\square + \xi_1 + \xi_2 + \xi_3$	$N_{H^+}^\square$	$N_{H^+}^\square + f_{H^+}.\xi_4 - f_{HCO_3^-}.\xi_4 - f_{CO_3^{2-}}.\xi_4$
5	OH ⁻	$N_{OH^-}^\square + \xi_1$	$N_{OH^-}^\square$	$N_{OH^-}^\square + f_{H^+}.\xi_4$
6	HCO ₃ ⁻	$N_{HCO_3^-}^\square + \xi_2 - \xi_3$	$N_{HCO_3^-}^\square$	$N_{HCO_3^-}^\square - f_{HCO_3^-}.\xi_4 + f_{CO_3^{2-}}.\xi_4$
7	CO ₃ ²⁻	$N_{CO_3^{2-}}^\square + \xi_3$	$N_{CO_3^{2-}}^\square + \xi_4$	$N_{CO_3^{2-}}^\square - f_{CO_3^{2-}}.\xi_4$
8	Ca ²⁺	$N_{Ca^{2+}}^\square$	$N_{Ca^{2+}}^\square + \xi_4$	$N_{Ca^{2+}}^\square$

The parameters of eq. (48) to compute $K_{EQ,j}(T, P)$ were retrieved from the PHREEQC's database WATEQ4F (BALL and NORDSTROM, 1991) and are displayed in TABLE 11, where T is in kelvin. The effect of pressure on the equilibrium constants were neglected.

$$\log_{10}(K_{EQ,j}) = A_1 + A_2 T + \frac{A_3}{T} + A_4 \log_{10}(T) + \frac{A_5}{T^2} \quad (48)$$

TABLE 11 EQUILIBRIUM CONSTANTS IN TERMS OF TEMPERATURE [K]

$K_{EQ,j}$	A_1	A_2	A_3	A_4	A_5
$K_{EQ,1}$	-283.971	-0.05069842	13323.0	102.24447	-1119669.0
$K_{EQ,2}$	-356.3094	-0.06091960	21834.37	126.8339	-1684915.0
$K_{EQ,3}$	-107.8871	-0.03252849	5151.79	38.92561	-563713.9
$K_{EQ,4}$	-171.9065	-0.077993	2839.319	71.595	0

Note that carbonic acid is an unstable chemical species so the equilibrium constant given for this reaction is for the apparent reaction of CO_2 and water to produce HCO_3^- and H^+ . It is important to distinguish the apparent equilibrium constant from the true equilibrium constant involving carbonic acid because they differ in value and on its representation in terms of the activities of the chemical species. For further information on this topic, see Pines et al. (2016).

The expressions of $K_{EQ,j}(\prod a_i^{v_{i,j}})$ must be written in terms of the extent of the reactions to compute the equilibrium condition in the speciation code using eq. (12). For the system presented in TABLE 8, the equilibrium constant $K_{EQ,j}(\prod a_i^{v_{i,j}})$ for each reaction is given in TABLE 12. Finally, the system of non-linear equations in eq. (12) is solved in this work by the MATLAB® command *mldivide*, automatically selecting the method to invert the Jacobian Matrix.

TABLE 12 EQUILIBRIUM CONSTANTS IN TERMS OF THE DEGREE OF ADVANCEMENT OF THE REACTIONS

j	Equilibrium constant
1	$K_{EQ,1} = \frac{\gamma_{\text{H}^+} \left(\frac{N_{0,\text{H}^+} + \xi_1 + \xi_2 + \xi_3}{\text{mass}_{\text{H}_2\text{O}}} \right) \gamma_{\text{OH}^-} \left(\frac{N_{0,\text{OH}^-} + \xi_1}{\text{mass}_{\text{H}_2\text{O}}} \right)}{a_{\text{H}_2\text{O}}}$
2	$K_{EQ,2} = \frac{\gamma_{\text{HCO}_3^-} \left(\frac{N_{0,\text{HCO}_3^-} + \xi_2 - \xi_3}{\text{mass}_{\text{H}_2\text{O}}} \right) \gamma_{\text{H}^+} \left(\frac{N_{0,\text{H}^+} + \xi_1 + \xi_2 + \xi_2}{\text{mass}_{\text{H}_2\text{O}}} \right)}{\gamma_{\text{CO}_2} \left(\frac{N_{0,\text{CO}_2} - \xi_2}{\text{mass}_{\text{H}_2\text{O}}} \right) a_{\text{H}_2\text{O}}}$
3	$K_{EQ,3} = \frac{\gamma_{\text{CO}_3^{2-}} \left(\frac{N_{0,\text{CO}_3^{2-}} + \xi_3}{\text{mass}_{\text{H}_2\text{O}}} \right) \gamma_{\text{H}^+} \left(\frac{N_{0,\text{H}^+} + \xi_1 + \xi_2 + \xi_3}{\text{mass}_{\text{H}_2\text{O}}} \right)}{\gamma_{\text{HCO}_3^-} \left(\frac{N_{0,\text{HCO}_3^-} + \xi_2 - \xi_3}{\text{mass}_{\text{H}_2\text{O}}} \right)}$

The WATEQ-Debye-Hückel equation was chosen to model ionic species. The parameters \hat{a}_i and b_i for the WATEQ equation were retrieved from the PHREEQC's database WATEQ4F (CHARLTON; PARKHURST, 2011). It is paramount that the molar weight of the species is collected from the same database to avoid simple mistakes, like the false creation or disappearance of

mass due to reactions. This work collected the molar weight of the species from the chemical portal (“Chemical Portal - Chemistry Online Education - Chemistry Online Education”, 2018) and their values are displayed in TABLE 13.

TABLE 13 CHEMICAL SPECIES PROPERTIES AND SUMMARY ACTIVITY COEFFICIENT MODELS USED IN THIS WORK.

ID	Species	Activity coefficient model	a_{WATEQ} [m]	b_{WATEQ} [kg/mol]	z	MW [g/mol]
1	H ₂ O	PHREEQC	N.A.	N.A.	0	18.01528
2	CO ₂	Modified Drummond (2018)	N.A.	N.A.	0	44.0095
3	CaCO ₃	Ideal	N.A.	N.A.	0	100.0869
4	H ⁺	WATEQ	9.0×10^{-10}	0	+1	1.00794
5	OH ⁻	WATEQ	3.5×10^{-10}	0	-1	17.00734
6	HCO ₃ ⁻	WATEQ	5.4×10^{-10}	0	-1	61.01684
7	CO ₃ ²⁻	WATEQ	5.4×10^{-10}	0	-2	60.0089
8	Ca ²⁺	WATEQ	5.0×10^{-10}	0.165	+2	40.078
9	Na ⁺	WATEQ	4.0×10^{-10}	0.075	+1	22.98977
10	Cl ⁻	WATEQ	3.5×10^{-10}	0.015	-1	35.453

Tolerance values and miscellaneous criteria for the numerical methods used in the algorithm in this work are presented in TABLE 14.

TABLE 14 MISCELLANEOUS CRITERIA FOR NUMERICAL METHODS IN THE EXAMPLE.

Parameter	Unit	Value	Main Program	Solubility code	Speciation code
$\xi_{crit,1}$	[mol]	1×10^{-6}	✓		
$\xi_{crit,2}$	[mol]	0.1	✓		
tol_{FVAL}	[-]	$\begin{bmatrix} 1 \times 10^{-14} \\ 1 \times 10^{-14} \\ 1 \times 10^{-14} \end{bmatrix}$			✓
tol_{ξ}	[mol]	$\begin{bmatrix} 1 \times 10^{-10} \\ 1 \times 10^{-10} \\ 1 \times 10^{-10} \end{bmatrix}$			✓
$tol_{\gamma_{CO_2}}$	[-]	1×10^{-7}		✓	
$\Delta \xi$	[mol]	1×10^{-8}			✓
ξ_0	[mol]	$\begin{bmatrix} 0.01 \times V_{cell} \\ 0.2 \times V_{cell} \\ 0.01 \times V_{cell} \end{bmatrix}$			✓
ξ_{stab}	[mol]	$\begin{bmatrix} 0.005 \times V_{cell} \\ 0.01 \times V_{cell} \\ 0.005 \times V_{cell} \end{bmatrix}$			✓

The kinetic dissolution rate of calcite is calculated from the data of Palandri and Kharaka (2004). Additionally, the reaction code includes the procedure to update the porosity, permeability and surface area over time using the models proposed by Panga et al. (2005) with $\beta = 1$. TABLE 15 summarizes the parameters required for eq. (37) and (38) for calcite. The values for p_u and q_u and $k_{T_{ref,u}}$ may require some tuning to fit the case, as in Hao et al. (2013).

TABLE 15 CALCITE DISSOLUTION PARAMETERS

u	Mechanism (u)	T_{ref} [K]	$k_{T_{ref},u}$ [mol.m ⁻² .s ⁻¹]	$E_{a,u}$ [J/mol]	$n_{H^+,u}$ [-]	$n_{(PCO_2),u}$ [-]	p_u [-]	q_u [-]
1	Acid	298.15	$10^{-0.3}$	14400	1.0	0.0	1.0	1.0
2	Neutral	298.15	$10^{-5.81}$	23500	0.0	0.0	1.0	1.0

SOURCE: (PALANDRI and KHARAKA, 2004).

The dissolution of calcite implies that the molality vector \mathbf{m}_i must be updated according to Table 10. The faster chemical equilibrium is updated, the lower the disequilibrium term in the rate of reaction becomes and the faster the dissolution reactions reach equilibrium. In this sense, the chemical equilibrium controls the rate of dissolution indirectly.

If too much dissolution occurs within the time step, the dissolved amount should be broken down into smaller parts as discussed in the adaptive control scheme of the time. If the extent of the dissolution reaction is higher than a critical value in the time step, the stabilization procedure acts to avoid numerical issues in the speciation code. The first step of the stabilization procedure is to represent the activities of HCO_3^- and CO_3^{2-} as functions of a_{CO_2} , as in eq. (49) and eq. (50).

$$m_{HCO_3^-} = \left(\frac{K_{EQ,2} \cdot a_{H_2O}}{a_{H^+} \gamma_{HCO_3^-}} \right) a_{CO_2} \quad (49)$$

$$m_{CO_3^{2-}} = \left(\frac{K_{EQ,2} K_{EQ,3} a_{H_2O}}{(a_{H^+})^2 \gamma_{CO_3^{2-}}} \right) a_{CO_2} \quad (50)$$

The total number of moles of dissolved inorganic carbon (N_{DIC}) is constant within the time step and is given by eq. (51), which yields eq. (52). Next, f_{H^+} , $f_{HCO_3^-}$ and $f_{CO_3^{2-}}$ are obtained from eq. (53) to eq. (55) It is possible to verify that $f_{H^+} = f_{HCO_3^-} + f_{CO_3^{2-}}$ so $f_{H^+} \cdot \xi_4 - f_{HCO_3^-} \cdot \xi_4 - f_{CO_3^{2-}} \cdot \xi_4 = 0$.

$$N_{DIC} = (m_{CO_2} + m_{HCO_3^-} + m_{CO_3^{2-}}) \cdot mass_{H_2O} \quad (51)$$

$$N_{DIC} = \left[\frac{1}{\gamma_{CO_2}} + \left(\frac{K_2 \cdot a_{H_2O}}{a_{H^+} \gamma_{HCO_3^-}} \right) + \left(\frac{K_2 K_3 a_{H_2O}}{(a_{H^+})^2 \gamma_{CO_3^{2-}}} \right) \right] \cdot a_{CO_2} \cdot mass_{H_2O} \quad (52)$$

$$f_{H^+} = \frac{2 \frac{1}{\gamma_{CO_2}} + 1 \left(\frac{K_{EQ,2} \cdot a_{H_2O}}{a_{H^+} \gamma_{HCO_3^-}} \right)}{\left[\frac{1}{\gamma_{CO_2}} + \left(\frac{K_{EQ,2} \cdot a_{H_2O}}{a_{H^+} \gamma_{HCO_3^-}} \right) + \left(\frac{K_{EQ,2} K_{EQ,3} a_{H_2O}}{(a_{H^+})^2 \gamma_{CO_3^{2-}}} \right) \right]} \quad (53)$$

$$f_{HCO_3^-} = \frac{\frac{1}{\gamma_{CO_2}}}{\left[\frac{1}{\gamma_{CO_2}} + \left(\frac{K_{EQ,2} \cdot a_{H_2O}}{a_{H^+} \gamma_{HCO_3^-}} \right) + \left(\frac{K_{EQ,2} K_{EQ,3} a_{H_2O}}{(a_{H^+})^2 \gamma_{CO_3^{2-}}} \right) \right]} \quad (54)$$

$$f_{CO_3^{2-}} = \frac{\frac{1}{\gamma_{CO_2}} + 1 \left(\frac{K_{EQ,2} \cdot a_{H_2O}}{a_{H^+} \gamma_{HCO_3^-}} \right)}{\left[\frac{1}{\gamma_{CO_2}} + \left(\frac{K_{EQ,2} \cdot a_{H_2O}}{a_{H^+} \gamma_{HCO_3^-}} \right) + \left(\frac{K_{EQ,2} K_{EQ,3} a_{H_2O}}{(a_{H^+})^2 \gamma_{CO_3^{2-}}} \right) \right]} \quad (55)$$

The results of the algorithm for 10 s of simulation with a time step of 0.01 s are shown in FIGURE 15, FIGURE 16 and IN THE context of this simulation, the solution is stagnant and chemical equilibrium is reached after some dissolution of calcite. As this mineral has a low solubility in water, the amount of dissolved calcite is low and the consequent changes in rock properties are modest in this case. On the other hand, once this model is implemented in a computational fluid dynamics application, it is expected that a considerable amount of mineral is dissolved, with the possibility of forming high permeability channels (wormholes) depending on injection conditions. This happens because fresh carbonated brine would reach the cells every Δt so the dissolution happens continuously. In addition, the ion species that originated from the dissolution of minerals are expected to remain in the brine solution only if the pH remains low enough. Otherwise, they will precipitate and possibly close pores, forming regions of high resistance to flow. This may be dangerous to the mechanical integrity of the reservoir and the equipment involved in the CWI because of the corresponding increase in the pressure loss.

FIGURE 17. As expected for a calcite rock, the pH value reaches a new plateau monotonically and increasingly slower, given the proximity of the chemical equilibrium (LEAL, 2014). Moreover, this change in pH is mainly due to a decrease in molality of H^+ , while its activity coefficient does not change considerably. The relative amount of CO_2 decreases over time as pH increases, as in the complete Bjerrum plot (HANRAHAN, 2012). In the context of this work, there is also the effect that the inorganic dissolved carbon in the solution increases over time due to dissolution reactions.

FIGURE 15 EVOLUTION OF VARIABLES IN TIME (A) PH, (B) DETAILED INFORMATION ON PH, (C) MOLALITY OF CARBON SPECIES (D) PARTIAL BJERRUM PLOT WITH PERCENTAGE OF CARBON SPECIES.

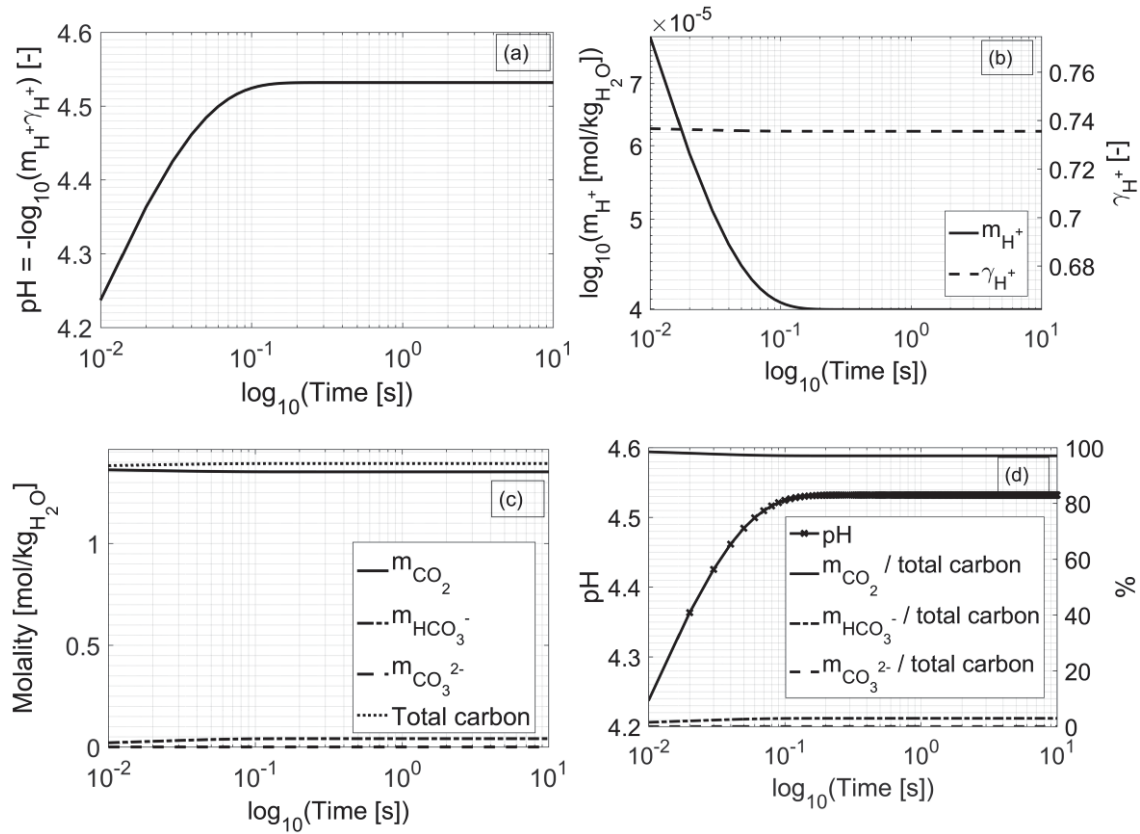
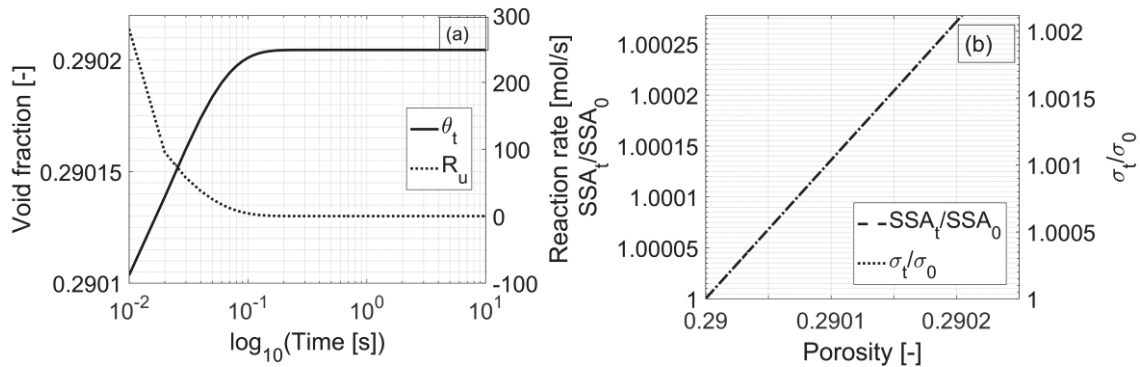


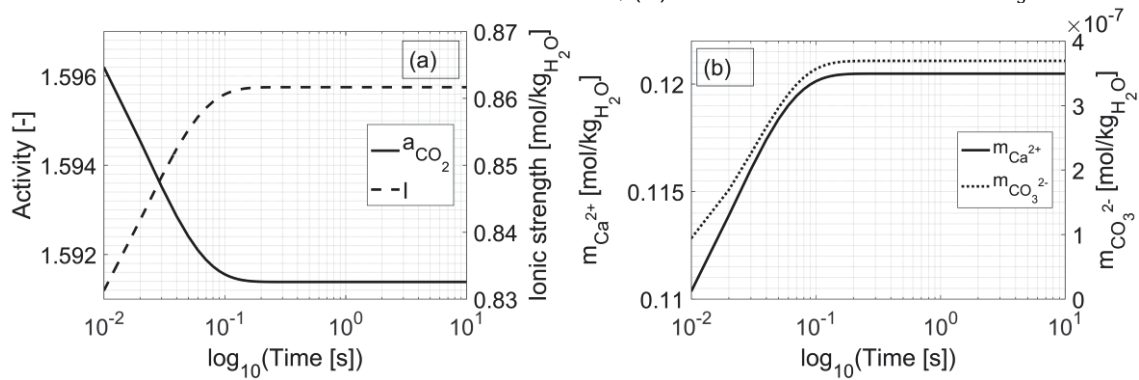
FIGURE 16 ROCK PROPERTIES AS A FUNCTION OF TIME (A) POROSITY AND DISSOLUTION RATE, (B) INDIRECT EFFECT OF DISSOLUTION RATE ON SPECIFIC SURFACE AREA AND PERMEABILITY.



In the context of this simulation, the solution is stagnant and chemical equilibrium is reached after some dissolution of calcite. As this mineral has a low solubility in water, the amount of dissolved calcite is low and the consequent changes in rock properties are modest in this case. On the other hand, once this model is implemented in a computational fluid dynamics application, it is expected that a considerable amount of mineral is dissolved, with the possibility of forming high permeability channels (wormholes) depending on injection conditions. This

happens because fresh carbonated brine would reach the cells every Δt so the dissolution happens continuously. In addition, the ion species that originated from the dissolution of minerals are expected to remain in the brine solution only if the pH remains low enough. Otherwise, they will precipitate and possibly close pores, forming regions of high resistance to flow. This may be dangerous to the mechanical integrity of the reservoir and the equipment involved in the CWI because of the corresponding increase in the pressure loss.

FIGURE 17 EVOLUTION OF IMPORTANT PROPERTIES OF THE SOLUTION IN TIME (A) ACTIVITY OF CO_2 AND IONIC STRENGTH, (B) MOLALITY OF Ca^{2+} AND CO_3^{2-} .



Note the reaction algorithm depends on many empirical parameters (e.g. p_u , q_u , β) that should be adjusted for a sample of the reservoir of interest to make the model more reliable. In addition, the relationship between the geometrical surface area and the reactive surface area is a complex function of pore size, pore distribution, and interconnectivity so the experimental determination of the reactive surface area is highly recommended, e.g. via the BET method.

4.3 ACTIVITY CONCENTRATION SCALE AND COMPARISON BETWEEN MODELS

In geochemistry, aqueous solutions often contain electrolytes. Mole fraction based activities and activity coefficients of solute species are not often used in this context. Most software, such as EQ3NR (WOLERY and DAVELER, 1992) and PHREEQC (CHARLTON and PARKHURST, 2011), use molality based activities. As such, all a_i and γ_i in this work are calculated in the molality

scale and are not directly comparable to the values from other concentration scales. The molalities at equilibrium condition, however, are comparable.

It interesting to verify the resulting performance from all choices in the algorithm proposed in this work with well-established models such as electrolyte-NRTL and Pitzer. A comparison between the results of the speciation code and Aspen Plus® 8.4 are presented in TABLE 16 for a synthetic brine.

TABLE 16 COMPARISON BETWEEN DIFFERENT THERMODYNAMIC MODELS AT $T = 60$ °C, $P_{EQ} = 100$ BAR, $m_{NaCl} = 0.5$ mol/kgH₂O AND $m_{CaCl_2} = 0.1$ mol/kgH₂O.

Species	Aspen® electrolyte-NRTL m_i [mol/kgH ₂ O]	Aspen® Pitzer m_i [mol/kgH ₂ O]	This work m_i [mol/kgH ₂ O]
CO ₂	0.8911	0.8907	0.8908
H ⁺	7.340×10^{-4}	1.123×10^{-3}	1.034×10^{-3}
OH ⁻	1.407×10^{-10}	2.182×10^{-10}	2.066×10^{-10}
HCO ₃ ⁻	7.340×10^{-4}	1.123×10^{-3}	1.034×10^{-3}
CO ₃ ²⁻	3.216×10^{-10}	7.316×10^{-10}	3.529×10^{-10}
Ca ²⁺	0.1	0.1	0.1
Na ⁺	0.5	0.5	0.5
Cl ⁻	0.7	0.7	0.7
pH	3.08	3.11	3.12

The results of the speciation in this work are noticeably close to the results using Pitzer for all chemical species except for CO₃²⁻. Electrolyte-NRTL results, however, differed by a larger margin, which was expected since WATEQ, as an extension of Debye-Hückel, is closer to Pitzer than electrolyte-NRTL in terms of theoretical grounds (BELVÈZE et al., 2004). These deviations may partially be due to the different source of $K_{EQ}(T, P)$ used in the speciation code.

Both Pitzer and electrolyte-NRTL are much more rigorous than the models used in this work, but these models require much more time and data for correct implementation, in addition to the extra computational effort each iteration in the simulation. Thus, the present algorithm is more versatile in terms of adding or removing chemical species from the system and it is expected that the results from this work are in agreement with Pitzer for the range of range of salinity and temperature that WATEQ-Debye-Hückel is applicable.

5 CONCLUSIONS

The algorithm integrated selected models into a complete and customizable procedure capable of successfully handling dissolution in carbonate rocks. The thermodynamic models treat the chemical species independently so the algorithm is readily extended to accommodate other chemical species, reactions, and minerals. Moreover, all secondary variables such as fugacity, density or the molality of CO₂ are now computed from system variables as temperature, pressure and salinity, which represents a huge advancement compared to the previous model developed at UFPR.

Additionally, the numerical derivatives in the Jacobian matrix allow the inclusion of more reactions with minor adaptations of the speciation code. More importantly, the pH value calculated by the algorithm proposed in this work (3.12), is noticeably close to the results generated by electrolyte-NRTL and Pitzer and (3.08 and 3.11, respectively). The pH value is crucial for properly calculating the dissolution rate of the carbonate minerals. This emphasizes that the many hypotheses made during the calculation of the activity coefficients of each species are valid within the tested range of system conditions.

The modification of γ_{CO_2} developed in this work offers the possibility of considering other chloride ions and proved to be a reasonable alternative to existing γ_{CO_2} models. It is easier to implement and provides results comparable to more traditional models like Duan and Sun (2003) for milder conditions even working with fewer parameters. Moreover, the errors with respect to the experimental values are within 9% for the first adjustment, i.e. without using validation data for training, while the error for the second adjustment is 4.5%. Thus, the activity model provides results with nearly the same accuracy of the model by Spycher and Pruess (2005), which has an accuracy of up to 8% within its temperature, pressure and salinity range.

The main limitation regarding the pseudo-homogeneous representation of the porous medium is that the cell must be small enough to capture the phenomena of interest, which leads to a compromise between the quality of the representation and the available computational resources. Nevertheless, this approach allows the use of equations developed to use in continuum media (e.g. Darcy-Brinkman, Kozeny-Carman) and is extendable to reservoir scale.

Further steps in this research would include simulation of the regions closer production wellbore where the pH is higher, favoring precipitation reactions. The pressure loss causes the formation of bubbles as well, so the chemical system and the flow equations much more complex. In addition, it is worth to consider the extension of the algorithm so it would contemplate microscale phenomena in a rock filled with oil, e.g. capillarity. These cases require multiphase flow calculations, as the formation of bubbles must include a flash calculation and a multiphase flow model. The presence of oil, however, must include a three-phase flash and perhaps an instability analysis along of a properly chosen multiphase flow model, e.g. the mixture model, where the phases are treated as interpenetrating continua.

REFERENCES

AHR, W. M. **Geology of Carbonate Reservoirs: The Identification, Description, and Characterization of Hydrocarbon Reservoirs in Carbonate Rocks**. John Wiley & Sons, 2008.

AL-MUTAIRI, S. M.; KOKAL, S. L. **EOR Potential in the Middle East: Current and Future Trends**. SPE EUROPEC/EAGE Annual Conference and Exhibition. **Anais...**Society of Petroleum Engineers, 4 April 2011. Available at: <<http://www.onepetro.org/doi/10.2118/143287-MS>>

ANSYS. **ANSYS Fluent 17.0 Help - Pressure-Velocity Coupling**. Available at: <https://www.sharcnet.ca/Software/Ansys/17.0/en-us/help/flu_th/flu_th_sec_uns_solve_pv.html>. Accessed on: 24 April 2018.

ASPEN TECHNOLOGY, I. Aspen Plus ® User Guide. **Aspen Technology, Inc.**, p. 936, 2000.

AZIN, R. et al. Measurement and modeling of CO₂ diffusion coefficient in Saline Aquifer at reservoir conditions. **Open Engineering**, v. 3, n. 4, 1 January 2013.

BALL, J. W.; NORDSTROM, D. K. User's Manual for WATEQ4F, with revised thermodynamic data base and test cases for calculating speciation of major, trace, and redox elements in natural waters. **U.S. Geological Survey Water-Resources Investigations Report**, v. 91–183, p. 1–188, 1991.

BELVÈZE, L. S.; BRENNECKE, J. F.; STADTHERR, M. A. Modeling of Activity Coefficients of Aqueous Solutions of Quaternary Ammonium Salts with the Electrolyte-NRTL Equation. **Industrial & Engineering Chemistry Research**, v. 43, n. 3, p. 815–825, 2004.

BLUNT, M. J. et al. Pore-scale imaging and modelling. **Advances in Water Resources**, v. 51, p. 197–216, January 2013.

BOYD, A. et al. Presalt Carbonate Evaluation for Santos Basin , Offshore Brazil. **Petrophysics**, v. 56, n. 6, p. 577–591, 2015.

BRAZIL, F. R. O. **Intended nationally determined contribution towards achieving the objective of the united nations framework convention on climate change**. Available at: <[http://www4.unfccc.int/submissions/INDC/Published Documents/Brazil/1/BRAZIL iNDC english FINAL.pdf](http://www4.unfccc.int/submissions/INDC/Published%20Documents/Brazil/1/BRAZIL%20INDC%20english%20FINAL.pdf)>. Accessed on: 19 abr. 2017.

BRINKMAN, H. C. A calculation of the viscous force exerted by a flowing fluid on a dense swarm of particles. **Flow, Turbulence and Combustion**, v. 1, n. 1, p. 27, 1 December 1949.

BURCHETTE, T. P. Carbonate rocks and petroleum reservoirs: a geological perspective from the industry. **Geological Society, London, Special Publications**, v. 370, n. 1, p. 17–37, 2012.

CADOGAN, S. P.; MAITLAND, G. C.; TRUSLER, J. P. M. Diffusion coefficients of CO₂ and N₂ in water at temperatures between 298.15 K and 423.15 K at pressures up to 45 MPa. **Journal of Chemical and Engineering Data**, v. 59, n. 2, p. 519–525, 13 February 2014.

Calcite. Institute of Experimental Mineralogy of Moscow. Available at: <http://database.iem.ac.ru/mincryst/s_carta.php?CALCITE+706>. Accessed on: 2 January 2018.

CHARLTON, S. R.; PARKHURST, D. L. Modules based on the geochemical model PHREEQC for use in scripting and programming languages. **Computers & Geosciences**, v. 37, n. 10, p. 1653–1663, 1 October 2011.

Chemical Portal - Chemistry Online Education - Chemistry Online Education. Available at: <<https://www.webqc.org/>>. Accessed on: 25 April 2018.

CHEN, N.; GUNZBURGER, M.; WANG, X. Asymptotic analysis of the differences between the Stokes-Darcy system with different interface conditions and the Stokes-Brinkman system. **Journal of Mathematical Analysis and Applications**, v. 368, n. 2, p. 658–676, August 2010.

CHOU, L.; GARRELS, R. M.; WOLLAST, R. Comparative study of the kinetics and mechanisms of dissolution of carbonate minerals. **Chemical Geology**, v. 78, n. 3–4, p. 269–282, December 1989.

COOPER, S. J. et al. TauFactor: An open-source application for calculating tortuosity factors from tomographic data. **SoftwareX**, v. 5, p. 203–210, 2016.

CRANK, J. Methods of Solution when the Diffusion Coefficient is Constant. In: **The mathematics of diffusion**. Clarendon Press, 1979. p. 414.

DOS SANTOS, H.; NEUMANN, R.; ÁVILA, C. A. Mineral Quantification with Simultaneous Refinement of Ca-Mg Carbonates Non-Stoichiometry by X-ray Diffraction, Rietveld Method. **Minerals**, v. 7, n. 9, p. 164, 2017.

DRUMMOND, E. S. **Boiling and mixing of hydrothermal fluids : chemical effects on mineral precipitation I**. University Park, Penn., Pennsylvania State University, Ph.D. thesis, 760 p

DUAN, Z.; MØLLER, N.; WEARE, J. H. An equation of state for the CH₄-CO₂-H₂O system: II. Mixtures from 50 to 1000°C and 0 to 1000 bar. **Geochimica et Cosmochimica Acta**, v. 56, n. 7, p. 2619–2631, 1992.

DUAN, Z.; SUN, R. An improved model calculating CO₂ solubility in pure water and aqueous NaCl solutions from 273 to 533 K and from 0 to 2000 bar. **Chemical Geology**, v. 193, n. 3–4, p. 257–271, February 2003.

FAN, Y.; DURLOFSKY, L. J.; TCHELEPI, H. A. A fully-coupled flow-reactive-transport formulation based on element conservation, with application to CO₂ storage simulations. **Advances in Water Resources**, v. 42, p. 47–61, June 2012.

FORMIGLI, J. **Pre-Salt Reservoirs Offshore Brazil: Perspectives and Challenges** Petrobrás, , 2007. Available at: <http://www.investidorpetrobras.com.br/download/1462/2007_Formigli_Miami_pre-sal.pdf>

FOROOZESH, J.; JAMIOLAHMADY, M.; SOHRABI, M. Mathematical modeling of carbonated water injection for EOR and CO₂ storage with a focus on mass transfer kinetics. **Fuel**, v. 174, p. 325–332, June 2016.

GARCÍA, J. E. Density of aqueous solutions of CO₂ Density of Aqueous Solutions of CO₂. 10 October 2001.

GOLFIER, F. et al. On the ability of a Darcy-scale model to capture wormhole formation during the dissolution of a porous medium. **Journal of Fluid Mechanics**, v. 457, p. 213–254, 9 April 2002.

GOLFIER, F. et al. Core-scale description of porous media dissolution during acid injection - Part I: theoretical development. **Computational & Applied Mathematics**, v. 23, n. 2–3, p. 173–194, 2004.

GOLFIER, F. et al. Core-Scale Description of Porous Media Dissolution During Acid Injection – Part II: Calculation of the Effective Properties. **Computational & Applied Mathematics**, v. 25, n. 1, p. 55–78, 2006.

GOMMES, C. J. et al. Practical methods for measuring the tortuosity of porous materials from binary or gray-tone tomographic reconstructions. **AIChE Journal**, v. 55, n. 8, p. 2000–2012, 2009.

GRAVA, W. **Aspects in CO₂ Management in Brazilian Pre-Salt O/G Production**. Petrobrás - CENPES PRO-CO₂, , 2014. Available at: <http://www.pucrs.br/cepac/download/ccsavancado/3.CO2_Management_Brazil_Grava.pdf>

GRIEWANK, A.; WALTHER, A. Introduction to Automatic Differentiation. **PAMM**, v. 2, n. 1, p. 45–49, 1 March 2003.

GUNTER, W. D.; PERKINS, E. H.; HUTCHEON, I. Aquifer disposal of acid gases: Modelling of water-rock reactions for trapping of acid wastes. **Applied Geochemistry**, v. 15, n. 8, p. 1085–1095, September 2000.

GUTA, L.; SUNDAR, S. Navier-stokes-brinkman system for interaction of viscous waves with a submerged porous structure. **Tamkang Journal of Mathematics**, v. 41, n. 3, p. 217–243, 2010.

HANRAHAN, G. **Key Concepts in Environmental Chemistry**. Academic Press, 2011.

HAO, Y. et al. CO₂-induced dissolution of low permeability carbonates. Part II: Numerical modeling of experiments. **Advances in Water Resources**, v. 62, p. 388–408, December 2013.

HELGESON, H. C.; KIRKHAM, D. H.; FLOWERS, G. C. Theoretical prediction of the thermodynamic behavior of aqueous electrolytes at high pressures and temperatures: IV. Calculation of activity coefficients, osmotic coefficients, and apparent molal and standard and relative partial molal properties to 600°C. **American Journal of Science**, v. 281, n. 10, p. 1249–1516, 1981.

IGLAUER, S. Dissolution Trapping of Carbon Dioxide in Reservoir Formation Brine – A Carbon Storage Mechanism. In: **Mass Transfer - Advanced Aspects**. InTech, 2011.

INSKEEP, W. P.; BLOOM, P. R. An evaluation of rate equations for calcite precipitation kinetics at pCO₂ less than 0.01 atm and pH greater than 8. **Geochimica et Cosmochimica Acta**, v. 49, n. 10, p. 2165–2180, 1985.

IZGEC, O. **Reactive Flow in Vuggy Carbonates: Methods and Models Applied to Matrix Acidizing of Carbonates**. Master Thesis, Texas A&M University, 2009.

JOHNSON, J. W.; OELKERS, E. H.; HELGESON, H. C. SUPCRT92: A software package for calculating the standard molal thermodynamic properties of minerals, gases, aqueous species, and reactions from 1 to 5000 bar and 0 to 1000°C. **Computers and Geosciences**, v. 18, n. 7, p. 899–947, August 1992.

KECHUT, N. I.; JAMIOLAHMADY, M.; SOHRABI, M. Numerical simulation of experimental carbonated water injection (CWI) for improved oil recovery and CO₂ storage. **Journal of Petroleum Science and Engineering**, v. 77, n. 1, p. 111–120, 2011.

KIELLAND, J. Individual Activity Coefficients of Ions in Aqueous Solutions. **Journal of the American Chemical Society**, v. 59, n. 9, p. 1675–1678, 1937.

LEAHY-DIOS, A.; FIROOZABADI, A. Unified model for nonideal multicomponent molecular diffusion coefficients. **AIChE Journal**, v. 53, n. 11, p. 2932–2939, 2007.

LEAL, A. M. M. **Computational methods for geochemical modelling: Applications to carbon dioxide sequestration**, 2014.

LEAL, A. M. M.; BLUNT, M. J.; LAFORCE, T. C. A chemical kinetics algorithm for geochemical modelling. **Applied Geochemistry**, v. 55, p. 46–61, 1 abr. 2015.

LI, L.; STEEFEL, C. I.; YANG, L. Scale dependence of mineral dissolution rates within single pores and fractures. **Geochimica et Cosmochimica Acta**, v. 72, n. 2, p. 360–377, January 2008.

LITTKE, R. et al. **Dynamics of complex intracontinental basins: The central european basin system**. Springer-Verlag Berlin Heidelberg, 2008.

LIU, Y. et al. Solubility of CO₂ in aqueous solutions of NaCl, KCl, CaCl₂ and their mixed salts at different temperatures and pressures. **The Journal of Supercritical Fluids**, v. 56, n. 2, p. 125–129, 2011.

LÓPEZ-CASTILLO, A.; DE SOUZA FILHO, J. C. Simulação do equilíbrio: O método de Monte Carlo. **Química Nova**, v. 30, n. 7, p. 1759–1762, 2007.

MACHADO, A. V. L. **Simulação numérica do escoamento de solução salina com CO₂ dissolvido em rochas carbonáticas**. Master Thesis, Universidade Federal do Paraná, 2015.

MCBRIDE-WRIGHT, M.; MAITLAND, G. C.; TRUSLER, J. P. M. Viscosity and density of aqueous solutions of carbon dioxide at temperatures from (274 to 449) K and at pressures up to 100 MPa. **Journal of Chemical and Engineering Data**, v. 60, n. 1, p. 171–180, 8 January 2015.

MCCAIN, W. D. **Properties of Petroleum Fluids**. Pennwell Books, 1990.

MCCAIN JR, W. D. Reservoir Fluid Property Correlations - State of the Art. **SPE Reservoir Engineers**, v. 6, n. 2, p. 8, 1991.

MOORTGAT, J.; LI, Z.; FIROOZABADI, A. Three-phase compositional modeling of CO₂ injection by higher-order finite element methods with CPA equation of state for aqueous phase. **Water Resources Research**, v. 48, n. 12, December 2012.

MORBIDELLI, M.; VARMA, A. Parametric sensitivity and runaway in chemical reactors. **Sadhana**, v. 10, n. 1–2, p. 133–148, 1987.

MOSTAGHIMI, P. Transport Phenomena Modelled on Pore-Space Images. **PhD thesis, Imperial College London**, 2012.

MUTORU, J. W.; LEAHY-DIOS, A.; FIROOZABADI, A. Modeling infinite dilution and Fickian diffusion coefficients of carbon dioxide in water. **AIChE Journal**, v. 57, n. 6, p. 1617–1627, 2011.

NICKALLS, R. W. D. A New Approach to Solving the Cubic: Cardan's Solution Revealed. **The Mathematical Gazette**, v. 77, n. 480, p. 354, November 1993.

NOIRIEL, C. et al. Changes in reactive surface area during limestone dissolution: An experimental and modelling study. **Chemical Geology**, v. 262, n. 3–4, p. 353–363, July 2009.

PALANDRI, J. L.; KHARAKA, Y. K. **A compilation of rate parameters of water-mineral interaction kinetics for application to geochemical modeling** USGS Open File Report, 2004. Available at: <<http://www.dtic.mil/cgi-bin/GetTRDoc?Location=U2&doc=GetTRDoc.pdf&AD=ADA440035>>.

PANGA, M. K. R.; ZIAUDDIN, M.; BALAKOTAIAH, V. **Two-scale continuum model for simulation of wormholes in carbonate acidization**. *AIChE Journal. Anais*, 2005.

PARKHURST, D. L.; APPELO, C. A. J. PHREEQC (Version 3) - A Computer Program for Speciation, Batch-Reaction, One-Dimensional Transport, and Inverse Geochemical Calculations. **Modeling Techniques, book 6**, p. 497, 2013.

PERKINS, E. H. et al. Critical review of classes of geochemical computer models adaptable for prediction of acidic drainage from mine waste rock. **Fourth International Conference on Acid Rock Drainage**, April 1995, p. 587–601, 1995.

PETERSOHN, E.; ABELHA, M. Brazil Pre-Salt - Libra - Assesment. 2013.

PINES, D. et al. How Acidic Is Carbonic Acid? **Journal of Physical Chemistry B**, v. 120, n. 9, p. 2440–2451, 2016.

PLUMMER, L. N.; WIGLEY, T. M. L.; PARKHURST, D. L. The kinetics of calcite dissolution in CO₂-water systems at 5C to 60C and 0.0 to 1.0 atm CO₂. **American Journal of Science**, v. 278, p. 179–216, 1978.

POKROVSKY, O. S. et al. Calcite, dolomite and magnesite dissolution kinetics in aqueous solutions at acid to circumneutral pH, 25 to 150 °C and 1 to 55 atm pCO₂: New constraints on CO₂ sequestration in sedimentary basins. **Chemical Geology**, v. 260, n. 3–4, p. 317–329, July 2009.

PRUTTON, C. F.; SAVAGE, R. L. The Solubility of Carbon Dioxide in Calcium Chloride-Water Solutions at 75, 100, 120° and High Pressures. **Journal of the American Chemical Society**, v. 67, n. 9, p. 1550–1554, 1945.

RAOOF, A. et al. PoreFlow: A complex pore-network model for simulation of reactive transport in variably saturated porous media. **Computers & Geosciences**, v. 61, p. 160–174, December 2013.

REUTERS. **Brazil pledges to cut carbon emissions 37% by 2025 | Environment. The Guardian.** Available at: <<https://www.theguardian.com/environment/2015/sep/28/brazil-pledges-to-cut-carbon-emissions-37-by-2025>>. Accessed on: 24 April 2018.

RUMPF, B. et al. Solubility of carbon dioxide in aqueous solutions of sodium chloride: Experimental results and correlation. **Journal of Solution Chemistry**, v. 23, n. 3, p. 431–448, 1994.

SAALTINK, M. W.; AYORA, C.; CARRERA, J. A mathematical formulation for reactive transport that eliminates mineral concentrations. **Water Resources Research**, v. 34, n. 7, p. 1649–1656, 1998

SALARI, H. et al. On estimating the water content of CO₂ in equilibrium with formation brine. **Petroleum Science and Technology**, v. 29, n. 19, p. 2037–2051, 2011.

SANAEI, A.; VARAVEI, A.; SEPEHRNOORI, K. **Mechanistic Modeling of Carbonated Waterflooding**. SPE Improved Oil Recovery Conference. Society of Petroleum Engineers, 13 April 2018. Available at: <<http://www.onepetro.org/doi/10.2118/190319-MS>>. Acesso em: 1 May 2018.

SILIN, D.; PATZEK, T. Pore space morphology analysis using maximal inscribed spheres. **Physica A: Statistical Mechanics and its Applications**, v. 371, n. 2, p. 336–360, 2006.

SOHRABI, M. et al. **Enhanced Oil Recovery and CO₂ Storage by Carbonated Water Injection**. International Petroleum Technology Conference. **Anais...** International Petroleum Technology Conference, 5 April. 2009. Available at: <<http://www.onepetro.org/doi/10.2523/IPTC-14070-ABSTRACT>>

SPYCHER, N.; PRUESS, K. CO₂-H₂O mixtures in the geological sequestration of CO₂. II. Partitioning in chloride brines at 12–100°C and up to 600 bar. **Geochimica et Cosmochimica Acta**, v. 69, n. 13, p. 3309–3320, July 2005.

SPYCHER, N.; PRUESS, K. A Phase-partitioning model for CO₂-brine mixtures at elevated temperatures and pressures: Application to CO₂-enhanced geothermal systems. **Transport in Porous Media**, v. 82, n. 1, p. 173–196, 17 March 2010.

SPYCHER, N.; PRUESS, K.; ENNIS-KING, J. CO₂-H₂O mixtures in the geological sequestration of CO₂. I. Assessment and calculation of mutual solubilities from 12 to 100°C and up to 600 bar. **Geochimica et Cosmochimica Acta**, v. 67, n. 16, p. 3015–3031, August 2003.

TAVAKOLIAN, M. et al. **Significant improvement in oil recovery and CO₂ storage by carbonated water injection (CWI)**. 3rd EAGE CO₂ Geological Storage Workshop: Understanding the Behaviour of CO₂ in Geological Storage Reservoirs. **Anais**. 27 March 2012. Available at: <<https://www.scopus.com/inward/record.uri?eid=2-s2.0-84896597826&partnerID=40&md5=edfb7e206d3b25cc56023bb6b1cd7f5c>>. Accessed on: 20 abr. 2018

THE MATHWORKS INC. **MATLAB** - MathWorks. Available at: <<http://www.mathworks.com/products/matlab/>>.

THOENEN, T. et al. **The PSI/Nagra Chemical Thermodynamic Database 12/07PSI Bericht Nr. 14-04**, 2014.

TONG, D.; TRUSLER, J. P. M.; VEGA-MAZA, D. Solubility of CO₂ in aqueous solutions of CaCl₂ or MgCl₂ and in a synthetic formation brine at temperatures up to 423 K and pressures up to 40 MPa. **Journal of Chemical and Engineering Data**, v. 58, n. 7, p. 2116–2124, 2013.

TURNER, C. H. et al. Simulation of chemical reaction equilibria by the reaction ensemble Monte Carlo method: A review. **Molecular Simulation**, v. 34, n. 2, p. 119–146, February 2008.

WANG, Y. et al. Experimental study of crossover from capillary to viscous fingering for supercritical CO₂-water displacement in a homogeneous pore network. **Environmental Science and Technology**, v. 47, n. 1, p. 212–218, 2013.

WOLERY, T. J.; DAVELER, S. A. Lawrence Livermore National Laboratory EQ6, A Computer Program for Reaction Path Modeling of Aqueous Geochemical Systems: Theoretical Manual, User's Guide, and Related Documentation (Version 7.0). 1992.

XIONG, Q.; BAYCHEV, T. G.; JIVKOV, A. P. Review of pore network modelling of porous media: Experimental characterisations, network constructions and applications to reactive transport. **Journal of Contaminant Hydrology**, v. 192, p. 101–117, September 2016.

ZARETSKIY, Y.; GEIGER, S.; SORBIE, K. Direct numerical simulation of pore-scale reactive transport: applications to wettability alteration during two-phase flow. **International Journal of Oil, Gas and Coal Technology**, v. 5, n. 2/3, p. 142, 2012.

ZARGHAMI, S.; BOUKADI, F.; AL-WAHAIBI, Y. Diffusion of carbon dioxide in formation water as a result of CO₂ enhanced oil recovery and CO₂ sequestration. **Journal of Petroleum Exploration and Production Technology**, v. 7, n. 1, p. 161–168, 17 March 2017.

ZHAO, H. et al. Carbon dioxide solubility in aqueous solutions of sodium chloride at geological conditions: Experimental results at 323.15, 373.15, and 423.15K and 150bar and modeling up to 573.15K and 2000bar. **Geochimica et Cosmochimica Acta**, v. 149, p. 165–189, January 2015.

APPENDIX 1 – FIT OF DATA FROM HELGESON (1981) FOR EXTENDED DEBYE-HÜCKEL PARAMETERS

Debye-Hückel parameters depend on solvent properties and temperature. The values used for water were collected from TABLE 17 and interpolated using Microsoft® Excel by a polynomial of second order, given in metric units in eq. (56) and (57), where T is in kelvin. Graphical representation of these functions are given in FIGURE 18.

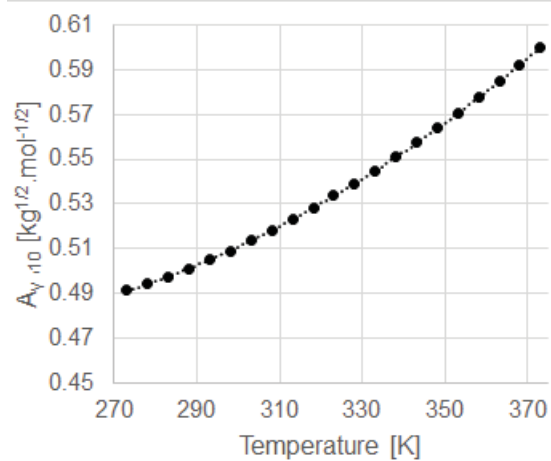
$$A_{\gamma,10} \left[kg^{\frac{1}{2}} mol^{-\frac{1}{2}} \right] = 4.7886 \times 10^{-6} T^2 - 2.0053 \times 10^{-3} T + 0.68151 \quad (56)$$

$$B_{\gamma,10} \left[\frac{kg^{1/2}}{mol\ m} \right] = 3.8628 \times 10^3 T^2 - 7.4407 \times 10^5 T + 3.1619 \times 10^9 \quad (57)$$

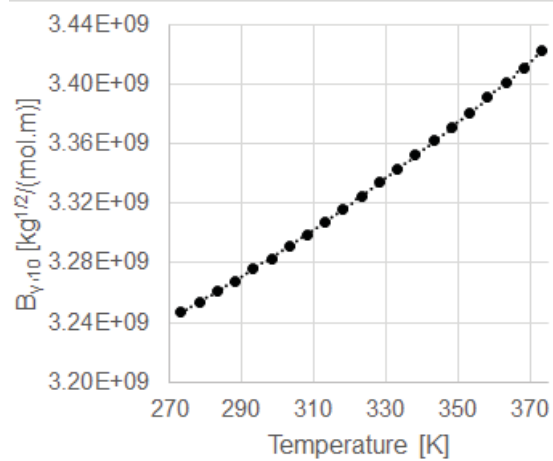
TABLE 17 DATA USED FOR COMPUTING DEBYE-HÜCKEL PARAMETERS

T	T	A _{γ,10}	B _{γ,10} × 10 ⁻⁸	B _{γ,10} × 10 ⁻⁹
[°C]	[K]	[kg ^{1/2} mol ^{-1/2}]	[kg ^{1/2} /(mol cm)]	[kg ^{1/2} /(mol m)]
0	273.15	0.4913	0.3247	3.247
5	278.15	0.4943	0.3254	3.254
10	283.15	0.4976	0.3261	3.261
15	288.15	0.5012	0.3268	3.268
20	293.15	0.5050	0.3276	3.276
25	298.15	0.5091	0.3283	3.283
30	303.15	0.5135	0.3291	3.291
35	308.15	0.5182	0.3299	3.299
40	313.15	0.5231	0.3307	3.307
45	318.15	0.5282	0.3316	3.316
50	323.15	0.5336	0.3325	3.325
55	328.15	0.5392	0.3334	3.334
60	333.15	0.5450	0.3343	3.343
65	338.15	0.5511	0.3352	3.352
70	343.15	0.5573	0.3362	3.362
75	348.15	0.5639	0.3371	3.371
80	353.15	0.5706	0.3381	3.381
85	358.15	0.5776	0.3391	3.391
90	363.15	0.5848	0.3401	3.401
95	368.15	0.5922	0.3411	3.411
100	373.15	0.5998	0.3422	3.422

SOURCE: ADAPTED FROM HELGESON ET AL. (1981).

FIGURE 18 (A) DATA FIT FOR PARAMETER $A_{y,10}$, (B) DATA FIT FOR PARAMETER $B_{y,10}$ 

(a)



(b)

APPENDIX 2 – BRIEF NOTES REGARDING THE EXPERIMENTS CWI IN CARBONATE MINERALS

This model assumes that the carbonated water reached equilibrium with CO₂ prior to injection in the reservoir and is further pressurized to injection pressure so as to assure single phase flow. Moreover, there is no oil phase.

This section shows why the model must follow these hypotheses in an experimental setup and make suggestions to circumvent problems. Both batch experiments and continuous reactors follow four main steps, which are the preparation of the carbonated water, pressurization of the system, a period where the pressure is constant and depressurization. Each has its nuances that should be isolated from the effects of the CWI to avoid false conclusions.

Prior to injection of carbonated water in the rock, there should be provided enough time for the CO₂ dissolve and diffuse in the liquid phase. The diffusion process of CO₂ in water is slow and several hours are required to reach the equilibrium condition in a deep layer in the absence of mechanical agitation (AZIN et al., 2013; CADOGAN et al., 2014; KECHUT et al., 2011).

During the positive ramp of pressure, the rock is subjected to a compression that can cause mechanical fractures, decreasing the porosity value and the size of the rock as a whole. This should not be confused with the effect of precipitation inside the rock, which also decreases local porosity, or dissolution on its borders, which changes the external surface of the rock as well.

During the negative ramp of pressure or during the continuous flow phase, if carbonated water is present inside the rock, the formation of bubbles is expected due to the decrease in CO₂ solubility, caused either by depressurization of the whole system or pressure drop during flow. This can change in flow patterns, modify the area available for reactions and permeability, enable other reaction mechanisms and possibly cause mechanical fractures, creating porosity that did not originate from the dissolution, but from the expansion of the gas phase when the bubble appears. This issue can be partly circumvented by further pressurizing the carbonated solution after reaching the equilibrium with CO₂ before the injection in the rock so as to have some leeway in terms of pressure drop to keep a single phase flow, in addition to injecting an oil phase or CO₂-free water for a period prior to depressurization. The decompression procedure in

itself is also capable of causing mechanical fractures, even with the absence of bubbles. There is no guarantee that this decompression effect fully compensate the compression effect because of hysteresis effects and plastic deformation.

One useful way to distinguish between the changes originated from chemical or mechanical causes would be to inject a neutral gas such as N_2 in the batch reactor and measure the effects of compression and decompression. Injection of CO_2 in the gas form in the absence of a liquid phase would result in the same effect as an inert, as there were no aqueous phases available, no ions could be produced when CO_2 entered the system. This prevents any dissolution as neither the H^+ ion nor the dissolution products Ca^{2+} and CO_3^{2-} could form without a proper medium. Besides, there would not be a saturated phase to create conditions to allow precipitation. As such, there would be no theoretical grounds to justify the presence of ions in the gas phase in the amount required to verify dissolution or precipitation reactions, suggesting that, without an aqueous phase, CO_2 cannot dissolve the rock at the conditions of the experiment.

A simulation using a Gibbs reactor, i.e. a reactor that minimizes the free energy of Gibbs, was performed in Aspen Plus, allowing all products and reactions in the Aspen Plus database and, when CO_2 is inserted without an aqueous phase, no reactions occurred. This proves that, in this case, thermodynamics should not favor any reactions. Thus, mechanical means should be the cause of all changes in the morphology of the rock in these conditions. On the other hand, when an aqueous phase is present, changes in porosity are hard to analyze, as there would be a mix of the chemical and mechanical effects.

The formation of a gas phase due to pressure drop is that the expansion may be enough to break the rock. Tackling mechanical fractures in this scheme is far too complex and is beyond the scope of this model. In order to interrupt the experiment while avoiding de-characterization of the situation inside the reactor, a fluid like CO_2 -free hexane can be injected into the rock prior to depressurization. This would simultaneously interrupt dissolution and avoid the formation of bubbles and subsequent precipitation of calcite. The depressurization is required to take the rock out of the reactor for post-processing (drying, micro-CT analysis).

ANNEX 1 – CALCULATION OF CO₂-BRINE EQUILIBRIUM

Spycher et al. (2003) and Spycher and Pruess (2005) developed a solubility model of CO₂ in a synthetic brine and tested their model in solutions of NaCl up to 6 m and CaCl₂ up to 4 m in the T-P grid of 12-100 °C and 1-600 bar, with errors up to 8% at ionic strength 6 molal. This work slightly changed their formulation so the model is applicable when more than one salt is present simultaneously.

The CO₂ solubility model proposed by Spycher and Pruess (2005) assumes (1) isofugacity for all species present in both phases, (2) their modified Redlich-Kwong EOS provides a good representation of the CO₂-rich phase, (3) all ions and salts are non-volatile, (4) infinite dilution of water in the CO₂-rich phase, (5) the water activity is close enough to unity and (6) the pH of the resulting solution is low enough that all inorganic carbon is the CO₂ present in that phase.

Classical mixing rules yield values for the intermolecular attraction parameter $a_{RK,mix}$ and the volume parameter $b_{RK,mix}$ equal to a_{RK,CO_2} and b_{RK,CO_2} , as in eq. (58) and (59). The parameters from Redlich-Kwong EoS shown in equations (60) to (61) were modified from a function of critical properties of the chemical species to the form of eq. (62) and (63).

$$a_{RK,mix} = \sum_{i=1}^{NC} \sum_{j=1}^{NC} y_i y_j a_{RK,ij} \therefore a_{RK,mix} = a_{RK,CO_2} \quad (58)$$

$$b_{RK,mix} = \sum_{i=1}^{NC} y_i b_{RK,ij} \therefore b_{RK,mix} = b_{RK,CO_2} \quad (59)$$

$$a_{RK,CO_2} = 7.54 \times 10^7 - 4.13 \times 10^4 T \quad (60)$$

valid for $283\text{ K} < T < 380\text{ K}$

$$a_{RK,H_2O-CO_2} = 7.89 \times 10^7 \text{ bar cm}^6 \text{ K}^{0.5} \text{ mol}^{-2} \quad (61)$$

$$b_{RK,CO_2} = 27.80 \text{ cm}^3/\text{mol} \quad (62)$$

$$b_{RK,H_2O} = 18.18 \text{ cm}^3/\text{mol} \quad (63)$$

The solution of the modified Redlich-Kwong EoS determines the molar volume of the H₂O-rich phase and the CO₂-rich phase, which are required to compute the fugacity coefficient of CO₂ and H₂O. Although there are numerical procedures to solve cubic EoS, the analytical approach is computationally faster and much simpler. Once the cubic equation of state is in the form of eq. (64), one

must collect the values of the coefficients c_{an} , d_{an} and e_{an} , and apply eq. (65) to (70) for the Redlich-Kwong EoS.

$$V_{mix}^3 + c_{an}V_{mix}^2 + d_{an}V_{mix} + e_{an} = 0 \quad (64)$$

$$c_{an} = \left(-\frac{RT}{P_{eq}} \right) \quad (65)$$

$$d_{an} = -\frac{RTb_{RK,mix}}{P_{eq}} + \frac{a_{RK,mix}}{P_{eq}T^{0.5}} - b_{RK,mix}^2 \quad (66)$$

$$e_{an} = -\frac{a_{RK,mix}b_{RK,mix}}{P_{eq}T^{0.5}} \quad (67)$$

$$Q_{an} = \frac{c_{an}^2 - 3d_{an}}{9} \quad (68)$$

$$L_{an} = \frac{2c_{an}^3 - 9c_{an}d_{an} + 27e_{an}}{54} \quad (69)$$

$$M_{an} = L_{an}^2 - Q_{an}^3 \quad (70)$$

If $M_{an} > 0$ there are three real roots, which are calculated by eq. (71) to (74).

$$\psi_{an} = \arccos\left(\frac{L_{an}}{\sqrt{Q_{an}^3}}\right) \quad (71)$$

$$V_{mix,1} = -\left[2\sqrt{Q_{an}} \cdot \cos\left(\frac{\psi_{an}}{3}\right)\right] - \frac{c_{an}}{3} \quad (72)$$

$$V_{mix,2} = -\left[2\sqrt{Q_{an}} \cdot \cos\left(\frac{\psi_{an} + 2\pi}{3}\right)\right] - \frac{c_{an}}{3} \quad (73)$$

$$V_{mix,3} = -\left[2\sqrt{Q_{an}} \cdot \cos\left(\frac{\psi_{an} - 2\pi}{3}\right)\right] - \frac{c_{an}}{3} \quad (74)$$

On the other hand, if $M_{an} < 0$, the equations has a single real root that can be determined using the parameters S'_{an} and T'_{an} in eq. (75) and (76) in (77).

$$S'_{an} = -\frac{L_{an}}{|L_{an}|} \cdot \sqrt[3]{|L_{an}| + \sqrt{M_{an}}} \quad (75)$$

$$T'_{an} = \frac{Q_{an}}{S'_{an}} \quad (76)$$

$$V_{mix} = S'_{an} + T'_{an} - \frac{c_{an}}{3} \quad (77)$$

If the cubic equation yields three roots, the value of V_{mix} used in the solubility model depends on which root is stable at system conditions, which is selected by the method of Nickalls (1993) using eq. (78) and (79).

$$w_1 = P_{eq}(V_{mix,g} - V_{mix,l}) \quad (78)$$

$$w_2 = RT \ln \left(\frac{V_{mix,g} - b_{mix}}{V_{mix,l} - b_{RK,mix}} \right) + \frac{a_{RK,mix}}{T^{0.5} b_{RK,mix}} \ln \left(\frac{(V_{mix,g} + b_{RK,mix}) V_{mix,l}}{(V_{mix,l} + b_{RK,mix}) V_{mix,g}} \right) \quad (79)$$

The decision criteria for choosing V_{mix} follows eq. (80) and eq. (81).

$$\text{If } (w_2 - w_1) \geq 0 \rightarrow V_{mix} = V_{mix,g} \quad (80)$$

$$\text{If } (w_2 - w_1) < 0 \rightarrow V_{mix} = V_{mix,l} \quad (81)$$

The fugacity coefficients ϕ_i are calculated using eq. (82), where h denotes all chemical species other than i that are present in the vapor phase.

$$\begin{aligned} \ln(\phi_i) = & \ln \left(\frac{V_{mix}}{V_{mix} - b_{RK,mix}} \right) + \left(\frac{b_{RK,i}}{V_{mix} - b_{RK,mix}} \right) \\ & - \left(\frac{2 \sum_{i=1}^{NC} y_i a_{RK,h-i}}{RT^{1.5} b_{RK,mix}} \right) \ln \left(\frac{V_{mix} + b_{RK,mix}}{V_{mix}} \right) \\ & + \left(\frac{a_{RK,mix} b_{RK,i}}{RT^{1.5} b_{RK,mix}^2} \right) \left[\ln \left(\frac{V_{mix} + b_{RK,mix}}{V_{mix}} \right) - \left(\frac{b_{RK,mix}}{V_{mix} + b_{RK,mix}} \right) \right] \\ & - \ln \left(\frac{P_{eq} V_{mix}}{RT} \right) \end{aligned} \quad (82)$$

Values of Henry's law constants for CO₂ in water $K_{H_2O,T,P}$ and $K_{CO_2,T,P}$ vary according to a function of temperature (expressed in °C), as in eq. (83) to (87).

$$\log(K_{H_2O,T,P_{ref}}) = -2.209 + 0.03097 T - 0.0001098 T^2 + 2.048 \times 10^{-7} T^3 \quad (83)$$

valid for 10 °C < T < 110 °C

$$\log(K_{CO_2(g),T,P_{ref}}) = 1.189 + 0.001304 T + 5.446 \times 10^{-5} T^2 \quad (84)$$

valid for 12 °C < T < 110 °C

$$\log(K_{CO_2(l),T,P_{ref}}) = 1.169 + 0.01368 T - 5.380 \times 10^{-5} T^2 \quad (85)$$

valid for 12 °C < T < 31 °C

The selection of the value of $K_{CO_2,T,P_{ref}}$ follows eq. (86) and (87).

$$\text{If } T < 31^\circ\text{C and } V_{mix} < 94 \text{ cm}^3 \rightarrow K_{H_2O,T,P_{ref}} = K_{CO_2(l),T,P_{ref}} \quad (86)$$

$$\text{Otherwise } K_{H_2O,T,P_{ref}} = K_{CO_2(g),T,P_{ref}} \quad (87)$$

These Henry's law constants are part of the model proposed by Spycher and Pruess (2005) and, as such, must be used instead of the Henry's law constants obtained by the unmodified Redlich-Kwong EoS.

The properties were lumped in the form of A_{spy} and B_{spy} in equations (88) and (89). Spycher and Pruess (2005) also calculated the averaged partial molar volumes over the range of their model, which are displayed in eq. (90) and (91).

$$A_{spy} = \frac{K_{H_2O,T,P_{ref}}}{\phi_{H_2O} P_{eq}} \exp\left(\frac{(P_{eq} - P_{ref})\bar{V}_{H_2O}}{RT}\right) \quad (88)$$

$$B_{spy} = \frac{\phi_{CO_2} P_{eq}}{55.508 \gamma_{x,CO_2} K_{CO_2,T,P_{ref}}} \exp\left(-\frac{(P_{eq} - P_{ref})\bar{V}_{CO_2}}{RT}\right) \quad (89)$$

$$\bar{V}_{H_2O} = 18.1 \text{ cm}^3/\text{mol} \quad (90)$$

$$\bar{V}_{CO_2} = 32.6 \text{ cm}^3/\text{mol} \quad (91)$$

Finally, the system is solved using eq. (92) and (93), while eq. (94) converts the molar fraction of CO_2 in the H_2O -rich phase to molality. If necessary, eq. (95) converts an activity coefficient on a molal to the molar fraction scale.

$$y_{H_2O} = \frac{(1 - B)55.508}{[(1/A) - B](\sum v_{tot,k} m_k + 55.508) + (\sum v_{tot,k} m_k)B} \quad (92)$$

$$x_{CO_2} = B(1 - y_{H_2O}) \quad (93)$$

$$m_{CO_2} = \frac{x_{CO_2} \cdot (\sum v_{tot,k} m_k + 55.508)}{(1 - x_{CO_2})} \quad (94)$$

$$\gamma_m = \frac{\gamma_x}{\left(1 + \frac{\sum m_i}{55.508}\right)} \left(1 + \frac{m_{CO_2}}{55.508}\right) \quad (95)$$

Three of the several activity coefficient models were tested by Spycher and Pruess (2005) are included in the code of this work: (1) Duan and Sun (2003), a modification of Rumpf et al. (1994) and (3) a modification of Drummond (1981).

Duan and Sun (2003) fitted a Pitzer model to a large set of experimental data for pure water and brine, covering the range 0 to 260 °C, 0 to 2000 bar, 0 to 6.5 molal NaCl and 0 to 3.9 molal CaCl₂. Their parameter γ_{DS}^* is not a true activity coefficient, as it actually is $m_{CO_2, H_2O} / m_{CO_2, brine}$ and is given from eq. (96) to (98).

$$\ln(\gamma_{DS}^*) = 2\lambda_{DS}(m_{Na^+} + m_{K^+} + 2m_{Ca^{2+}} + 2m_{Mg^{2+}}) + \xi_{DS}m_{Cl^-}(m_{Na^+} + m_{K^+} + m_{Ca^{2+}} + m_{Mg^{2+}}) - 0.07m_{SO_4^{2-}} \quad (96)$$

$$\lambda_{DS} = -0.411370585 + 6.07632013 \times 10^{-4} T + \frac{97.5347708}{T} - \frac{0.0237622469 P_{EQ}}{T} + \frac{0.0170656236 P_{EQ}}{(630 - T)} + 1.41335834 \times 10^{-5} T \ln(P_{EQ}) \quad (97)$$

$$\xi_{DS} = 3.36389723 \times 10^{-4} - 1.98298980 \times 10^{-5} T + \frac{2.12220830 \times 10^{-3} P_{EQ}}{T} - \frac{5.24873303 \times 10^{-3} P_{EQ}}{(630 - T)} \quad (98)$$

Alternatively, a modified version of Rumpf et al. (1994), given by eq. (99) to (101), provides the γ_{CO_2} on the molality scale using a Pitzer formulation.

$$\ln(\gamma_{m,CO_2}) = 2B^{(0)}(m_{Na^+} + m_{K^+} + 2m_{Ca^{2+}} + 2m_{Mg^{2+}}) + 3\Gamma m_{Cl^-}(m_{Na^+} + m_{K^+} + m_{Ca^{2+}} + m_{Mg^{2+}}) \quad (99)$$

$$B^{(0)} = 0.254 - \frac{76.82}{T} - \frac{10656}{T^2} + \frac{6.312 \times 10^3}{T^3} \quad (100)$$

$$\Gamma = -0.0028 \quad (101)$$

ANNEX LIST – VIRTUAL DOCUMENTS

This master thesis has the financial support of the Brazilian Government. As such, the codes developed in this master thesis are of public domain under solicitation to the author at gustavoquillo@hotmail.com. All files are provided in their natural extension (e.g. .m for a MATLAB® code) and as .pdf in the digital version of this master thesis.

Part 1

1. MainProgram.m: calls other algorithms where appropriate.
2. massH2OMcCain.m: calculates the density of brine under reservoir conditions and the mass of each species present in the cell;
3. myfun.m: auxiliary function required to call the fsolve function to compare results of the Newton-Raphson method using Levenberg-Marquardt;
4. ReactionCheck.m: verifies if the extent of the reaction is too large and divides the time step into smaller parts according to the criterium established in the section Reaction Check;
5. ReactionCode.m: computes the rate of dissolution of calcite and applies changes in rock structure, as presented in the section Reaction Code;
6. SolubilityCode.m: computes the solubility of CO₂ in brine;
7. SpeciationCode.m: applies the Newton-Raphson method with numerical derivatives as explained in the section Speciation Model;
8. StabilizeSystem.m: prepares a better initial guess for the Speciation Code if the dissolution reaction was too fast;
9. PostProcessing.m: generates graphs and reports.

Part 2

1. estimador.m: estimates the optimal parameters for the modification of Drummond (1981) using the particle swarm optimization and many deterministic methods. In addition, it calculates the individual and joint confidence interval for each parameter.
2. fobj.m: objective function used during parameter estimation
3. fobjaux.m: objective function used when calculating the Hessian matrix;

4. fobjaux2.m: objective function used for lsqnonlin;
5. geterror.m: calculates the result predict by the model and compares with the experimental value;
6. Hessiana.m: calculates the Hessian matrix using numerical derivatives.

Part 3

10. MasterThesis_aPLOT.m: plots the results for the molality of CO₂ in the aqueous phase and the content of H₂O in the CO₂-rich phase. It includes two modes, the calculation mode and the plot mode;
11. MasterThesis_g_molalityfunc.m: generates the sum of the squared errors used to fit the parameters of the modified version of Drummond (1981).
12. Particleswarm.m: calls MasterThesis_g_molalityfunc.m and find the best parameters for the modified version of Drummond (1981).
13. Molality_from_wt_calc.m: converts data from Liu et al. (2011) and Tong et al. (2013) to the molality concentration scale.